

Reactive Trace Gases within and above a Grassland Canopy: Challenges for Flux and Transport Process Determination

A dissertation submitted to the
FACULTY OF BIOLOGY, CHEMISTRY AND GEOSCIENCES
AT THE UNIVERSITY OF BAYREUTH

for the degree of

DR. RER. NAT.

presented by

DANIEL PLAKE

Dipl. Landschaftsökologe

born 15. July 1981

in Neuenkirchen

Bayreuth, January 2014

Reactive Trace Gases within and above a Grassland Canopy:
Challenges for Flux and Transport Process Determination

Supervised by PROF. DR. ANDREAS HELD

Die vorliegende Arbeit wurde in der Zeit von Dezember 2009 bis Januar 2014 in Bayreuth am Lehrstuhl für Atmosphärische Chemie unter Betreuung von Herrn Professor Dr. Andreas Held angefertigt.

Vollständiger Abdruck der von der Fakultät für Biologie, Chemie und Geowissenschaften der Universität Bayreuth genehmigten Dissertation zur Erlangung des akademischen Grades eines Doktors der Naturwissenschaften (Dr. rer. nat.).

Dissertation eingereicht am:	20. Januar 2014
Zulassung durch die Promotionskommission:	29. Januar 2014
Wissenschaftliches Kolloquium:	15. April 2014
Amtierender Dekan:	<i>Prof. Dr. Rhett Kempe</i>

Prüfungsausschuss:

Prof. Dr. Andreas Held (Erstgutachter)

Prof. Dr. Thomas Foken (Zweitgutachter)

Prof. Dr. Cyrus Samimi (Vorsitz)

Prof. Dr. Christiane Werner Pinto

Contents

Contents.....	I
List of Manuscripts.....	III
Acknowledgements.....	V
Summary.....	VII
Zusammenfassung.....	IX
Synthesis.....	1
1 Introduction.....	1
1.1 Objectives of this thesis.....	5
2 Experimental.....	7
2.1 Site description.....	7
2.2 Experimental setup.....	8
3 Results.....	11
3.1 Technical advancements.....	11
3.1.1 A novel automated thoron profile system.....	11
3.1.2 Ozone fluxes measured with the dynamic chamber technique.....	12
3.2 Scientific advancements.....	15
3.2.1 In-canopy transport.....	15
3.2.2 Timescales of transport and chemistry.....	17
3.2.3 Canopy reduction of nitric oxides within a natural grassland canopy.....	20
3.2.4 Ozone fluxes at a natural grassland.....	21
3.2.5 Ozone flux divergence.....	22
4 Conclusions.....	25
References.....	29
List of Appendices.....	35
Appendix A: Individual Contribution to the Joint Publications.....	37
Appendix B: Thoron Profile System.....	39
Appendix C: Ozone Deposition Measured with the Dynamic Chamber Method.....	65
Appendix D: Chemical Divergence of the NO-NO ₂ -O ₃ Triad.....	97
Erklärungen.....	121

List of Manuscripts

The dissertation is presented in cumulative form. It consists of three individual but thematically linked manuscripts. The first manuscript has been published in a peer-reviewed journal. The second manuscript has been submitted to a peer-reviewed journal. The third manuscript will be submitted for publication in the near future.

Published manuscript

PLAKE, D. and TREBS, I., 2013. An automated system for selective and continuous measurements of vertical thoron profiles for the determination of transport times near the ground. *Atmospheric Measurement Techniques*, 6(4): 1017-1030.

Submitted manuscript

PLAKE, D., STELLA, P., MORAVEK, A., MAYER, J.C., AMMANN, C., HELD, A. and TREBS, I., 2014. Comparison of ozone deposition measured with the dynamic chamber and the eddy covariance method. *Agricultural and Forest Meteorology*, submitted.

Manuscript to be submitted

PLAKE, D., SÖRGEL, M., STELLA, P., HELD, A. and TREBS, I., 2014. Influence of meteorology and anthropogenic pollution on chemical divergence of the NO-NO₂-O₃ triad above and within a natural grassland canopy. *Biogeosciences*, to be submitted.

Other publications, not included in this thesis

MESTROT, A., PLAKE, D., TREBS, I., VELESCU, A., ROSCHER, C., MILCU, A., ROY, J., OELMANN, Y. and WILCKE, W., 2014. Measuring nitrogen foliar uptake using ¹⁵N labeled NO₂ gas. *Journal of Experimental Botany*, in preparation.

FOKEN, T., MEIXNER, F.X., FALGE, E., ZETZSCH, C., SERAFIMOVICH, A., BARGSTEN, A., BEHRENDT, T., BIERMANN, T., BREUNINGER, C., DIX, S., GERKEN, T., HUNNER, M., LEHMANN-PAPE, L., HENS, K., JOCHER, G., KESSELMEIER, J., LUERS, J., MAYER, J.C., MORAVEK, A., PLAKE, D., RIEDERER, M., RUTZ, F., SCHEIBE, M., SIEBICKE, L., SÖRGEL, M., STAUDT, K., TREBS, I., TSOKANKUNKU, A., WELLING, M., WOLFF, V. and ZHU, Z., 2012. Coupling processes and exchange of energy and reactive and non-reactive trace gases at a forest site - results of the EGER experiment. *Atmospheric Chemistry and Physics*, 12(4): 1923-1950.

Acknowledgements

I am very grateful to my daily advisor and group leader Ivonne Trebs for her scientific and personal support, her valuable guidance throughout the entire PhD, her commendable proof-reading skills, and her tireless commitment for the professional needs of her collaborators. A boss, who holds the work-live balance of his staff in a priority position, is a good boss! Ivonne, I very much appreciate all the help.

I am very thankful to my doctoral advisor Andreas Held for his personal and scientific support, his availability for fruitful discussions, his stake in proofreading as well as his thematic direction throughout my PhD time. Andreas, you are someone to count on!

Special thanks to Christof Ammann who was scientifically and personally involved in this PhD from the beginning to the end. His great experience in the investigated subject guaranteed advices of high value, preferentially conveyed during late afternoon telephone calls.

I warmly thank Franz X. Meixner for assisting in methodological issues, whenever needed. His positive impulsive nature illuminated some hard working days.

I would like to thank the members of the AG Trebs (now AG Sörgel) and other recent and former working colleagues, with whom I frequently discussed all possible scientific and also general matters in front of my office door. The first to mention is Alexander Moravek for being a very close friend and also working colleague since nearly seven years now. Fruitful discussions with him and the feedback from him impacted solely positive on my PhD life and, thus, also this thesis. Many thanks also to Robert Oswald for his scientific advices but most importantly for being responsible for good mood and coffee breaks in our hard working office. Many thanks also to Patrick Stella for co-working on two manuscripts and his company during regular working days and conferences. Thanks to Michael Welling for contributing with technical details on the measurement setup and with logistical and technical support during the field campaign. Thanks to Eva Falge for the help with plant species and LAI determination as well as for scientific advice. Thanks to Jens C. Mayer for providing micrometeorological measurements. Thanks to Daniel Moran for helping with the field installations. I want to thank Matthias Sörgel for his scientific advice. Further I want to thank Michael Ermel, Stefan Wolf and Dianming Wu for their cheerful company.

I thank Andi Andreae and the Max-Planck Society for funding me. Andi Andreae contributed helpful scientific advice as member of my PhD advisory committee.

I would like to thank the colleagues at the Max-Planck-Institute for Chemistry who contributed to this thesis. Special thanks to Michael Flanz at the electronic department for the support with the data acquisition and the colleagues at the mechanical workshop for the construction important components of my measurement setup.

I am grateful to Mr. H. Gross for the electrical installations at the field site and for the logistical support.

I thank Derek Lane-Smith for discussing the setup of the Thoron system.

I am indebted to Annette Röttger and Anja Honig at the Physikalisch-Technische Bundesanstalt (PTB, Braunschweig, Germany) for their help in validating the sensitivity of the RAD7 monitors for Thoron.

I am grateful to my friend Mia Terashima for reviewing the synthesis.

Many, many thanks to my family and friends! Without your support this thesis could not have come into existence and daily life would be gray without you.

Not gray but blonde is the person who owns my biggest debt of gratitude: my love Evridiki. The simultaneous PhD-life brought us together and led us through sunny and cloudy times. Finally, we managed and reached the end of the tunnel together. A shiny, most-likely female treasure is waiting there for us to color our future lives. Many, many thanks for being with me and always supporting me!

Summary

Nitrogen oxide (NO), nitrogen dioxide (NO₂) and ozone (O₃) constitute a reactive trace gas triad, which is highly important for the oxidizing capacity of the atmosphere, the functioning of ecosystems and climate change. Terrestrial ecosystems, such as grasslands, represent considerable sources and sinks for the NO-NO₂-O₃ triad and, thus, are crucial for atmospheric budgets of these species. The experimental quantification of surface-atmosphere exchange of the NO-NO₂-O₃ triad is difficult, and permanent flux monitoring networks are still at their infancy. Due to their fast reactivity, vertical gradients and fluxes of these species differ significantly from the respective theoretical descriptions for non-reactive trace gases. This effect is referred to as “chemical flux divergence”. Compared to the layer above, plant canopies exhibit an increased aerodynamic resistance, resulting in prolonged transport times of air within the canopy. This may provide sufficient time for in-canopy flux divergence and for interactions of trace gases such as the NO-NO₂-O₃ triad with plants. A prominent example is the fate of soil-emitted NO that undergoes chemical reaction with O₃ within the canopy and is subsequently recaptured by the surrounding vegetation in the form of NO₂. This process is referred to as “NO_x canopy reduction” (NO_x = NO+NO₂). NO_x canopy reduction is commonly applied in global atmospheric chemistry and transport models, but was never investigated for grassland canopies, which cover vast terrestrial areas.

This thesis focusses on the following topics investigated for a natural grassland canopy: (i) the quantification of in-canopy transport characteristics such as aerodynamic resistances and transport times, (ii) validation of the dynamic chamber technique for routine O₃ flux measurements at low canopy ecosystems and (iii) the analysis of chemical flux divergence and NO_x canopy reduction.

The quantification of in-canopy transport characteristics is of a major importance for the investigation of sources, sinks and net fluxes of reactive trace gases within plant canopies. A novel automated measurement system for selective vertical Thoron (Tn) profiles near the earth’s surface has been presented and evaluated, and its suitability for the direct and reliable determination of transport times within a natural grassland canopy has been demonstrated. For the first time, a rigorous determination of systematic and random error of Tn concentrations was performed under field conditions for this type of measurement system. In-canopy transport times were calculated and their uncertainty from the individual errors of the Tn concentration measurements was propagated. The directly measured in-canopy transport times were compared with two empirical parameterizations that are frequently used in modeling studies. The disability of the parameterizations to reproduce the entire diurnal course of the in-canopy transport has been proven. An agreement with the measured transport times was

either found during daytime or during nighttime, depending on the parameterization. The in-canopy transport characteristics constituted as base for the investigation of chemical flux divergence and NO_x canopy reduction.

Nowadays, eddy covariance (*EC*) is the state of the art method to quantify turbulent exchange fluxes. *EC* requires high-frequency trace gas instruments that are not always available. In the absence of such instruments, fluxes can also be determined using e.g., chamber techniques. However, up to date fluxes of depositing compounds have been rarely determined using chamber techniques, mainly due to a modification of the aerodynamic conditions for the trace gas transport within the chamber. O_3 deposition fluxes measured at a natural grassland site by the dynamic chamber technique are presented and, for the first time, validated against the *EC* method. The raw O_3 fluxes of the dynamic chamber method were corrected for gas-phase chemistry and for the modification of the aerodynamic resistances. Simultaneously measured carbon dioxide and water vapor fluxes by both methods were comparable during daytime, documenting an equal vegetation activity inside and outside the chambers. The final corrected O_3 deposition fluxes of both methods deviated on average by only 11 % during daytime. This demonstrates the capability of the dynamic chamber method to capture representative O_3 deposition fluxes for low canopy ecosystems. The canopy resistance to O_3 , an important parameter in modeling studies, was assessed by both methods and showed a characteristic diurnal cycle with minimum hourly median values of 180 s m^{-1} (chambers) and 150 s m^{-1} (*EC*) before noon. By using the O_3 fluxes resulting from the *EC* method, it could be shown that the non-stomatal pathway dominated the total O_3 deposition to the natural grassland canopy.

For the first time, transport times, aerodynamic resistances, vertical profiles of NO - NO_2 - O_3 mixing ratios and micrometeorological quantities were simultaneously measured within and above a natural grassland canopy, and delivered insights on potential NO_x canopy reduction and flux divergence. A canopy decoupling was observed during day and nighttime from vertical temperature profiles resulting in inverse stability conditions in the lower and upper grassland canopy. For the lower canopy this interestingly implied a daytime stable stratification and a nighttime unstable stratification. The diurnal courses of in-canopy transport characteristics reflected the stratification. The grassland showed parallels with Amazonian rainforest canopies from the literature. Unfortunately, NO_x canopy reduction could not be quantified due to insignificant NO soil emissions at the site. Nevertheless, the obtained results clearly allowed the conclusion that NO_x canopy reduction in grassland canopies of similar structure is generally very efficient during daytime at sites where NO is emitted. In addition, a chemical flux divergence for O_3 was determined between the *EC* measurement height and the canopy top. In contrast to previous studies, the chemical flux divergence resulted in a net chemical O_3 production during daytime, leading to 10 % underestimation of the O_3 flux by the *EC* method.

Zusammenfassung

Stickstoffmonoxid (NO), Stickstoffdioxid (NO₂) und Ozon (O₃) stellen eine reaktive Spurengas-Triade dar, welche von größter Bedeutung für die Oxidierungskapazität der Atmosphäre, die Funktionsfähigkeit von Ökosystemen und den Klimawandel ist. Terrestrische Ökosysteme, wie z.B. Grasland, repräsentieren bedeutende Quellen und Senken für die NO-NO₂-O₃-Triade und sind damit von entscheidender Bedeutung für atmosphärische Budgets dieser Stoffe. Die experimentelle Quantifizierung des Austausches der NO-NO₂-O₃-Triade zwischen Erdoberfläche und Atmosphäre ist diffizil und permanente Fluss Monitoring Netzwerke stecken noch immer im Anfangsstadium. Aufgrund der schnellen Reaktivität dieser Spezies weichen die dazugehörigen vertikalen Gradienten und Flüsse in erheblichem Maße von der theoretischen Beschreibung für nicht-reaktive Spurengase ab. Dieser Effekt wird als „chemische Flussdivergenz“ bezeichnet. Im Vergleich zu der darüber liegenden Schicht weisen Pflanzenbestände einen erhöhten aerodynamischen Widerstand auf, was zu einer Verlängerung von Transportzeiten der Luft in Pflanzenbeständen führt. Dieses kann zur Folge haben, dass sich innerhalb von Pflanzenbeständen ausreichend Zeit für Flussdivergenzen und Interaktionen von Spurengasen wie z.B. der NO-NO₂-O₃-Triade mit Pflanzen bietet. Ein bekanntes Beispiel ist der Verbleib von bodenemittiertem NO im Pflanzenbestand, welches nach chemischer Reaktion mit O₃ in Form von NO₂ von der umgebenden Vegetation wiederaufgenommen wird. Dieser Vorgang wird als „NO_x-Verringerung im Bestand“ (NO_x = NO+NO₂) bezeichnet. Atmosphärenchemie- und Transportmodelle wenden für globale Berechnung die NO_x-Verringerung im Bestand an. Diese wurde jedoch niemals explizit für Graslandbestände untersucht, ein Ökosystemtyp, welche erhebliche terrestrische Flächen bedeckt.

Diese Arbeit konzentriert sich auf die folgenden ein natürliches Grasland betreffenden Themen: (i) die Quantifizierung von Transporteigenschaften wie aerodynamischen Widerständen und Transportzeiten innerhalb des Bestandes, (ii) die Validierung eines dynamischen Kammer-systems für routinemäßige Messungen von O₃ Flüssen in Ökosystemen mit geringer Bestandshöhe und (iii) die Analyse von chemischer Flussdivergenz und NO_x-Verringerung im Bestand.

Die Quantifizierung von innerbestandlichen Transporteigenschaften ist von grundlegender Bedeutung für die Untersuchung von Quellen, Senken und netto Flüssen von reaktiven Spurengasspezies in Pflanzenbeständen. Ein neuartiges und automatisiertes Messsystem für selektive Thoron (Tn) Vertikalprofile in Bodennähe ist präsentiert und evaluiert worden. Seine Eignung für die direkte und verlässliche Bestimmung von Transportzeiten innerhalb von Graslandbeständen konnte demonstriert werden. Erstmals wurde eine rigorose Bestimmung von systematischen und zufälligen Messfehlern für Tn-Konzentrationen unter Feldbedingun-

gen für diese Art von Messsystem durchgeführt. Innerbestandliche Transportzeiten wurden berechnet und deren Unsicherheit ausgehend von den individuellen Messfehlern der T_n -Konzentrationen fortgepflanzt. Die direkt gemessenen innerbestandlichen Transportzeiten wurden mit zwei häufig in Modelluntersuchungen benutzten empirischen Parametrisierungen verglichen. Dabei wurde die Unzulänglichkeit beider Parametrisierungen zur Reproduktion des gesamten Tagesganges der innerbestandlichen Transportzeiten belegt. Eine Übereinstimmung mit den gemessenen Transportzeiten wurde dabei je nach Parametrisierung entweder nur für am Tag oder nur in der Nacht gefunden. Die innerbestandlichen Transporteigenschaften dienten als Basis für die Untersuchung von Flussdivergenzen und die NO_x -Verringerung.

Eddy Kovarianz (*EC*) ist die dem aktuellen Stand der Technik entsprechende Methode zur Quantifizierung von turbulenten Austauschflüssen. *EC* erfordert Messinstrumente mit hochfrequenter zeitlicher Auflösung, die nicht immer zur Verfügung stehen. In einem solchen Fall können Flüsse z.B. auch mit Kammermethoden bestimmt werden. Allerdings wurden Flüsse von deponierenden Komponenten bislang nur selten mit Kammermethoden bestimmt, was hauptsächlich an der Problematik der Veränderung von aerodynamischen Bedingungen für die Spurengase durch die Kammer selbst liegt. An einem Standort mit natürlichem Graslandbestand mit der dynamischen Kammermethode gemessene O_3 -Depositionsflüsse werden präsentiert und erstmalig gegen die *EC*-Methode validiert. Die O_3 -Rohflüsse der dynamischen Kammermethode wurden für Gasphasenchemie und die Modifikation der aerodynamischen Widerstände korrigiert. Eine gute Übereinstimmung der simultan mit beiden Methoden gemessenen Kohlenstoffdioxid- und Wasserdampfdampf Flüsse belegten eine gleichwertige Vegetationsaktivität inner- und außerhalb der Kammern. Nach der finalen Korrektur wichen die O_3 -Depositionsflüsse beider Methoden am Tag nur um 11 % voneinander ab, was die Fähigkeit der dynamischen Kammermethode zur Messung repräsentativer Depositionsflüsse für Ökosysteme mit niedriger Vegetation belegt. Der Widerstand des Graslandbestandes für O_3 , ein wichtiger Parameter in Modellierungsstudien, wurde mit beiden Methoden erfasst. Dieser war einem charakteristischen Tagesgang unterworfen mit dem spätmorgendlichen Minimum der stündlichen Medianwerte von 180 s m^{-1} (Kammern) und 150 s m^{-1} (*EC*). Des Weiteren konnte durch Nutzung der *EC*- O_3 -Flüsse gezeigt werden, dass die totale O_3 -Deposition vorrangig nicht-stomatär erfolgt.

Erstmalig wurden Transportzeiten, aerodynamische Widerstände, Vertikalprofile der NO - NO_2 - O_3 -Triade und mikrometeorologische Größen simultan innerhalb und oberhalb eines natürlichen Grasbestandes gemessen. Die Messungen lieferten Einblicke in Themen, wie potentieller NO_x -Verringerung im Bestand und chemischer Flussdivergenz. Eine Entkoppelung verbunden mit umgekehrten Stabilitätsbedingungen des oberen und unteren Teils des Grasbestandes wurde während des gesamten Tages durch Vertikalprofile der Temperatur beobachtet.

Interessanterweise beinhaltet dies für den unteren Teil des Grasbestandes am Tag eine stabile und in der Nacht eine instabile Schichtung, was auch im Tagesgang der innerbestandlichen Transporteigenschaften zu sehen war. Literaturvergleiche ergaben, dass einige Parallelen zwischen dem untersuchten Grasland und Regenwaldbeständen im Amazonasgebiet bestehen. Aufgrund nicht-signifikanter NO-Bodenemissionen am untersuchten Standort konnte leider die NO_x-Verringerung im Bestand nicht quantifiziert werden. Trotzdem ließen die Ergebnisse dieser Studie die generelle Schlussfolgerung zu, dass am Tag die NO_x-Verringerung in Grasbeständen ähnlicher Struktur mit signifikanten NO-Bodenemissionen äußerst effektiv ist. Außerdem wurde eine O₃-Flussdivergenz zwischen der *EC*-Messhöhe und der Bestandshöhe bestimmt. Diese stellte tagsüber eine O₃-Produktion dar und steht damit im Widerspruch zu bisherigen Veröffentlichungen zu diesem Thema. Die O₃ Flussdivergenz sorgte für eine zehnprozentige Unterschätzung des O₃ Flusses durch die *EC*-Methode.

SYNTHESIS

1 Introduction

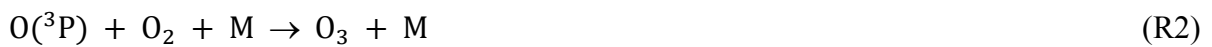
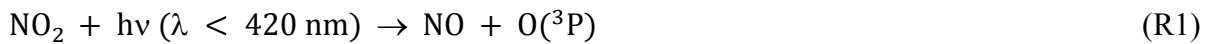
Besides nitrogen, oxygen and argon, the major constituents of the Earth's atmosphere, a large number of gases exist, which are characterized by concentrations far below 1 %; the trace gases. The low atmospheric abundance of trace gases strictly contrasts their importance. On the one hand, the natural greenhouse effect is provided by atmospheric trace gases such as carbon dioxide (CO₂) or methane (CH₄), allowing humans to live on Earth (e.g., MITCHELL, 1989). On the other hand, the industrialization resulted in increased anthropogenic emissions and, subsequently, led to a substantial rise of atmospheric trace gas levels (e.g., IPCC, 2007). That is why besides atmospheric aerosols, many trace gases are considered as air pollutants, as they can cause hazardous environmental and health damages at global and local levels. An exemplary and uncompleted list comprises (i) the anthropogenic greenhouse effect among others caused by increased CO₂, CH₄, nitrous oxide (N₂O) or ozone (O₃) levels (e.g., IPCC, 2007); (ii) acidic rain by emissions of precursor substances such as sulfur dioxide (SO₂) or nitrogen dioxide (NO₂) (e.g., DUYZER and FOWLER, 1994; KHEMANI et al., 1994); (iii) damaging effects on human health in locations with elevated O₃, NO₂ or SO₂ concentrations (e.g., GILLILAND et al., 2004; KIM et al., 2013); (iv) ecosystem eutrophication by deposition of anthropogenic emitted trace gases such as NO₂ or ammonia (NH₃) (e.g., DUYZER and FOWLER, 1994; NEMITZ et al., 2000); (iv) direct damage to plants resulting from stomatal uptake of O₃ or NO₂ (e.g., SIGNAL et al., 2007; GREITNER et al., 1994).

Investigative explorations of such effects require knowledge on the atmospheric composition, the underlying transport and the respective source-sink distribution of respective trace gases, all of which are variable in space and time. Depending on the respective scientific question, different spatial and temporal scales might be addressed. For investigations at a global scale, such as future climate predictions, global atmospheric models are the methods of choice (cf., IPCC, 2007). Exhaust plumes of cities can be studied by using regional observations and/or models (e.g., ZHENG et al., 2013). Nevertheless, current and future global models, as well as those on a regional or ecosystem scale (e.g., BALDOCCHI, 1988), rely on results of small scale field measurements as crucial input parameters such as micrometeorological trace gas fluxes (MONCRIEFF et al., 1997).

Eddy covariance (e.g., FOKEN et al., 2012a) is the state-of-the-art micrometeorological measurement technique to derive net ecosystem fluxes e.g., for CO₂. Huge efforts have been carried out to install flux measurement networks (e.g., CarboEurope in DOLMAN et al. (2006)), as these data have a great value e.g., for climate change research. In cases when instruments

suitable for eddy covariance are not available, also profile methods can be used for flux measurements. Enclosure methods such as static or dynamic chambers, however, can be operated to identify and quantify sources and sinks of trace gases in ecosystem compartments such as soils (e.g., GUT et al., 2002b) or branches (e.g., BOURTSOUKIDIS et al., 2012). While static chambers are used for non-reactive species, dynamic chambers are additionally suitable to determine fluxes of fast reacting compounds. Furthermore, the dynamic chamber technique is able to yield net ecosystem exchange fluxes of trace gases (e.g., HIROTA et al., 2010), in cases where the canopy of the ecosystem under consideration is up to approximately the same height as the used chamber.

However, respective investigations using either numerical models or field measurements become substantially more complicated when chemical reactive species are investigated. Reactive trace gases such as nitric oxide (NO) and NO₂ play a crucial role in atmospheric chemistry since they act as key catalysts for the production of O₃ and, thus, are linked to the generation of hydroxyl radicals (OH) (CRUTZEN, 1973), the major oxidant of the atmosphere. The most significant tropospheric source for O₃ is initiated by NO₂ photolysis and subsequent reaction of the resulting ground state oxygen atom (O(³P)) with molecular oxygen:



When O₃ is present, it may oxidize NO and re-form NO₂:



In the absence of additional reactions, R1–R3 constitute a null cycle, which led to the term NO-NO₂-O₃ triad. Beside R1–R3, NO is oxidized by peroxy radicals representing an additional important net O₃ production pathway in the troposphere (WARNECK, 2000).

Terrestrial ecosystems play a key role for the emission and removal of trace gases such as the NO-NO₂-O₃ triad, which strongly impact atmospheric chemistry and climate (ARNETH et al., 2010). That is why several previous studies investigated the corresponding source-sink distributions. NO is known to be mainly net emitted from nearly all soil types (e.g., FOWLER et al., 2009). These emissions contribute with ~20 % to the global NO_x (NO+NO₂) emissions (IPPC, 2007). Dry-deposition to terrestrial ecosystems, especially to plant canopies, is an important sink for tropospheric O₃ and NO₂ (e.g., FOWLER et al., 2009). While the net ecosystem exchange of NO₂ can be bi-directional depending on the ambient NO₂ levels and the magnitude of simultaneous NO soil emissions (e.g., PILEGAARD et al., 1998), O₃ is exclusively deposited to ecosystem elements such as plants or soils (e.g., FOWLER et al., 2009). MASSMAN et al. (2000) nicely summarized results of conducted O₃ flux experiments. Certainly, additional

field campaigns on O₃ fluxes have been carried out to date (e.g., STELLA et al., 2013a) and knowledge on O₃ deposition has slightly improved. But nevertheless, permanent flux measurement networks for the members of the NO-NO₂-O₃ are, in contrast to CO₂, not yet established. Thus, any further step leading towards continuous NO-NO₂-O₃ flux measurements represents a highly important contribution for atmospheric research.

Physical transport of trace gases in air can occur through: (i) pure molecular diffusion, (ii) turbulent transport or (iii) convection. While the relatively slow molecular diffusion is only important in laminar boundary layers at the millimeter range above surfaces, the approximately five orders of magnitude faster turbulent transport comes into play with increasing distances to surfaces. An air parcel is convectively transported when its temperature or moisture differs from the surrounding air, and the transport efficiency depends on the magnitude of the difference. LENSCHOW (1982) pointed out that the fast characteristic chemical timescale of the NO-NO₂-O₃ triad (R1–R3) is in the order of seconds to minutes which is the typical range of typical turbulent transport times in the atmospheric boundary layer. This implies that a gradient or flux of a fast reacting compound measured at a field site can be (i) either due to physical transport towards or from a sink or source, respectively, as well as (ii) due to chemistry. Accordingly, a deviation from the constant flux assumption (e.g., SWINBANK, 1968) due to chemical reactions and interconversion of reactive compounds is termed “chemical flux divergence” (e.g., DE ARELLANO et al., 1993). Chemical flux divergences can lead to large difficulties in the interpretation of experimental data and their implication into models.

A major challenge for the investigation of surface-atmosphere exchange fluxes of reactive trace gases is the presence of plant canopies. Over rough surfaces, such as plant canopies, physical transport of matter is dominated by low-frequency turbulence events called “coherent structures” (e.g., FINNIGAN, 2000; THOMAS and FOKEN, 2007). These consist of ejection of air from, and sweeps into the canopy, promoting the development of a vertical motion that may penetrate deep into the canopy. The attenuation of turbulence within canopies is strongly dependent on the canopy structure. Compared to the air layer above, a substantial modification of the residence time of the air within the canopy may occur, whose amplitude is a function of the height above the ground and the time of the day. This may provide sufficient time for (i) promoting in-canopy chemical flux divergence and (ii) recapturing of either the directly emitted compounds such as NH₃ in NEMITZ et al. (2000) or reaction products (e.g., NO₂) to be deposited and taken up by plants and soil (e.g., MEIXNER, 1994). The whole process (with respect to the emitted compounds) is typically called “canopy reduction”, which implies that the canopy processes result in a decrease in the effective emission flux into the atmosphere (e.g., YIENGER and LEVY, 1995). For instance, only a fraction (~20 %) of soil biogenic NO emissions typically leave e.g., rain forest canopies, because a large part is oxidized by O₃ and

the product NO_2 is subsequently recaptured mainly through uptake by plant stomata and soil (JACOB and WOFYSY, 1990). Consequently, sources and sinks of reactive trace gases are influenced by vegetation canopies and canopy interactions provide a main link between surface emissions and the atmospheric burden of e.g., NO_x .

Global atmospheric chemistry and transport models account for this by applying NO_x canopy reduction factors for different canopy types (e.g., YIENGER and LEVY, 1995). However, these estimates are based on only one single experiment in the Amazon Basin (BAKWIN et al., 1990) and the subsequent model analysis (JACOB and WOFYSY, 1990). Thereafter, these were empirically adapted to other canopies (e.g., YIENGER and LEVY, 1995). As the canopy structure determines the in-canopy turbulence attenuation, a highly critical factor for chemical flux divergence and, thus, the canopy reduction itself, such an adaption to other canopies of substantial structural difference might be invalid. For instance, forests hold the bulk leaf area index in the upper canopy, which is fundamentally different in grassland canopies, where the bulk leaf area index is located near the soil (e.g., JÄGGI et al., 2006; RIPLEY and REDMAN, 1976). Furthermore, mean distances between plant elements of only some millimeters (AYLOR et al., 1993) reflect the enormous density within the lower part of grassland canopies. The great importance of grasslands as land cover class is demonstrated by the terrestrial land surface coverage of globally 41 % and Europe-wide 19 % (KASANKO et al., 2011; SUTTIE et al., 2005), emphasizing the relevance for atmospheric budgets of NO_x . In comparison to forests, the number of experiments carried out on in-canopy processes of grasslands is very low. Although, the lack of experimental data on NO_x canopy reduction is known for decades, only minor progress has been made to improve measurement methods and experimental strategies. Nevertheless, improvements in this topic are crucial to derive also modeling schemes. These may help to characterize and quantify turbulence-chemistry interactions and to incorporate in-canopy processes, the influence of the canopy structure and turbulence in global chemistry and transport models (GANZVELD et al., 2002a; GANZVELD et al., 2002b).

1.1 Objectives of this thesis

The motivation of this PhD thesis was the investigation of the NO-NO₂-O₃ exchange at a natural grassland ecosystem. Certain aspects of this topic were individually addressed before but a specific study on exchange and chemistry considering the entire NO-NO₂-O₃ triad above and within a grassland canopy is still lacking. Both, the vast global terrestrial coverage of grasslands as well as the importance of the NO-NO₂-O₃ triad for ozone production, the oxidizing capacity of the atmosphere and the functioning of ecosystems underline the need for an experimental investigation on this topic. The investigation of turbulence-chemistry and plant canopy interactions such as NO_x canopy reduction or chemical flux divergences within and above a grassland canopy necessitated the conduction of an intensive field campaign using appropriate instrumentation.

This kind of research requires information on characteristic timescales of processes involved for different layers within and above the canopy. Beside knowledge on the chemical timescales, which can be addressed by the kinetics of the respective chemical reactions of the participating reactants, transport times are crucial to evaluate potential flux divergences. Common micrometeorological approaches can be used for the quantification of transport times. However, experimental difficulties in dense plant canopies such as grasslands can complicate associated measurements. For instance, the obstruction of ultra-sonic anemometer pathways by grass blades must be avoided (e.g., NEMITZ et al., 2009). An alternative method according to LEHMANN et al. (1999) uses vertical profiles of Thoron (Tn), a radioactive isotope of the noble gas radon (Rn), for the direct quantification of average transport times. This technique was applied in some studies before (e.g., GUT et al., 2002b; HENS, 2009; LEHMANN et al., 1999; NEMITZ et al., 2009). However, all of these studies derived the vertical Tn profiles from non-simultaneous measurements using instruments that were non-selective for Tn, which presumably caused large measurement errors (NEMITZ et al., 2009). This highlights the need for an advanced setup that can be used to derive reliable transport characteristics of grassland canopies such as in-canopy transport times and aerodynamic resistances prerequisite to the investigation on turbulence-chemistry interactions.

Eddy covariance requires fast instruments which are not always available. In the absence of such instruments, alternative flux measurement techniques are required in order to increase the flux data coverage of important trace gases such as the NO-NO₂-O₃ triad. Chamber based methods are typically used for the determination of emission fluxes (e.g., BOURTSOUKIDIS et al., 2012; GUT et al., 2002b). Due to experimental difficulties (for details see PAPE et al., 2009) they have only seldom been used for flux measurements of depositing compounds such as O₃. Nevertheless, chamber systems that are designed for long-term measurements of NO

soil emissions, often operate NO₂ and O₃ instruments simultaneously for reasons of chemistry corrections (e.g., PAPE et al., 2009). Such a system could constitute a flux measurement alternative for depositing compounds at low vegetation ecosystems, if these experimental difficulties can be overcome. In this way the O₃ flux data coverage could be increased.

Accordingly, the objectives of this thesis can be summarized as follows:

- (1) provision of reliable tools for the measurement of required quantities:
 - (i) development and evaluation of a selective thoron profile system for the direct quantification of in-canopy transport characteristics such as transport times and aerodynamic resistances (treated in PLAKE and TREBS (2013, Appendix B));
 - (ii) technical advancement and validation of a dynamic chamber system for the measurement of exchange fluxes of depositing compounds such as O₃ on low canopy ecosystems (treated in PLAKE et al. (2014b, Appendix C))
- (2) determination of the impact of turbulence-chemistry interactions for the exchange of the NO-NO₂-O₃ triad above and within a natural grassland canopy under different meteorological and air pollutant conditions (treated in PLAKE et al. (2014a, Appendix D))
- (3) quantification and characterization of NO_x canopy reduction and chemical flux divergence of O₃ at a natural grassland site (treated in PLAKE et al. (2014a, Appendix D))

2 Experimental

2.1 Site description

The results presented in this thesis were obtained during an intensive field experiment, aiming at the surface-atmosphere exchange of reactive trace gases at a natural grassland site. It took place from July to October 2011 at the estate of the Mainz-Finthen Airport near to the Rhine-Main city region in Rhineland-Palatinate, Germany (Fig. 2.1). The small airport was predominantly used by sports airplanes. The site was situated about 9 km south-west of the city center of Mainz and topographically located on a plateau 150 m above the Rhine valley. Small villages and motorways surrounded the site in a distance of 2 to 6 km and 4 to 15 km, respectively. The land use of the adjacent area was mainly agricultural, characterized by vineyards, orchards and crops. In south-western direction the fetch was largest without significant anthropogenic pollution sources.

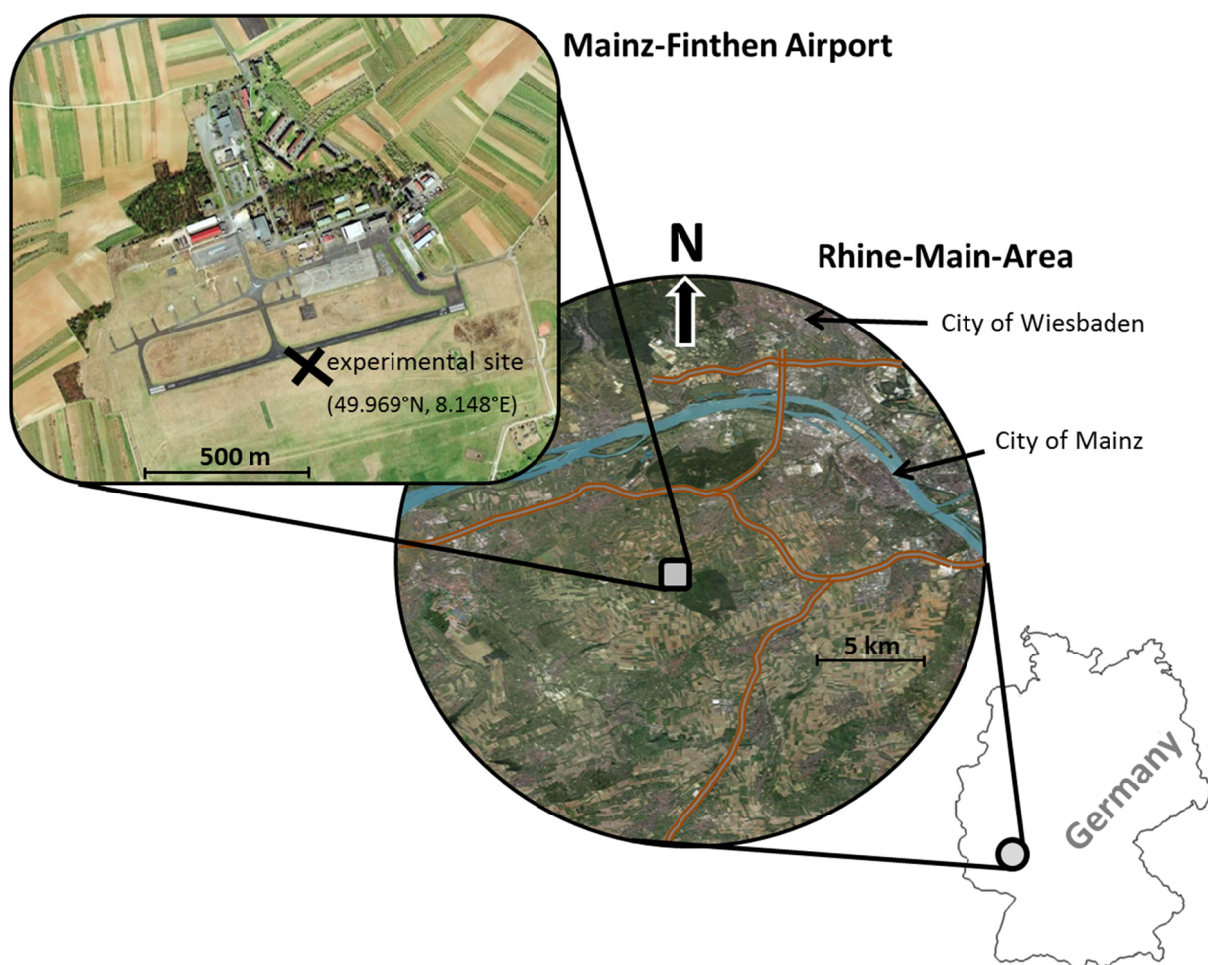


Fig. 2.1. Location of the experimental site on the estate of the Mainz-Finthen-Airport in vicinity of the cities of Mainz and Wiesbaden within the Rhine-Main-Area, Germany. The course of nearby motorways is indicated.

The vegetation canopy at the site constituted a steppe-like natural grassland ecosystem (cf. Fig. 2.2a), categorized as false oat-grass (*Arrhenatherion elatioris*) plant community and covering an area of 0.7 x 2.0 km (predominately extending from east to west). The mean canopy height (h_c) was 0.6 m. The total leaf area index (LAI) (green and brown leaves) was $4.8 \text{ m}^2 \text{ m}^{-2}$ (unit henceforth omitted), which is relatively low compared to intensively managed grasslands. The vertical LAI profile (Fig. 2.2b) indicated a high biomass density in the lower canopy layer below 0.2 m, which is typical for natural grasslands. 85 % of the total LAI was located here. The canopy was characterized by a proportion of about 40 % senescent or dead leaves. In the past, parts of the site were occasionally subject to management activities such as sheep grazing or scrub clearance. The soil was dry and sandy, exhibiting only low nutrient supply to the vegetation of $\sim 0.7 \text{ mg kg}^{-1}$ soil nitrate and $\sim 20 \text{ mg kg}^{-1}$ ammonium in the upper 5 cm (OSWALD et al., 2013).

2.2 Experimental setup

Prior to the field experiment, an extended period of time was devoted to developmental engineering of basically two major measurement systems that constituted the basis of this thesis (see Fig. 2.3): (i) the novel vertical thoron (Tn) profile system and (ii) the combined vertical near surface profile and dynamic chamber system for reactive trace gases. The first system was planned, piece by piece constructed based on accompanying laboratory tests and programming, until it was finally set into operation. The second system is an extension of an already existing dynamic chamber system, which was combined with a vertical trace gas profile. Beside the essential hardware modification for this system, the sampling schedule was

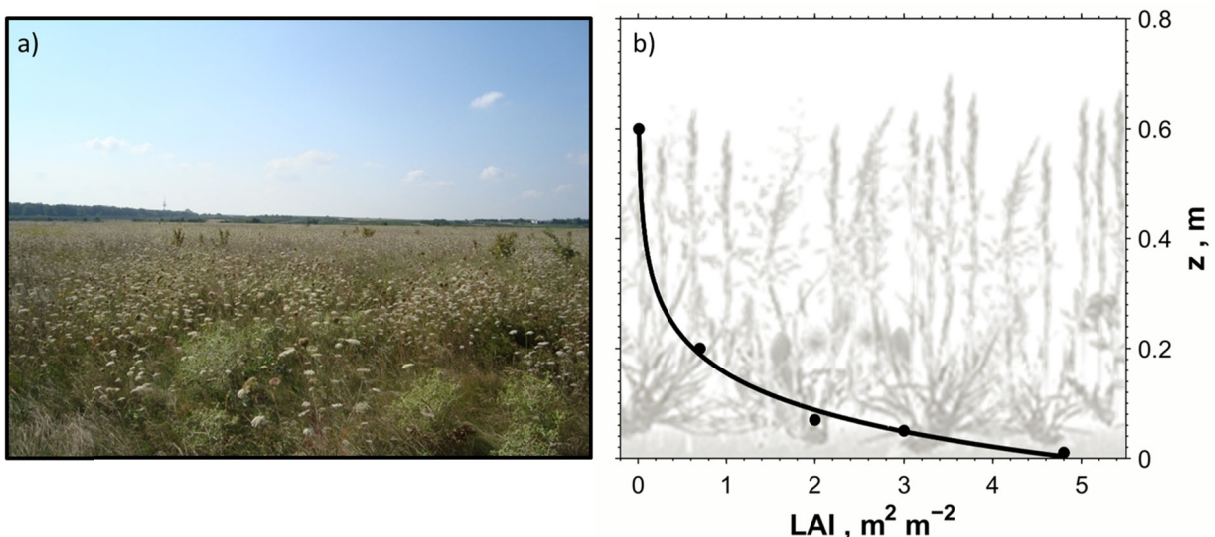


Fig. 2.2. (a) Photograph of the steppe-like grassland canopy at the Mainz-Finthen site; (b) vertical leaf area index (LAI) profile within the canopy, (b) taken from PLAKE et al. (2014b, Appendix C), modified.

restructured based on response time tests, and the automation of the entire system was achieved by programming flexible and reliable software.

The novel Tn profile system was designed to attain information on in-canopy transport, such as transport times. Gaseous Tn is an isotope of the noble gas radon (Rn) and is known to be soil-emitted and not to be taken up by plants. The only atmospheric removal process of Tn is radioactive decay at a half-life time of 55.6 s (decay rate $\lambda = 0.0125 \text{ s}^{-1}$). This implies that under the assumption of homogeneous soil emissions the vertical profile of Tn contains information on the average characteristic time of transport. Thus, bulk average transport times (τ_{tr} in s) between a lower (z_l) and an upper measurement height (z_u) can be directly derived by the vertical Tn concentration (C_{Tn} in Bq m^{-3}) profile (LEHMANN et al., 1999) as:

$$\tau_{tr} = \ln \left[\frac{C_{Tn_{z_l}}}{C_{Tn_{z_u}}} \right] / \lambda \quad (1)$$

The technique is henceforth abbreviated as Tn tracer technique. The novel Tn profile system was operated during the experiment by using simultaneously three Tn analyzers at three heights ($z_1 - z_3$). Further details on the Tn tracer technique and the measurement setup are given in PLAKE and TREBS (2013, Appendix B).

The near surface profile and the dynamic chamber system were combined in order to determine fluxes of the NO-NO₂-O₃ triad and additionally of CO₂ and H₂O through the soil-atmosphere interface and to simultaneously yield information on the corresponding vertical distribution. A dynamic chamber covers a specific soil area (A in m^2). A flow of ambient air through the dynamic chamber headspace (Q in $\text{m}^3 \text{ s}^{-1}$) allows the achievement of a steady state between the corresponding mixing ratios in- (μ_{IN}) and outside of the chamber (μ_{OUT} both e.g., in ppb). The flux (F_{CH} e.g., in $\text{nmol m}^{-2} \text{ s}^{-1}$) is basically a function of the mixing ratio difference (PAPE et al., 2009):

$$F_{CH} = \frac{Q}{A} \cdot \rho_d \cdot [\mu_{OUT} - \mu_{IN}] \quad (2)$$

with ρ_d being the molar density of dry air (in mol m^{-3}). During the experiment three dynamic chambers and three inlet heights of the near surface profile system were operated simultaneously. One set of analyzers measured NO, NO₂, O₃, CO₂ and H₂O mixing ratios. The use of switching valves enabled the sequential sampling in- and outside the three chambers and at the three near surface profile inlets. Further details on the setup, flux and error calculation as well as on chemical corrections are given in PLAKE et al. (2014b, Appendix C).

An eddy covariance system was operated throughout the campaign as a reference for the CO_2 , H_2O and O_3 flux measurements as well as for deriving essential micrometeorological quantities such as friction velocity (u_*) or stability parameters (details given in PLAKE et al., 2014b, Appendix C). In addition, vertical profiles of temperature, relative humidity and wind speed were measured. Standard meteorology, global radiation and the NO_2 photolysis frequency were also recorded. All equipment was operated simultaneously for the data collection phase of the field experiment from 04 August to 26 September 2011.

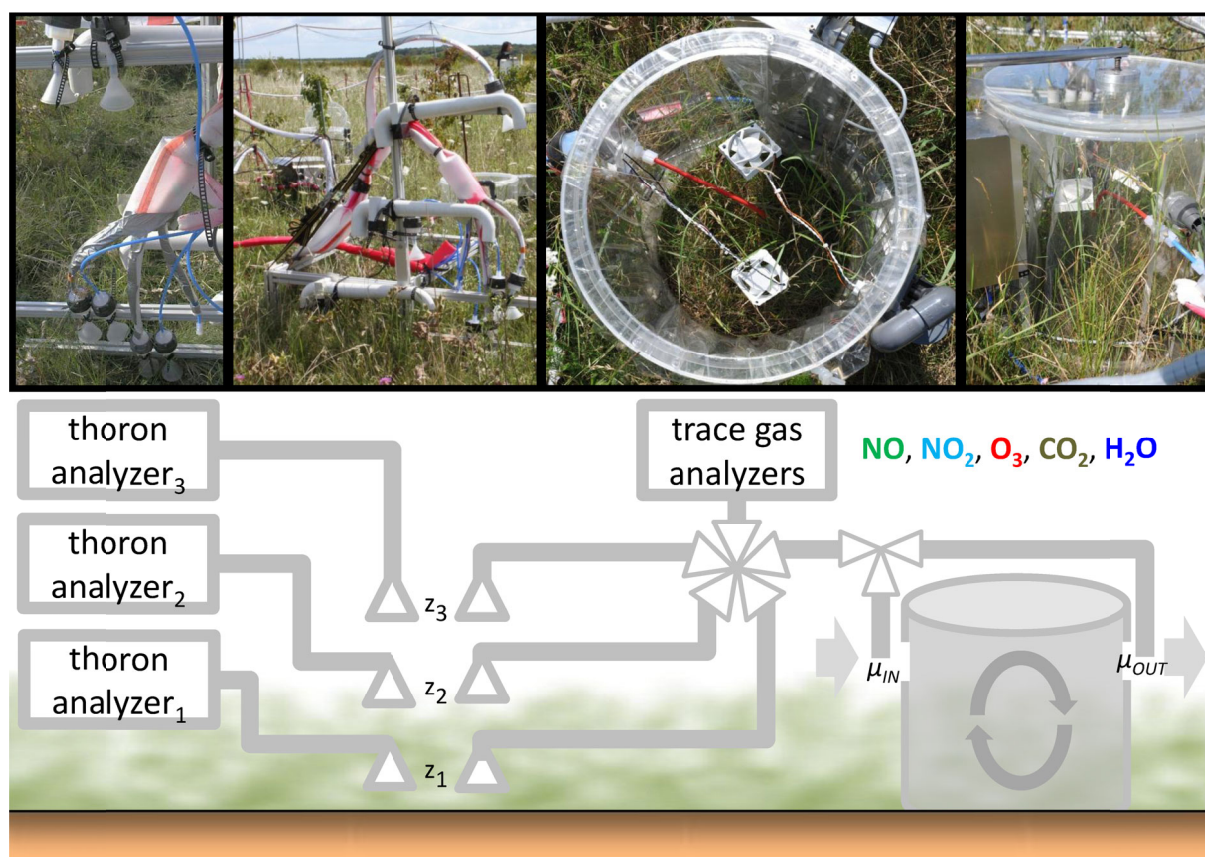


Fig. 2.3. Schematic sketch of the major measurement systems utilized in this study and their practical installation at the field site: (i) the novel vertical profile system for the simultaneous determination of thoron concentration at z_1 – z_3 using three individual analyzers; (ii) the combined near surface trace gas profile and dynamic chamber system for sequential sampling of three heights (z_1 – z_3) and the inlet (μ_{IN}) and outlet (μ_{OUT}) of three dynamic chambers using switching valves and one set of analyzers per gas (NO , NO_2 , O_3 , CO_2 and H_2O).

3 Results

3.1 Technical advancements

3.1.1 A novel automated thoron profile system

The concentrations of Tn were measured with three commercially available instruments (RAD7, DurrIDGE, Billerica, USA). The RAD7 uses a solid state alpha detector for alpha particle counting and electronic alpha spectrometry. A special feature of these instruments is their ability to distinguish Rn from Tn, which is very rare for currently available commercial Rn monitors. Thus, Tn concentrations in previous studies were typically measured using e.g. two non-selective Rn and Tn instruments in series. The first instrument measured the sum of Tn and Rn, the isotope separation was made by a defined Tn decay volume installed between both instruments, and the Tn concentration was then obtained by subtraction of the Rn signal (instrument 2) from the sum of Tn and Rn (instrument 1) (e.g., GUT et al., 2002b; HENS, 2009; LEHMANN et al., 1999; NEMITZ et al., 2009). Furthermore, vertical Tn profiles were obtained with such systems by sequential sampling at different heights using switching valves, which resulted in additional uncertainties due to potential non-stationarities. In contrast, the novel system developed for this study and presented in PLAKE and TREBS (2013, Appendix B) provides simultaneously measured vertical Tn profiles using Tn selective instruments, thus minimizing potential error sources. In addition, the remaining systematic and random errors of the Tn concentration readings were carefully quantified and propagated to yield the uncertainty of the determined transport times, which was never reported by any previous study before.

The precondition of relative humidity of $< 10\%$ within the Tn instruments was excellently achieved throughout the campaign by actively drying each sample-air flow (2 L min^{-1}) using Nafion dryers (Perma Pure, Toms River, USA). Each instrument's Tn sensitivity was verified against the world's first primary standard for Tn activity concentration in air at the Physikalisch-Technische Bundesanstalt (PTB, Braunschweig, Germany). For the first time a rigorous determination of systematic and random errors of the Tn concentration readings was performed for this type of measurement system under field conditions. Beside low systematic errors among the three instruments ($\leq 3\%$), the obtained median precisions for three concentration classes (> 100 , $100\text{--}15$ and $< 15\text{ Bq m}^{-3}$) were 8.8, 23.2 and 132.1 % for Tn. The individual errors of the Tn concentration measurements were propagated to determine the uncertainty of the transport times (τ_{tr}). During 51 measurement days, 44 % of the transport times showed a good data quality with relative uncertainties below 50 %. In contrast, only

22 % of all determined transport times exhibited uncertainties higher than 100 %, caused by absolute T_n gradients lower than $70 \text{ Bq m}^{-3} \text{ m}^{-1}$.

3.1.2 Ozone fluxes measured with the dynamic chamber technique

The sophisticated dynamic chamber system for the determination of emission fluxes presented in PAPE et al. (2009) was a base for this study. A substantial further optimization of the hardware setup and the sampling cycle led to an achievement of the following goals: (i) decreasing the likelihood of non-stationary events during a single chamber measurement, (ii) improving the time resolution for flux determination, (iii) ensuring representative rainfall amounts and soil moisture in the chambers by long open phases during 90 % of the day (iv) gaining simultaneous information on the vertical distribution of the investigated trace gases and (v) eliminating water vapor interferences on the measurements of NO (MATTHEWS et al., 1977) and O_3 (WILSON and BIRKS, 2006) mixing ratios. Details on the system are given in PLAKE et al. (2014b, Appendix C). PAPE et al. (2009) provided the essential correction to account for gas-phase chemical reactions of the NO-NO₂-O₃ triad within the dynamic chamber (*CH*) headspace. The *CH* fluxes corrected for gas-phase chemistry are henceforth referred to as CH_{gp} .

The application of a dynamic chamber leads to a modification of the aerodynamic and diffusive transport, which results in altered trace gas mixing ratios within the *CH* headspace. This is of minor importance for quantifying fluxes of soil-emitted compounds, such as NO, because the emission flux is hardly influenced by (moderate) changes in the aboveground gas concentration and environmental conditions. However, for deposited trace gases, such as O_3 , the modification of the turbulent resistive scheme is highly relevant as the deposition flux depends on the mixing ratio and is often limited by the turbulent transport. Thus, for a reliable quantification of deposition fluxes using the *CH* method, a modified resistive scheme has to be quantified and corrected for. In this study, a corresponding correction presented by PAPE et al. (2009) was applied. The canopy height h_c at the Mainz-Finthen grassland site slightly exceeded the *CH* height (0.43 m), which did not affect the undisturbed *CH* closure as the uppermost canopy was characterized by sparse grass spandices. However, in contrast to PAPE et al. (2009), this resulted in significantly differing O_3 mixing ratios at the height of the *CH* inlet (0.2 m) compared to the above-canopy reference height (3.0 m). Consequently, the correction equation given in PAPE et al. (2009) was extended by the ratio of the corresponding O_3 mixing ratios (for details see PLAKE et al. (2014b, Appendix C)). The finally corrected *CH* flux is henceforth referred to as CH_{cor} .

Eddy covariance (*EC*), the state-of-the-art flux measurement technique, was chosen as reference to validate the derived O_3 deposition fluxes by the *CH* method. Prerequisites for a mean-

ingful O_3 flux comparison were (i) similar vegetation structure and activity within (ii) the mostly overlapping footprints of both methods. Good daytime agreements of the independently derived CO_2 and H_2O fluxes (deviations by only 10 and 1 %, respectively) and of the canopy resistance to O_3 (deviation by 25 %) supported the assumption of a comparable vegetation structure. Finally, a footprint analysis (cf., PLAKE et al., 2014b, Appendix C) confirmed all prerequisites to be fulfilled.

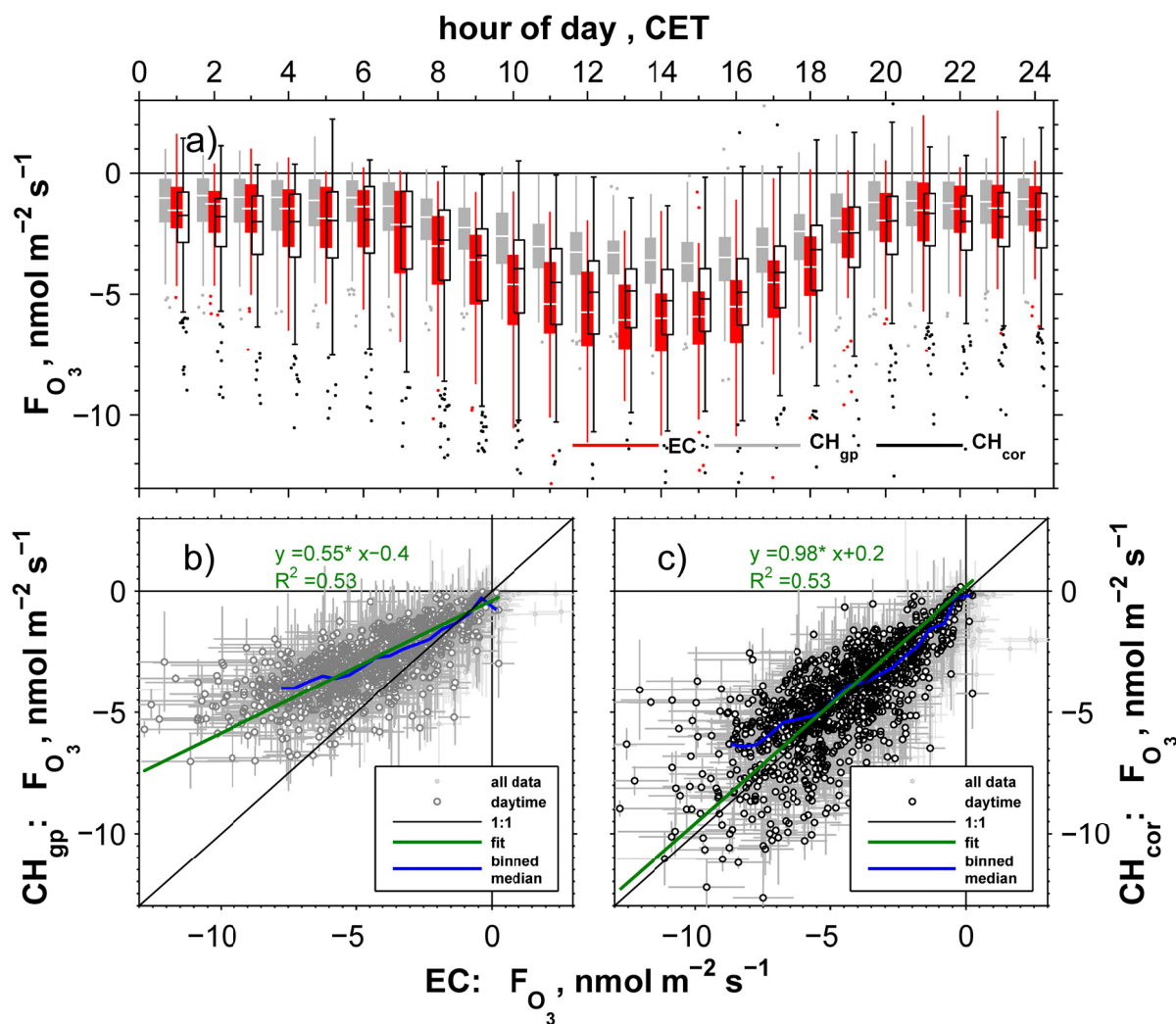


Fig. 3.1. Comparison of O_3 fluxes determined by the eddy covariance (EC) and the dynamic chamber (CH) methods presented as (a) diurnal cycles using hourly box plot statistics and (b)–(c) scatter plots. All data from 04 August–26 September 2011 are included. Daytime values refer to global radiation $> 10\ W\ m^{-2}$. O_3 fluxes determined by the CH method are shown in (b) as only gas-phase chemistry-corrected (CH_{gp}) and in (c) as finally corrected (CH_{cor}). The bivariate weighted least-squares fitting by the Williamson-York method (CANTRELL, 2008) was used for the regression analysis. A binned median illustrates deviations from the fit. Figure taken from PLAKE et al. (2014b, Appendix C)

The subsequent O₃ flux comparison revealed an obvious underestimation of the O₃ flux by the *CH* method when only corrected for gas-phase chemistry (CH_{gp}) as shown in the diurnal course and the scatter plot (Fig. 3.1a,b). However, the *CH* method's capability of determining representative O₃ fluxes could be clearly demonstrated when comparing the finally corrected *CH* flux (CH_{cor}) with the *EC* method. The diurnal courses of both corresponding O₃ fluxes (Fig. 3.1a) are characterized by widely overlapping interquartile boxes. Also, the bivariate fit in the corresponding scatter plot (Fig. 3.1c) underlines the good conformity. On average, the deviation between both methods was quantified to be only 11 % during daytime. Beside the good agreement of the overall O₃ flux data set PLAKE et al. (2014b, Appendix C) have also shown that the advanced setup of the *CH* system enables the determination of reliable O₃ fluxes even for 30 min averaging intervals. Furthermore, they found the relative O₃ flux error of the *CH* method below 25 % with u_* being higher than 0.22 m s⁻¹. The median O₃ flux error of the *CH* method throughout the campaign was 32 % during daytime and 58 % during nighttime.

3.2 Scientific advancements

3.2.1 In-canopy transport

Aerodynamic resistances (R_a) are important input parameters for modeling studies on surface-atmosphere exchange fluxes. They represent transport times through a layer, normalized by the layer thickness ($R_a = \tau_{tr}/\Delta z$). When the thicknesses of two layers under consideration differ, the effectiveness of transport can be represented by the corresponding aerodynamic resistances. On the other hand, transport times are required to evaluate the influence of chemical reactions on fluxes (e.g., Damköhler numbers see Sect. 3.2.2).

Aerodynamic in-canopy resistances (R_{ac}) are typically parameterized as a function of u_* and LAI (e.g., PERSONNE et al., 2009; VAN PUL and JACOBS, 1994). These parameterizations are based on experiments above e.g., crops such as maize (VAN PUL and JACOBS, 1994) and consider a vertically homogeneous leaf distribution (PERSONNE et al., 2009). However, this approximation may differ substantially within grassland canopies, as their structure is characterized by high biomass density in the lowest layer (cf. Fig. 2.2b).

The great advantage of the Tn tracer technique is the direct assessment of measured R_{ac} values for various layers, which are presented in Fig. 3.2 as diurnal courses. The vertical R_{ac} profile indicated a strongly decreasing aerodynamic transport efficiency with height. For instance, during daytime R_{ac} in the lowest canopy layer was found two orders of magnitude and during nighttime one order of magnitude higher than R_a in the layer above the canopy. Furthermore, R_{ac} in the lower canopy exhibited an inversed diurnal course (highest during daytime, lowest during nighttime) compared to the aerodynamic resistances in the upper canopy or above it. The inversed diurnal courses were caused by the analogously inverted stability conditions in the corresponding layers. These are visualized by vertical temperature profiles in Fig. 3.3, which indicate temperature inversions during both day and nighttime. During daytime the upper canopy and the above-canopy layer were characterized by unstable stratification, as the main turnover of short wave radiation into heat took place around the upper end of the lower canopy layer. The lower canopy layer instead showed stable stratification, as the air in the lower canopy was cooled by heat dissipation towards the soil. During nighttime longwave upwelling radiation cooled the upper canopy yielding lowest temperatures around the upper end of the lower canopy layer and a stable stratification above, whereas within the lower canopy the release of upward thermal plumes originating from the warmer soil body resulted in convective transport and, thus, unstable stratification. Before, the resulting partial canopy decoupling was only observed for differently structured canopies such as forests (e.g., KRUIJT et al., 2000) or crops (e.g., JACOBS et al., 1994; NEMITZ et al., 2000). The magnitude and the diurnal course of R_{ac} in the lower grassland canopy were astonishingly comparable to

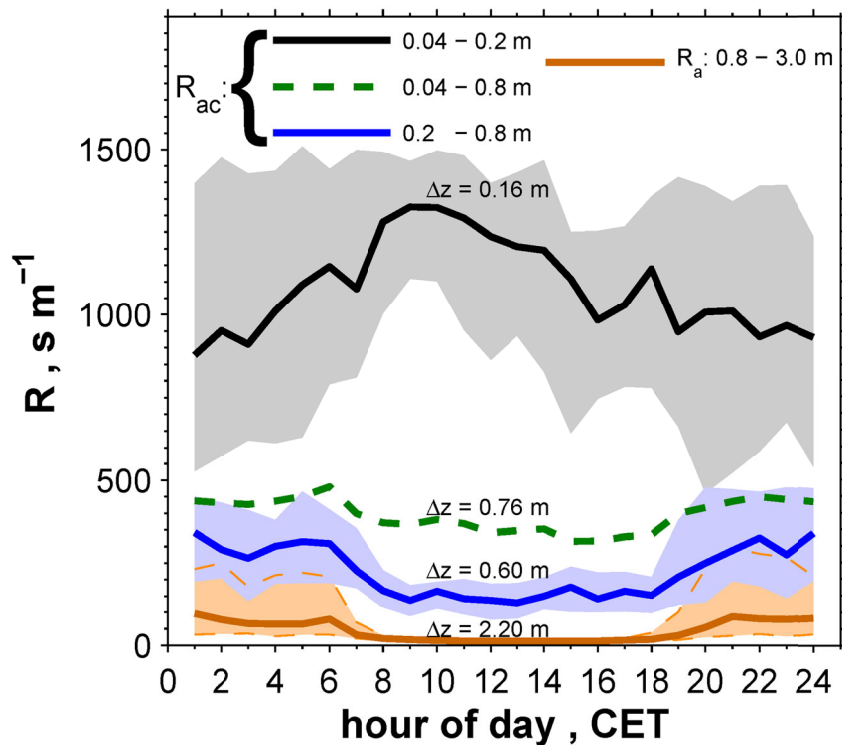


Fig. 3.2. Diurnal courses of in-canopy aerodynamic resistances (R_{ac}) for individual layers: lower canopy (0.04–0.2 m), upper canopy (0.2–0.8 m), whole canopy (0.04–0.8 m) at the Mainz-Finthen grassland site (median and shaded interquartile ranges). For comparison, the aerodynamic resistance above the canopy (R_a : 0.8–3.0 m) is also displayed. The layer thickness (Δz) is indicated. The plot includes all data from 19 August until 26 September 2011. Figure taken from PLAKE et al. (2014a, Appendix D), modified.

R_{ac} values given in literature for the lowest meter of Amazonian rain forest (GUT et al., 2002a). The inversed diurnal course of R_{ac} in the lower and upper canopy resulted in a rather small diurnal variation of R_{ac} representing the whole canopy, which again was found to be analogous within an Amazonian rain forest canopy (SIMON et al., 2005).

A literature comparison revealed the R_{ac} representing the whole grassland canopy being at least 3–4 times higher than corresponding values for forests (cf. PLAKE et al., 2014a, Appendix D). In other words, the transport efficiency was found to be at least 3–4 times higher in forest canopies, which is mainly due to the high biomass density in the lower grassland canopy. Accordingly, PLAKE et al. (2014a, Appendix D) found that corresponding transport times through the whole canopy (canopy flushing times) can be longer by 400 % in grassland canopies than in forests. This is astonishing as the height of grassland canopies is small compared to forest (h_c of grasslands only around 1–10 % compared to h_c of forests). In addition, they found that canopy flushing times of grasslands can also be shorter than those of forests.

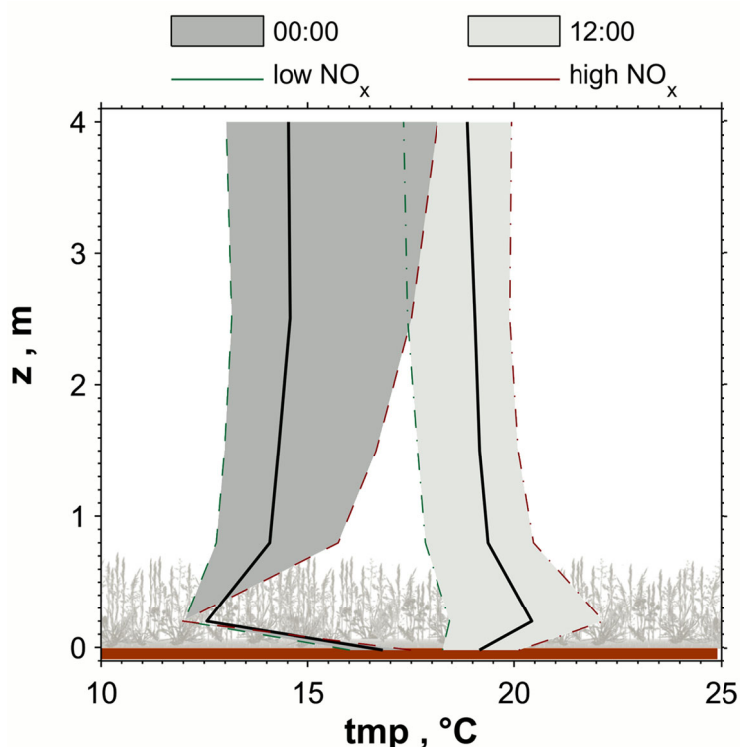


Fig. 3.3. Median vertical temperature profiles representing the thermal stratification at 00:00 and 12:00 CET considering data from 19 August to 26 September 2011 (black lines) at the Mainz-Finthen grassland site. Also the respective thermal stratification during high and low NO_x periods (explained in Sect. 3.2.2) is presented. Figure taken from PLAKE et al. (2014a, Appendix D), modified.

For instance, this may be the case when grassland, which is relatively sparse in the lower canopy, is compared to a dense and tall forest.

PLAKE and TREBS (2013, Appendix B) compared the directly measured canopy flushing times with the parameterizations of VAN PUL and JACOBS (1994) and PERSONNE et al. (2009), that are frequently used in modeling studies. The measured canopy flushing times revealed the lowest scatter. None of the parameterizations was able to reproduce the entire diurnal course of the in-canopy transport. An agreement with the measured canopy flushing times was either found during daytime (PERSONNE et al., 2009) or nighttime (VAN PUL and JACOBS, 1994), underlining the value of the direct in-canopy transport measurements and the need for more experimental confirmation of such empirical parameterizations.

3.2.2 Timescales of transport and chemistry

The particular air chemical situation at the site was strongly related to the prevailing meteorological conditions. Winds from a south western direction of high wind speed ($> 3 \text{ m s}^{-1}$) were connected to relatively low NO_x levels ($< 5 \text{ ppb}$) indicating minor anthropogenic impact.

Contrastingly, winds from the north eastern sector were characterized by low wind speed ($< 3 \text{ m s}^{-1}$) and relatively high NO_x levels ($> 5 \text{ ppb}$). In order to gain insights on transport-chemistry interactions under contrasting meteorological and air chemical conditions, eleven and nine days were identified by specific criteria as low and high NO_x periods, respectively. These were separately analyzed for the entire data set (for details see PLAKE et al., 2014a, Appendix D).

The higher wind speed prevailing during day and nighttime of the low NO_x periods yielded low vertical differences in temperature (cf. Fig. 3.3) and trace gases (cf. PLAKE et al., 2014a, Appendix D). In contrast, the nighttime of the high NO_x periods was characterized by extraordinary stable stratification in the upper canopy and above forming a “canopy lid” (median temperature difference 4.0–0.2 m: 6 K). Under these conditions mixing ratios of exclusively depositing compounds such as O_3 were as low as 1 ppb in the lower canopy, whereas exclusively emitted compounds such as Rn were trapped within the canopy and showed strongly enhanced concentrations. In contrast, the simultaneous NO mixing ratios in the lower canopy were only weakly enhanced, suggesting rather low NO soil emissions, which was in accordance with the results of the dynamic chamber technique that detected insignificant NO soil emissions (cf. PLAKE et al., 2014b, Appendix C). The daytime conditions of the high NO_x periods were characterized by distinctly enhanced NO_x mixing ratios during the morning hours, a diurnal O_3 maximum in the afternoon (for both see PLAKE et al. (2014a, Appendix D)) and pronounced unstable stratification during daytime (cf. Fig. 3.3).

The ratio of the transport time and the chemical timescale (τ_{ch}) for the NO- NO_2 - O_3 triad (LENSCHOW, 1982), the so-called Damköhler number ($DA = \tau_{tr}/\tau_{ch}$), is used as an indicator for potential chemical divergence (e.g., STELLA et al., 2013a). Typically, Damköhler numbers equal to unity or above indicate a strong potential chemical divergence. When Damköhler numbers are smaller than 0.1, chemical reactions are considered of minor importance, whereas within the critical range between unity and 0.1, a chemical divergence cannot be excluded. For the first time PLAKE et al. (2014a, Appendix D) derived transport times, chemical timescales and Damköhler numbers from measurements individually for the lower and the upper canopy and the above-canopy layer as given in Fig. 3.4.

During daytime the chemical timescale showed a weak vertical profile with lowest values above the canopy and highest values in the lower canopy. The chemical timescales between the low and high NO_x periods only slightly differed. During daytime the transport times were found equally fast as the chemical timescales in the lower canopy, somewhat faster in the upper canopy and around two to five times faster in the above-canopy layer. The fastest transport above the canopy occurred during the low NO_x periods due to the higher wind speed, whereas the transport in the lowest canopy layer interestingly showed the opposite

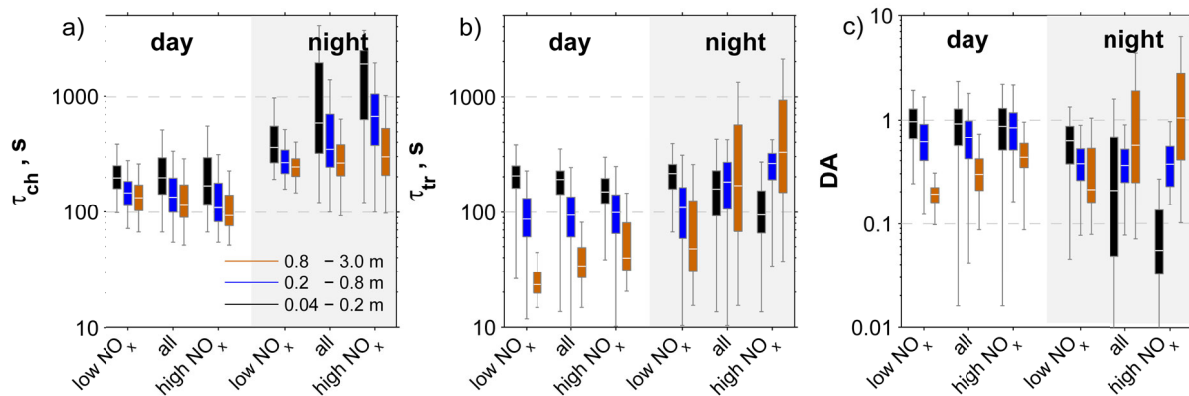


Fig. 3.4. Comparison of box plot statistics for chemical timescales (τ_{ch}), transport times (τ_{tr}) and Damköhler numbers ($DA = \tau_{tr}/\tau_{ch}$) within the lower canopy (0.04–0.2 m), the upper canopy (0.2–0.8 m) and the above-canopy layer (0.8–3.0 m) during daytime and nighttime including all data from 19 August until 26 September 2011 separated for the low and high NO_x periods at the Mainz-Finthen grassland site. Figure taken from PLAKE et al. (2014a, Appendix D).

trend due to the thermal stratification (cf. Sect. 3.2.1). Consequently, the daytime Damköhler numbers indicated the highest likelihood for chemical divergence in the lower canopy, followed by the upper canopy and the above-canopy layer. The likelihood for chemical divergence was lowest above the canopy during the low NO_x periods.

During nighttime the vertical profile of the chemical timescale showed the same pattern as during daytime but quantitatively shifted upwards resulting in much higher values. This was especially pronounced for the lower canopy during the high NO_x periods, where the chemical timescale was one order of magnitude higher than during daytime, caused by the very low mixing ratios of NO , NO_2 and O_3 in this layer (cf. PLAKE et al. (2014a, Appendix D)). During nighttime the above-canopy and lower canopy transport times showed the same reversed dependency on the wind speed but even stronger pronounced. In this context, a rather unexpected pattern was the faster transport time in the lower canopy than in the above-canopy layer during the highly stable nights of the high NO_x periods. Thus, the vertical profile of Damköhler numbers was inverted during nighttime of the high NO_x periods. Above the canopy equally fast timescales of chemistry and transport indicated potential chemical divergence. In contrast, the twenty times faster timescale of transport compared to chemistry in the lower canopy resulted in the only instance within the entire data set, in which Damköhler numbers clearly indicated no potential chemical divergence. This finding agrees very well with RUMMEL (2005) who found at nighttime the transport timescale in the lowest layer of an Amazonian rainforest to be faster than the chemical timescale.

Nevertheless, it should be noted that Damköhler numbers within plant canopies are not fully representative for all processes, since besides transport and chemistry, additional sources and sinks for trace gases exist within plant canopies. These are specific for each trace gas and will be discussed in the next sections.

3.2.3 Canopy reduction of nitric oxides within a natural grassland canopy

Due to the insignificant NO soil emissions at the Mainz-Finthen experiment site, potential NO_x canopy reduction could unfortunately not be directly quantified. The unique data set of this study was nevertheless used to derive more general conclusions on NO_x canopy reduction within natural grassland canopies by comparing the derived timescales of transport and chemistry with the characteristic timescale of NO₂ uptake by the plant canopy. The timescale of NO₂ plant uptake ($\tau_u(NO_2)$) integrated over the whole canopy was estimated based on a resistance model (BALDOCCHI, 1988) following an approach of RUMMEL (2005) and is presented in Fig. 3.5 (for details see PLAKE et al. (2014a, Appendix D)).

During daytime the timescale of NO₂ plant uptake was typically the shortest amongst all timescales relevant for NO₂ closely followed by the chemical timescale. Thus, for a similar canopy with significant NO soil emissions, this would imply an efficient in-canopy conversion of NO to NO₂ during daytime, followed by an effective NO₂ plant uptake as the transport was found to be 2-3 times slower. The high biomass density in the lower canopy (cf. Fig. 2.2b) dampens the photolysis of NO₂ at the soil-canopy interface. Furthermore, the stable stratification during daytime (cf. Fig. 3.3) strongly inhibits the aerodynamic transport at the soil-canopy interface (cf. Fig. 3.4b). Altogether, this indicates strong NO_x canopy reduction occurring during daytime in such grassland ecosystems, if the precondition of significant NO soil emissions is fulfilled.

However, during nighttime the timescale of NO₂ plant uptake was found to be very large. Hence, the role of turbulence-chemistry interactions (Damköhler number) was dominating over biological uptake processes and, thus, determined the fate of potentially soil-emitted NO. During rather windy nights (low NO_x periods) the Damköhler numbers indicated an efficient formation of NO₂ within the canopy which is due to (i) the sufficient supply of O₃ from above and (ii) the slowest transport occurring in the lower canopy under such conditions. Thus, such nighttime conditions would most likely favor simultaneous NO₂ and NO canopy emission fluxes. In contrast, during nights of low wind speed (high NO_x periods) the extremely stable stratified upper canopy leads to the breakdown of the O₃ supply from above (cf. Sect. 3.2.2). Within the canopy the reaction of residual O₃ and soil-emitted NO would compete with the O₃ surface deposition until the remaining O₃ almost entirely disappeared. Subsequently, a mixture of NO and NO₂ would be trapped inside the canopy. Besides some minor in-canopy NO₂

losses (see above), a distinct NO and NO₂ release may occur in the morning hours, as has been observed for forests (cf. DORSEY et al., 2004; FOKEN et al., 2012b; JACOB and WOFSY, 1990).

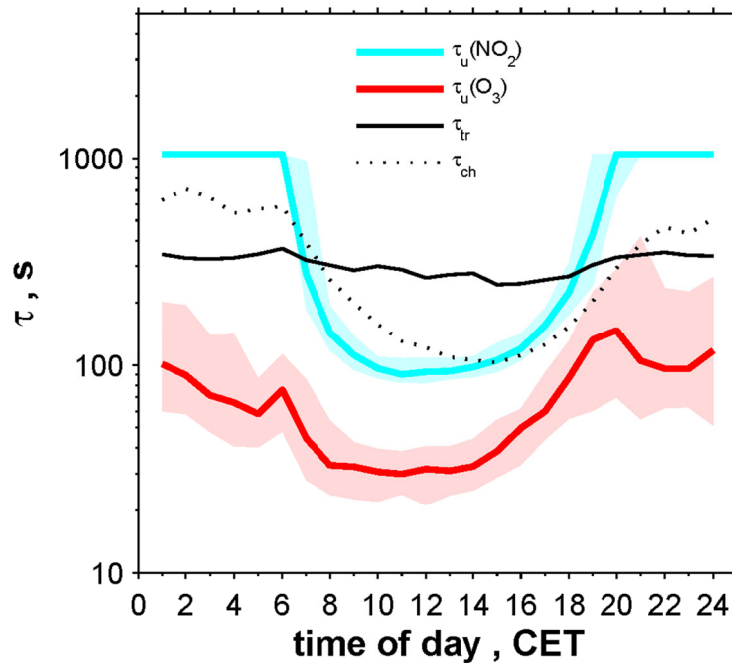


Fig. 3.5. Comparison of median diurnal timescales of plant uptake by the vegetation canopy ($\tau_u(NO_2)$, $\tau_u(O_3)$) with interquartile ranges, transport through the whole canopy (τ_{tr}) and the characteristic chemical timescale (τ_{ch}) within the canopy layer (0.04–0.8 m) considering all data from 19 August to 26 September 2011 at the Mainz-Finthen grassland site. Figure taken from PLAKE et al. (2014a, Appendix D).

3.2.4 Ozone fluxes at a natural grassland

The O₃ deposition fluxes determined during the late summer period at the nutrient poor natural grassland site using the *EC* method, ranged from -0.5 to -3 nmol m⁻² s⁻¹ (25th to 75th percentile boxes) during nighttime and from -2 to -7 nmol m⁻² s⁻¹ (maximal median: -6 nmol m⁻² s⁻¹) during daytime (see Fig. 3.3). In literature O₃ fluxes to grassland ecosystems are still not as abundant as those to forests or crops. However, considering available grassland studies, the Mainz-Finthen site was among those with relatively low O₃ deposition fluxes (cf. e.g., MASSMAN et al., 2000), which appears sensible due to the nutrient poor site characteristics and the rather high proportion of senescent dead leaves.

O₃ deposition towards terrestrial ecosystems occurs through various pathways depending on vegetation and soil characteristics that vary in space and time. Amongst these pathways are

plant stomatal uptake and also non-stomatal pathways, such as cuticular deposition or soil deposition. In this study the measured O_3 deposition flux by the *EC* method was partitioned into its stomatal and non-stomatal contribution (for details see PLAKE et al., 2014b, Appendix C). Daily averages of the stomatal and non-stomatal O_3 deposition fluxes were 27 and 73 %, respectively, revealing dominant O_3 deposition through the non-stomatal pathway throughout the day. Considering daytime only (global radiation $> 10 \text{ W m}^{-2}$) the average partitioning to the stomatal and non-stomatal pathways was almost equal with 47 and 53 %, respectively. Thus, the non-stomatal deposition was found the major O_3 deposition pathway at the natural grassland canopy, which is in contrast to other studies on intensively managed grassland and crop canopies (BASSIN et al., 2004; MESZAROS et al., 2009; STELLA et al., 2013b). However, the partitioning results are in line with LAMAUD et al. (2009) who found a strong relative humidity (*RH*) dependence of the stomatal and non-stomatal contribution. At a senescent maize crop, they found non-stomatal pathway for $RH > 60 \%$, but stomatal O_3 deposition for $RH < 60 \%$ to provide the dominating portion of the total O_3 deposition flux. They attributed this to (i) a decrease of stomatal conductance under high *RH* (e.g., EMBERSON et al., 2000) and (ii) to an increase in cuticular deposition with *RH* (e.g., ALTIMIR et al., 2006; 2004). Throughout the campaign in Mainz-Finthen the median diurnal *RH* just above the canopy ($z = 0.8 \text{ m}$) was only below 60 % for three hours per day, which elucidates the dominating non-stomatal O_3 deposition flux. In addition, two further arguments underline the non-stomatal dominance of the O_3 deposition: (i) several nights of high wind speeds that exhibited relatively high nighttime O_3 fluxes contributed entirely to the non-stomatal O_3 deposition and (ii) in contrast to intensively managed plots, a relative high proportion of biologically inactive brown leaf area ($> 40 \%$) prevailed at the unmanaged natural grassland, which did not contribute to stomatal O_3 uptake but to non-stomatal O_3 deposition. Chemical reactions of O_3 with e.g., soil-emitted NO or plant emitted volatile organic compounds (VOCs) that potentially also contribute significantly to the non-stomatal O_3 deposition pathway (e.g., KURPIUS and GOLDSTEIN, 2003). Nevertheless, at the Mainz-Finthen site these were unimportant due to the very low emissions of both NO from the soil and VOCs from the canopy (cf. PLAKE et al., 2014b, Appendix C).

3.2.5 Ozone flux divergence

Similar as for NO_2 (cf. Sect. 3.2.3), the application of in-canopy Damköhler numbers for O_3 can be problematic, as plant uptake and deposition to plant and soil surfaces constitute additional O_3 pathways besides chemistry (cf. Sect. 3.2.4). In this context, the timescale of O_3 plant uptake and soil deposition ($\tau_u(O_3)$) was estimated similarly as for NO_2 (for details see PLAKE et al. (2014a, Appendix D)) and compared to the transport times and the chemical timescale displayed in Fig. 3.5. The plant uptake and soil deposition of O_3 was found signifi-

cantly faster than chemistry or transport throughout the day. Thus, the comparison of the relevant timescales revealed that in-canopy Damköhler numbers were irrelevant for O₃. Nevertheless, this should not be taken as a general statement for grassland sites as for sites with strong NO soil emissions, such as intensively managed grasslands, the chemical timescale would be considerably lower and, thus, most likely partly comparable to the timescale of O₃ plant uptake and soil deposition.

The above-canopy Damköhler numbers were found within the critical range throughout the day and under all conditions (cf. Fig. 3.4c). Thus, a chemical divergence for O₃ could not be excluded and had to be further investigated in order to validate the measured O₃ deposition fluxes of the *EC* method (Sect. 3.2.4). Following a simplified approach by DUYZER et al. (1995), which only considers R1 and R3 and the measured fluxes of NO, NO₂ and O₃, the O₃ flux divergence was quantified to be less than 1 %. This was mainly due to the insignificant NO soil emissions at the site.

Nevertheless, regularly elevated NO mixing ratios during the morning hours, when the O₃ levels were still relatively low, led to small O₃/NO ratios, which raised the suspicion of a potential chemical impact on the O₃ fluxes (cf. PLAKE et al. (2014a, Appendix D)). Thus, a net chemically induced O₃ flux ($F_c(O_3)$) due to the simultaneous O₃ production ($P(O_3)$) by R1–R2 and O₃ loss ($L(O_3)$) by R3 was quantified as integral over the above-canopy layer according to RUMMEL et al. (2007) and is presented in Fig. 3.6. The resulting median net chemically induced O₃ flux ranged between 0.6 and -0.05 nmol m⁻² s⁻¹, representing a net O₃ production during daytime and a small net loss during nighttime. Thus, in median the O₃ flux was underestimated by 10 % during daytime and overestimated by 3 % during nighttime. The chemically induced O₃ flux was highly variable and one order of magnitude higher during the high NO_x than during the low NO_x periods. The O₃ production was due to a deviation from the NO-NO₂-O₃ photostationary state by a surplus of NO₂, based on NO oxidation by e.g. peroxy radicals or other oxidants. This finding is interesting as previous studies only reported O₃ losses when dealing with the chemical flux divergence of O₃. The net O₃ losses were caused by the outbalancing of the reactions of O₃ with NO (e.g., DORSEY et al., 2004) or VOCs (e.g., KURPIUS and GOLDSTEIN, 2003) emitted by soil or plants, respectively. However, the O₃ fluxes presented in Sect. 3.2.4 were not corrected for this process, since the method is prone to high uncertainties caused by (i) calculation of the net effect as a difference of two counteracting chemical reactions and (ii) not involving all chemical reactions important for O₃.

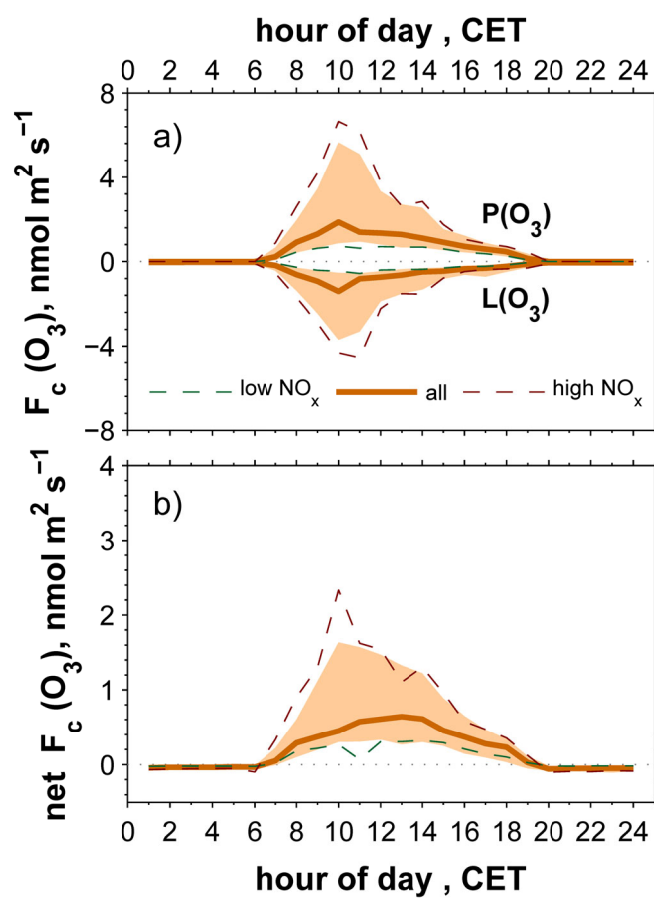


Fig. 3.6. Diurnal courses showing (a) photochemical O_3 production ($P(O_3)$) and chemical O_3 loss ($L(O_3)$) and (b) the net effect of both ($F_c(O_3)$) within the above-canopy layer (0.8–3.0 m) considering all data from 19 August to 26 September 2011 (medians and shaded interquartile ranges) and separated for the low and high NO_x periods (medians) at the Mainz-Finthen grassland site. Figure taken from PLAKE et al. (2014a, Appendix D).

4 Conclusions

The main findings of this study can be summarized as follows:

- (1) The careful development and thorough characterization of the novel automated Tn profile system by PLAKE and TREBS (2013, Appendix B) ensured good system performance and reliable results during a field campaign. For the first time vertical Tn profiles were measured simultaneously using Tn selective instruments. The Tn tracer technique allowed the direct quantification of transport characteristics such as transport times and aerodynamic resistances for various layers within a natural grassland canopy. Such transport characteristics are typically parameterized due to their difficult experimental accessibility. The directly measured canopy flushing times from the Tn tracer technique helped to discover the insufficiency of two commonly used empirical parameterizations in predicting correct values for grassland canopies throughout the entire diurnal course. The parameterizations only agreed either during day or during nighttime. The vast terrestrial coverage of grasslands underlines the need for reliable parameterizations of in-canopy transport characteristics for grasslands. The Tn tracer technique constitutes a powerful tool for this purpose, which should be used in future works.
- (2) By applying the Tn tracer technique, PLAKE et al. (2014a, Appendix D) showed the aerodynamic resistance in the lower grassland canopy to be two orders of magnitude during daytime and by one order of magnitude during nighttime higher, as the according above-canopy aerodynamic resistance. The sharp decrease from canopy bottom to top is mainly due to the high biomass density within the lower canopy of grasslands, leading to an extremely high aerodynamic resistance here. Correspondingly, the aerodynamic resistance of the whole grassland canopy was shown to be at least 3–4 times higher than corresponding values for forests. Therefore, canopy flushing times can be longer by 400 % for grassland canopies than for forests, even if the canopy height of grasslands is only around 1–10 % compared to forests.
- (3) It was shown by PLAKE et al. (2014a, Appendix D) that grasslands can be prone to canopy decoupling throughout the day. In their study, temperature inversions yielded (i) unstable conditions in the upper canopy and simultaneous stable conditions in the lower canopy during daytime and conversely, (ii) stable conditions in the upper canopy and simultaneous unstable conditions in the lower canopy during nighttime. Consistently, the directly measured aerodynamic resistances and transport times representing the upper and lower canopy underwent contrasting diurnal courses. Thus, during daytime, when the aerodynamic resistances and transport times in the upper canopy were lowest, they were highest in the lower canopy. During nighttime, when they

showed their diurnal maxima in the upper canopy, their diurnal minima prevailed in the lower canopy.

- (4) For the first time the comprehensive data set of PLAKE et al. (2014a, Appendix D) allowed the comparison of directly measured transport times, chemical timescales and Damköhler numbers for various layers within and above a grassland canopy. Their analysis on transport-chemistry interactions with respect to contrasting meteorological and air-chemical conditions (high and low NO_x periods) revealed for daytime conditions that the highest likelihood for chemical divergence prevailed in the lower canopy, followed by the upper canopy and the above-canopy layer. At this time, the likelihood within the above-canopy layer was lowest during the low NO_x periods. During daytime the magnitude of the Damköhler number was mainly determined by the transport time. The nighttime conditions during the low NO_x periods were found entirely different from those during the high NO_x periods. During the low NO_x periods the turbulence-chemistry interactions remained almost similar to those during daytime. In contrast, the extraordinary strong temperature inversion during the high NO_x periods yielded for the lowest canopy layer (i) the longest chemical timescales and (ii) the shortest transport times, which resulted in a reversed Damköhler number profile. Above the canopy, equally fast chemistry and transport indicated potential chemical divergence, whereas in the lower canopy the twenty times faster timescale of transport compared to chemistry resulted in the only instance within the entire data set, where the Damköhler numbers clearly indicated no potential chemical divergence.
- (5) The grassland canopy investigated in PLAKE et al. (2014a, Appendix D) exhibited surprisingly many parallels with results reported from Amazonian rain forest canopies by other studies. Among these were (i) comparable magnitude of the aerodynamic resistances within the lower part of both canopies, (ii) inversed diurnal courses of the aerodynamic resistances in the lower and upper part of both canopies resulting in only small diurnal variations of the aerodynamic resistances representing the whole canopies and (iii) nighttime transport being faster than the corresponding chemical timescale of the NO - NO_2 - O_3 triad within the lowest canopy layers.
- (6) The insignificant NO soil emissions at the site inhibited the quantification of the NO_x canopy reduction within the grassland canopy. Nevertheless, the unique data set presented by PLAKE et al. (2014a, Appendix D) allowed the derivation of some general conclusions on NO_x canopy reduction within natural grassland canopies by comparing measured timescales of transport and chemistry with the characteristic timescale of NO_2 uptake by the plant canopy. Their results indicated for a grassland canopy of similar structure with significant NO soil emissions an efficient daytime conversion of soil-emitted NO to NO_2 (high Damköhler number) and subsequent effective plant up-

take (fast timescale of NO_2 plant uptake). This leads to strong NO_x canopy reduction within the highly dense and stable stratified lower canopy during daytime. During nighttime NO_2 plant uptake was found insignificant and, thus, the turbulence-chemistry interactions (Damköhler number) determine the fate of soil-emitted NO. During rather windy nights (low NO_x periods) the efficient formation of NO_2 within the canopy (high Damköhler numbers) favors simultaneous NO_2 and NO canopy emission fluxes. Nights of low wind speed (high NO_x periods) are connected to an extremely stable stratified upper canopy, suppressing the vertical exchange and, thus, causing the breakdown of the O_3 supply from above. Subsequently, soil-emitted NO is trapped as a mixture of NO and NO_2 within the lower canopy until the morning. The results of PLAKE et al. (2014a, Appendix D) are the first that indicate strong NO_x canopy reduction for grasslands based on direct in-canopy measurements. Nevertheless, a quantification of the NO_x canopy reduction for grasslands is unfortunately still lacking, but the used measurement setup was shown to be definitely suitable for this purpose. Thus, the implementation of an advanced NO_x canopy reduction algorithm in global atmospheric transport and chemistry models can certainly be achieved in the future.

- (7) PLAKE et al. (2014b, Appendix C) determined O_3 deposition fluxes at the Mainz-Finthen site which were, compared to other studies, in the lower range for grassland sites. With respect to the nutrient poor site characteristics and the rather high proportion of senescent dead leaves, their results are reasonable. A partitioning analysis of the O_3 flux revealed that the non-stomatal deposition was the major O_3 deposition pathway towards the natural grassland canopy. This was attributed to high relative humidity, the senescence of the canopy and several nights of high wind speed during the experiment.
- (8) PLAKE et al. (2014a, Appendix D) found plant uptake and soil deposition of O_3 being significantly faster than chemistry or transport in the investigated canopy throughout the day. Thus, at the investigated site in-canopy Damköhler numbers were irrelevant for O_3 . In contrast to other studies, a chemical divergence for O_3 due to reactions with ecosystem-emitted NO or VOCs was not detected at the Mainz-Finthen site. A potential chemical divergence throughout the day, as indicated by the above-canopy Damköhler numbers, together with partly comparable O_3 and NO levels (small O_3/NO ratios), led to the estimation of a net chemically induced O_3 flux. In contrast to previous studies, the results revealed a net O_3 production during daytime, resulting in an underestimation of the median daytime O_3 fluxes determined by PLAKE et al. (2014b, Appendix C) by 10 %. The O_3 production resulted from a deviation from the $\text{NO-NO}_2\text{-O}_3$ photostationary state by a surplus of NO_2 , based on NO oxidation by e.g. per-

oxy radicals or other oxidants. In previous studies, the photochemical O₃ production was most likely hidden by the outbalancing of O₃ reactions with NO or VOCs. Above-canopy Damköhler numbers did not hint towards a chemical flux divergence.

- (9) PLAKE et al. (2014b, Appendix C) successfully advanced a dynamic chamber system and investigated the applicability for flux determinations of depositing compounds, such as O₃. By validation against eddy covariance, the state-of-the-art flux measurement method, they demonstrated that the dynamic chamber method is suitable to reliably determine diurnal courses as well as 30 min averages of O₃ fluxes. Under certain conditions, the corresponding relative flux errors were shown to be well below 25 %. The prerequisites of representative vegetation structure and activity of the enclosed vegetation were fulfilled. The results of PLAKE et al. (2014b, Appendix C) revealed that O₃ fluxes can be determined as a complementary component of standard NO flux measurements by dynamic chamber systems. Such systems generally run simultaneous O₃ mixing ratio measurements for gas-phase chemistry corrections. These systems can easily be used for continuous O₃ and also NO₂ flux measurements in order to extend the knowledge on the deposition of these gases and on the underlying processes for a large range of low canopy ecosystems. Solely one additional 3D ultra-sonic anemometer, required for the correction of the resistive scheme, has to be installed at a reference level above the canopy. For cases when the canopy is slightly higher than the chambers, such as in PLAKE et al. (2014b, Appendix C), an additional O₃ mixing ratio measurement above the canopy is needed at the reference level. Overall, it has been shown that the dynamic chamber method definitely constitutes an alternative for O₃ flux measurements at low canopy ecosystems in cases when the eddy covariance method cannot be applied. Arguments favoring the dynamic chamber against the eddy covariance method are: (i) applicability of chamber methods on micro plots for investigations on gas exchange of different vegetation species and management forms, (ii) a more direct determination of canopy resistance that is required as input for process and modeling studies, (iii) well-defined gas-phase chemistry corrections for reactive compounds in the well-mixed chamber headspace (elimination of potential flux divergence).

References

- ALTIMIR, N. et al., 2006. Foliage surface ozone deposition: a role for surface moisture? *Biogeosciences*, 3(2): 209-228.
- ALTIMIR, N., TUOVINEN, J.P., VESALA, T., KULMALA, M. and HARI, P., 2004. Measurements of ozone removal by Scots pine shoots: calibration of a stomatal uptake model including the non-stomatal component. *Atmospheric Environment*, 38(15): 2387-2398.
- ARNETH, A. et al., 2010. Terrestrial biogeochemical feedbacks in the climate system. *Nature Geoscience*, 3(8): 525-532.
- AYLOR, D.E., WANG, Y.S. and MILLER, D.R., 1993. Intermittent wind close to the ground within a grass canopy. *Boundary-Layer Meteorology*, 66(4): 427-448.
- BAKWIN, P.S., WOFSY, S.C., FAN, S.M., KELLER, M., TRUMBORE, S.E. and DACOSTA, J.M., 1990. Emission of nitric-oxide (NO) from tropical forest soils and exchange of NO between the forest canopy and atmospheric boundary-layers. *Journal of Geophysical Research-Atmospheres*, 95(D10): 16755-16764.
- BALDOCCHI, D., 1988. A multi-layer model for estimating sulfur-dioxide deposition to a deciduous oak forest canopy. *Atmospheric Environment*, 22(5): 869-884.
- BASSIN, S., CALANCA, P., WEIDINGER, T., GEROSA, G. and FUHRER, E., 2004. Modeling seasonal ozone fluxes to grassland and wheat: model improvement, testing, and application. *Atmospheric Environment*, 38(15): 2349-2359.
- BIGNAL, K.L., ASHMORE, M.R., HEADLEY, A.D., STEWART, K. and WEIGERT, K., 2007. Ecological impacts of air pollution from road transport on local vegetation. *Applied Geochemistry*, 22(6): 1265-1271.
- BOURTSOUKIDIS, E., BONN, B., DITTMANN, A., HAKOLA, H., HELLEN, H. and JACOBI, S., 2012. Ozone stress as a driving force of sesquiterpene emissions: a suggested parameterisation. *Biogeosciences*, 9(11): 4337-4352.
- CANTRELL, C.A., 2008. Technical note: review of methods for linear least-squares fitting of data and application to atmospheric chemistry problems. *Atmospheric Chemistry and Physics*, 8(17): 5477-5487.
- CRUTZEN, P., 1973. Discussion of chemistry of some minor constituents in stratosphere and troposphere. *Pure and Applied Geophysics*, 106(5-7): 1385-1399.
- DE ARELLANO, J., DUYNKERKE, P.G. and BUILTJES, P.J.H., 1993. The divergence of the turbulent-diffusion flux in the surface-layer due to chemical-reactions - the NO-O₃-NO₂ System. *Tellus Series B-Chemical and Physical Meteorology*, 45(1): 23-33.
- DOLMAN, A.J. et al., 2006. The CarboEurope regional experiment strategy. *Bulletin of the American Meteorological Society*, 87(10): 1367-1379.
- DORSEY, J.R. et al., 2004. Oxidized nitrogen and ozone interaction with forests. I: Experimental observations and analysis of exchange with Douglas fir. *Quarterly Journal of the Royal Meteorological Society*, 130(600): 1941-1955.

- DUYZER, J. and FOWLER, D., 1994. Modeling land-atmosphere exchange of gaseous oxides of nitrogen in Europe. *Tellus Series B-Chemical and Physical Meteorology*, 46(5): 353-372.
- DUYZER, J.H., DEINUM, G. and BAAK, J., 1995. The interpretation of measurements of surface exchange of nitrogen-oxides - correction for chemical-reactions. *Philosophical Transactions of the Royal Society a-Mathematical Physical and Engineering Sciences*, 351(1696): 231-248.
- EMBERSON, L.D., WIESER, G. and ASHMORE, M.R., 2000. Modelling of stomatal conductance and ozone flux of Norway spruce: comparison with field data. *Environmental Pollution*, 109(3): 393-402.
- FINNIGAN, J., 2000. Turbulence in plant canopies. *Annual Review of Fluid Mechanics*, 32: 519-571.
- FOKEN, T., AUBINET, M. and LEUNING, R., 2012a. The eddy covariance method. In: M. Aubinet, T. Vesala and D. Papale (Editors), *Eddy covariance*. Springer, Dordrecht, Heidelberg, London, New York, pp. 438.
- FOKEN, T. et al., 2012b. Coupling processes and exchange of energy and reactive and non-reactive trace gases at a forest site - results of the EGER experiment. *Atmospheric Chemistry and Physics*, 12(4): 1923-1950.
- FOWLER, D. et al., 2009. Atmospheric composition change: ecosystems-atmosphere interactions. *Atmospheric Environment*, 43(33): 5193-5267.
- GANZEVELD, L.N., LELIEVELD, J., DENTENER, F.J., KROL, A.C. and ROELOFS, G., 2002a. Atmosphere-biosphere trace gas exchanges simulated with a single-column model. *Journal of Geophysical Research*, 107(D16): ACH8-1-21.
- GANZEVELD, L.N., LELIEVELD, J., DENTENER, F.J., KROL, M.C., BOUWMAN, A.J. and ROELOFS, G.J., 2002b. Global soil-biogenic NO_x emissions and the role of canopy processes. *Journal of Geophysical Research-Atmospheres*, 107(D16).
- GILLILAND, F., MILLSTEIN, J., MARGOLIS, H., LURMANN, F.W., LI, Y.F., AVOL, E. and PETERS, J.M., 2004. Effects of prenatal exposure to O₃, PM₁₀, NO₂, and CO on birth weight in full-term pregnancies: Results from the children's health study (CHS). *Epidemiology*, 15(4): S34-S34.
- GREITNER, C.S., PELL, E.J. and WINNER, W.E., 1994. Analysis of aspen foliage exposed to multiple stresses - ozone, nitrogen deficiency and drought. *New Phytologist*, 127(3): 579-589.
- GUT, A. et al., 2002a. Exchange fluxes of NO₂ and O₃ at soil and leaf surfaces in an Amazonian rain forest. *Journal of Geophysical Research-Atmospheres*, 107(D20): LBA 27-1-LBA 27-15.
- GUT, A. et al., 2002b. NO emission from an Amazonian rain forest soil: Continuous measurements of NO flux and soil concentration. *Journal of Geophysical Research-Atmospheres*, 107(D20): LBA 24-1-LBA 24-10.
- HENS, K., 2009. Der bodennahe, vertikale, turbulente Transport von ²²²Rn, ²²⁰Rn und anderen Spurengasen im Stammraum eines Fichtenbestandes, Johannes Gutenberg - Universität, Mainz, 93 pp.

- HIROTA, M., ZHANG, P.C., GU, S., SHEN, H.H., KURIYAMA, T., LI, Y.N. and TANG, Y.H., 2010. Small-scale variation in ecosystem CO₂ fluxes in an alpine meadow depends on plant biomass and species richness. *Journal of Plant Research*, 123(4): 531-541.
- IPPC, 2007. *Climate Change 2007: the physical science basis. Contribution of working group I to the fourth assessment report of the Intergovernmental Panel on Climate Change.* University Press, Cambridge, UK.
- JACOB, D.J. and WOFSY, S.C., 1990. Budgets of reactive nitrogen, hydrocarbons, and ozone over the amazon-forest during the wet season. *Journal of Geophysical Research-Atmospheres*, 95(D10): 16737-16754.
- JACOBS, A.F.G., VANBOXEL, J.H. and ELKILANI, R.M.M., 1994. Nighttime free-convection characteristics within a plant canopy. *Boundary-Layer Meteorology*, 71(4): 375-391.
- JÄGGI, M., AMMANN, C., NEFTEL, A. and FUHRER, J., 2006. Environmental control of profiles of ozone concentration in a grassland canopy. *Atmospheric Environment*, 40(28): 5496-5507.
- KASANKO, M., PALMIERI, A. and COYETTE, C., 2011. Land cover/ land use statistics. In: C. Coyette and H. Schenk (Editors), *Agriculture and Fishery Statistics.* Eurostat, Luxembourg, pp. 158.
- KHEMANI, L.T., MOMIN, G.A., RAO, P.S.P., PILLAI, A.G., SAFAI, P.D., MOHAN, K. and RAO, M.G., 1994. Atmospheric pollutants and their influence on acidification of rain water at an industrial-location on the west-coast of India. *Atmospheric Environment*, 28(19): 3145-3154.
- KIM, H.H. et al., 2013. Analysis of the association between air pollution and allergic diseases exposure from nearby sources of ambient air pollution within elementary school zones in four Korean cities. *Environmental Science and Pollution Research*, 20(7): 4831-4846.
- KRUIJT, B. et al., 2000. Turbulence statistics above and within two Amazon rain forest canopies. *Boundary-Layer Meteorology*, 94(2): 297-331.
- KURPIUS, M.R. and GOLDSTEIN, A.H., 2003. Gas-phase chemistry dominates O₃ loss to a forest, implying a source of aerosols and hydroxyl radicals to the atmosphere. *Geophysical Research Letters*, 30(7).
- LAMAUD, E., LOUBET, B., IRVINE, M., STELLA, P., PERSONNE, E. and CELLIER, P., 2009. Partitioning of ozone deposition over a developed maize crop between stomatal and non-stomatal uptakes, using eddy-covariance flux measurements and modelling. *Agricultural and Forest Meteorology*, 149(9): 1385-1396.
- LEHMANN, B.E., LEHMANN, M., NEFTEL, A., GUT, A. and TARAKANOV, S.V., 1999. Radon-220 calibration of near-surface turbulent gas transport. *Geophysical Research Letters*, 26(5): 607-610.
- LENSCHOW, D.H., 1982. Reactive trace species in the boundary-layer from a micrometeorological perspective. *Journal of the Meteorological Society of Japan*, 60(1): 472-480.
- MASSMAN, W.J., MUSSELMAN, R.C. and LEFOHN, A.S., 2000. A conceptual ozone dose-response model to develop a standard to protect vegetation. *Atmospheric Environment*, 34(5): 745-759.

- MATTHEWS, R.D., SAWYER, R.F. and SCHEFER, R.W., 1977. Interferences in chemiluminescent measurement of NO and NO₂ emissions from combustion systems. *Environmental Science & Technology*, 11(12): 1092-1096.
- MEIXNER, F.X., 1994. Surface exchange of odd nitrogen oxides, *Nova Acta Leopoldina*; The terrestrial nitrogen cycle as influenced by man. *Nova Acta Leopoldina*, pp. 299-348.
- MESZAROS, R. et al., 2009. Measurement and modelling ozone fluxes over a cut and fertilized grassland. *Biogeosciences*, 6(10): 1987-1999.
- MITCHELL, J.F.B., 1989. The Greenhouse-Effect and Climate Change. *Reviews of Geophysics*, 27(1): 115-139.
- MONCRIEFF, J., VALENTINI, R., GRECO, S., SEUFERT, G. and CICCIOLO, P., 1997. Trace gas exchange over terrestrial ecosystems: Methods and perspectives in micrometeorology. *Journal of Experimental Botany*, 48(310): 1133-1142.
- NEMITZ, E. et al., 2009. Turbulence characteristics in grassland canopies and implications for tracer transport. *Biogeosciences*, 6(8): 1519-1537.
- NEMITZ, E., SUTTON, M.A., GUT, A., SAN JOSE, R., HUSTED, S. and SCHJOERRING, J.K., 2000. Sources and sinks of ammonia within an oilseed rape canopy. *Agricultural and Forest Meteorology*, 105(4): 385-404.
- OSWALD, R. et al., 2013. HONO emissions from soil bacteria as a major source of atmospheric reactive nitrogen. *Science*, 341(6151): 1233-1235.
- PAPE, L., AMMANN, C., NYFELER-BRUNNER, A., SPIRIG, C., HENS, K. and MEIXNER, F.X., 2009. An automated dynamic chamber system for surface exchange measurement of non-reactive and reactive trace gases of grassland ecosystems. *Biogeosciences*, 6(3): 405-429.
- PERSONNE, E. et al., 2009. SURFATM-NH₃: a model combining the surface energy balance and bi-directional exchanges of ammonia applied at the field scale. *Biogeosciences*, 6(8): 1371-1388.
- PILEGAARD, K., HUMMELSHOJ, P. and JENSEN, N.O., 1998. Fluxes of ozone and nitrogen dioxide measured by eddy correlation over a harvested wheat field. *Atmospheric Environment*, 32(7): 1167-1177.
- PLAKE, D., SÖRGEL, M., STELLA, P., HELD, A. and TREBS, I., 2014a. Influence of meteorology and anthropogenic pollution on chemical divergence of the NO-NO₂-O₃ triad above and within a natural grassland canopy. *Biogeosciences*, to be submitted.
- PLAKE, D., STELLA, P., MORAVEK, A., MAYER, J.C., AMMANN, C., HELD, A. and TREBS, I., 2014b. Comparison of ozone deposition measured with the dynamic chamber and the eddy covariance method. *Agricultural and Forest Meteorology*, submitted.
- PLAKE, D. and TREBS, I., 2013. An automated system for selective and continuous measurements of vertical thoron profiles for the determination of transport times near the ground. *Atmospheric Measurement Techniques*, 6(4): 1017-1030.
- RIPLEY, E.A. and REDMAN, R.E., 1976. Grassland. In: J.L. Monteith (Editor), *Vegetation and the atmosphere*. Acad. Press, London.
- RUMMEL, U., 2005. Turbulent exchange of ozone and nitrogen oxides between an Amazonian rain forest and the atmosphere, University of Bayreuth, Bayreuth, 246 pp.

- RUMMEL, U., AMMANN, C., KIRKMAN, G.A., MOURA, M.A.L., FOKEN, T., ANDREAE, M.O. and MEIXNER, F.X., 2007. Seasonal variation of ozone deposition to a tropical rain forest in southwest Amazonia. *Atmospheric Chemistry and Physics*, 7(20): 5415-5435.
- SIMON, E. et al., 2005. Lagrangian dispersion of Rn-222, H₂O and CO₂ within Amazonian rain forest. *Agricultural and Forest Meteorology*, 132(3-4): 286-304.
- STELLA, P., KORTNER, M., AMMANN, C., FOKEN, T., MEIXNER, F.X. and TREBS, I., 2013a. Measurements of nitrogen oxides and ozone fluxes by eddy covariance at a meadow: evidence for an internal leaf resistance to NO₂. *Biogeosciences*, 10(9): 5997-6017.
- STELLA, P., PERSONNE, E., LAMAUD, E., LOUBET, B., TREBS, I. and CELLIER, P., 2013b. Assessment of the total, stomatal, cuticular, and soil 2 year ozone budgets of an agricultural field with winter wheat and maize crops. *Journal of Geophysical Research: Biogeosciences*: 1120-1132.
- SUTTIE, J.M., REYNOLDS, S.G. and BATELLO, C., 2005. Introduction. In: J.M. Suttie, S.G. Reynolds and C. Batello (Editors), *Grasslands of the World*. FAO, Rome.
- SWINBANK, W.C., 1968. A comparison between predictions of dimensional analysis for constant-flux layer and observations in unstable conditions. *Quarterly Journal of the Royal Meteorological Society*, 94(402): 460-&.
- THOMAS, C. and FOKEN, T., 2007. Flux contribution of coherent structures and its implications for the exchange of energy and matter in a tall spruce canopy. *Boundary-Layer Meteorology*, 123(2): 317-337.
- VAN PUL, W.A.J. and JACOBS, A.F.G., 1994. The conductance of a maize crop and the underlying soil to ozone under various environmental-conditions. *Boundary-Layer Meteorology*, 69(1-2): 83-99.
- WARNECK, P., 2000. *Chemistry of the natural atmosphere*. Academic Press, San Diego, California, 927 pp.
- WILSON, K.L. and BIRKS, J.W., 2006. Mechanism and elimination of a water vapor interference in the measurement of ozone by UV absorbance. *Environmental Science & Technology*, 40(20): 6361-6367.
- YIENGER, J.J. and LEVY, H., 1995. Empirical-model of global soil-biogenic NO_x emissions. *Journal of Geophysical Research-Atmospheres*, 100(D6): 11447-11464.
- ZHENG, J. et al., 2013. Volatile organic compounds in Tijuana during the Cal-Mex 2010 campaign: Measurements and source apportionment. *Atmospheric Environment*, 70: 521-531.

LIST OF APPENDICES**APPENDIX A:.....37**

Individual contribution to the joint publication

APPENDIX B:.....39

PLAKE, D. and TREBS, I., 2013. An automated system for selective and continuous measurements of vertical thoron profiles for the determination of transport times near the ground. *Atmospheric Measurement Techniques*, 6(4): 1017-1030.

APPENDIX C:.....65

PLAKE, D., STELLA, P., MORAVEK, A., MAYER, J.C., AMMANN, C., HELD, A. and TREBS, I., 2014. Comparison of ozone deposition measured with the dynamic chamber and the eddy covariance method. *Agricultural and Forest Meteorology*, submitted.

APPENDIX D:.....97

PLAKE, D., SÖRGEL, M., STELLA, P., HELD, A. and TREBS, I., 2014. Influence of meteorology and anthropogenic pollution on chemical divergence of the NO-NO₂-O₃ triad above and within a natural grassland canopy. *Biogeosciences*, to be submitted.

APPENDIX A

INDIVIDUAL CONTRIBUTION TO THE JOINT PUBLICATIONS

This cumulative thesis consists of three manuscripts, which were composed in close cooperation with other researchers. In this section the individual contribution to each joint publication is specified.

APPENDIX B

PLAKE, D. and TREBS, I., 2013. An automated system for selective and continuous measurements of vertical thoron profiles for the determination of transport times near the ground. *Atmospheric Measurement Techniques*, 6(4): 1017-1030.

The novel automated system was fully designed by D. PLAKE. He ordered the required hardware components, assembled the system, ran test measurements, organized the calibration and was the only operator of the system during the entire field experiment. The side-by-side measurement setup idea was his. He fully performed the data analysis. He drafted and wrote the entire paper.

I. TREBS gave helpful suggestions during the system planning and testing phase. She provided valuable guidance through some difficult phases of the data analysis process. Her proofreading advanced the manuscript.

APPENDIX C

PLAKE, D., STELLA, P., MORAVEK, A., MAYER, J.C., AMMANN, C., HELD, A. and TREBS, I., 2014. Comparison of ozone deposition measured with the dynamic chamber and the eddy covariance method. *Agricultural and Forest Meteorology*, submitted.

D. PLAKE was fully responsible for the combination of the vertical profile and dynamic chamber system for reactive trace gases. He advanced the switching schedule, ordered required hardware components, assembled the system, ran test measurements, regularly calibrated the essential measurements systems and was the only operator of the combined vertical profile and dynamic chamber system during the entire field experiment. He actively supported the conduction of the eddy covariance and micrometeorological measurements. The bulk data analysis was performed by him. He drafted and wrote the entire paper.

P. STELLA contributed with helpful discussions on the resistive scheme and with revising the manuscript.

A. MORAVEK helped with the conduction and analysis of the eddy covariance measurements. Furthermore, many discussions with him helped to improve the manuscript.

J.C. MAYER was conducive to the study by installing and maintaining micrometeorological hardware.

C. AMMANN, contributed ideas during the data analysis and during the writing of the manuscript. He carefully reviewed the manuscript.

A. HELD added helpful ideas during the data analysis and during the writing of the manuscript. He contributed to this manuscript by many fruitful discussions and by diligent proofreading.

I. TREBS had a hand in many details from measurement setup, over data analysis up to drafting of the manuscript.

APPENDIX D

PLAKE, D., SÖRGEL, M., STELLA, P., HELD, A. and TREBS, I., 2014. Influence of meteorology and anthropogenic pollution on chemical divergence of the NO-NO₂-O₃ triad above and within a natural grassland canopy. Biogeosciences, to be submitted.

The bulk of the essential measurements for the manuscript were made by D. PLAKE (see also Appendix A, B). He was fully responsible for calibration, data analysis and the conceptual design and the drafting of the manuscript.

M. SÖRGEL helped with some advisory ideas concerning the data analysis.

P. STELLA contributed by revising the manuscript.

A. HELD provided useful guidance through some conceptual difficulties. The discussions with him helped improve the manuscript. In addition, he carefully proofread the manuscript.

I. TREBS contributed helpful ideas concerning the data analysis. Her proofreading advanced the manuscript.

APPENDIX B

Atmos. Meas. Tech., 6, 1017–1030, 2013
www.atmos-meas-tech.net/6/1017/2013/
doi:10.5194/amt-6-1017-2013
© Author(s) 2013. CC Attribution 3.0 License.



An automated system for selective and continuous measurements of vertical Thoron profiles for the determination of transport times near the ground

D. Plake¹ and I. Trebs^{1*}

[1] Max Planck Institute for Chemistry, Biogeochemistry Department, P. O. Box 3060, 55020 Mainz, Germany.

* now at: Centre de Recherche Public - Gabriel Lippmann, Department Environment and Agrobiotechnologies, 41 rue du Brill, L-4422 Belvaux, Luxembourg

Correspondence to: D. Plake (daniel.plake@mpic.de)

Received: 14 December 2012 – Published in Atmos. Tech. Discuss.: 25 January 2013

Revised: 25 March 2013 – Accepted: 26 March 2013 – Published: 16 April 2013

Abstract

The quantification of in-canopy transport times is of a major importance for the investigation of sources, sinks and net fluxes of reactive trace gases within plant canopies. The Damköhler number, which compares timescales of chemical reactions with transport times, is a widely applied measure to evaluate flux divergences. In this study, we present and evaluate a novel automated measurement system for selective vertical Thoron (Tn) profiles near the earth's surface and demonstrate its suitability for the direct and reliable determination of transport times within a natural grassland canopy. For the first time, we perform a rigorous determination of systematic and random uncertainties of Tn (and Rn) concentrations under field conditions for this type of measurement system. The obtained median precisions for three concentration classes ($>100 \text{ Bq m}^{-3}$, $100\text{--}15 \text{ Bq m}^{-3}$, $<15 \text{ Bq m}^{-3}$) were 8.8 %, 23.2 % and 132.1 % for Tn (and 16.6 %, 25.0 %, 99.2 % for Rn). We calculate in-canopy transport times (τ) and propagate their uncertainty from the individual errors of the Tn concentration measurements. A

quality assessment of τ for the field experiment during a period of 51 days revealed a good data quality with 44 % of the relative uncertainties below 50 %. The occurrence of transport time uncertainties higher than 100 % was caused by absolute Tn gradients lower than $70 \text{ Bq m}^{-3} \text{ m}^{-1}$, which was found for 22 % of all determined transport times. In addition, the method was found to be highly sensitive to the Tn concentrations at the upper of the two inlet heights (z_u). Low values of $C_{Tn_{z_u}}$ result in high absolute uncertainties of the transport time. A comparison with empirical parameterizations revealed a much lower scatter for the τ values determined from our measurements. We found an excellent agreement with τ values obtained by the in-canopy resistance approach used e.g., in the SURFATM model during daytime, while the SURFATM model significantly overestimated transport times during nighttime.

1 Introduction

The two isotopes ^{220}Rn (Thoron) and ^{222}Rn (Radon) are generated in rocks and natural soils, where their respective mother nuclides Thorium (^{232}Th) and Uranium (^{238}U) occur as common radioactive atoms. Thoron (Tn) and Radon (Rn) can migrate into the atmosphere if the location of the production is close enough to the soil-atmosphere interface. The half-life times ($T_{0.5}$) are 55.6 s for Tn and 3.8 d for Rn (Lide, 2004), and limit the transport distances within the soil and the atmosphere. Above the soil Tn and Rn atoms undergo dilution and transport in atmospheric air until they are removed by radioactive decay, which is their only removal process. In flat terrains with homogeneous emission rates Tn and Rn concentrations therefore always decrease with height. Due to its relatively long $T_{0.5}$, Rn is widely used as tracer for regional and global atmospheric transport (cf. Dorr et al., 1983; Zahorowski et al., 2004) and in global circulation models (cf. Brost and Chatfield, 1989; Zhang et al., 2008). In contrast, Tn is excellent for studying meteorological processes in the lowest decameters above soil (Israel, 1965).

Soil is to a large extent covered by plant canopies, such as forest, crop or natural grassland, which act as sources and sinks of reactive trace gases. Canopies strongly influence the vertical wind profile and other micrometeorological parameters, which drive the trace gas exchange (cf. Finnigan, 2000). The first meter above soil is of significant importance for the surface-atmosphere exchange fluxes of trace gases, since the eddy diffusivity (K) changes by three orders of magnitude (cf. Ikebe and Shimo, 1972), and the transition from turbulent to diffusive transport occurs. The transport time of the air within this layer determines the effectiveness of (a) chemical reactions and inter-conversion of reactive trace gases (termed “chemical flux divergence” (De Arellano et al., 1993)) and (b) the deposition and uptake to/by plants and soil of either the directly emitted compounds or their reaction products. For instance, due to long in-canopy transport times only a fraction of soil biogenic nitric oxide (NO) emissions may leave a canopy, because a large part is oxidized by ozone (O_3) and the product nitrogen dioxide (NO_2) is subsequently recaptured mainly through uptake by soil and plant stomata (“canopy reduction”) (e.g., Yienger and Levy, 1995). The calculation of Damköhler numbers, which compare chemical timescales to transport times (τ), is a widely applied approach to evaluate the influence of chemistry on exchange fluxes (e.g., Dlugi et al., 2010). Typically, τ or K may be derived using micrometeorological techniques such as the eddy covariance and the flux-gradient approach. However,

their application is limited within plant canopies where low turbulence prevails and e.g., the Monin-Obukov similarity theory does not hold (Denmead and Bradley, 1985). In addition, practical reasons complicate their in-canopy application (e.g., short distance between wind sensors and branches).

Rn is mainly used as a tracer in studies focusing on vertical spatial scales of meters to kilometers above soil (e.g., Liu et al., 1984). Some studies present mean residence times for tall forest canopies (e.g., Trumbore et al., 1990; Ussler et al., 1994; Martens et al., 2004) derived using Rn canopy inventory models (for details see Trumbore et al., 1990). A similar method was used by Simon et al. (2005), who calculated vertical τ profiles from Rn measurements inside a rainforest canopy.

In contrast, studies dealing with Tn mainly focus on the layer adjacent to the ground, where its concentration is determined by the competition of transport and the fast radioactive decay. Rn decay can be neglected in this layer because of its longer $T_{0.5}$. Butterweck et al. (1994) point out that even in a dense canopy, where most micrometeorological methods fail, the turbulent exchange can be characterized with the help of Tn. Lehmann et al. (1999) describe the characteristic vertical range for Tn ($z^* = (K/\lambda)^{1/2}$, where $\lambda = \ln 2 / T_{0.5} = 0.0125 \text{ s}^{-1}$ is the radioactive decay rate (Hänsel and Neumann, 1995) and $K = 10^{-3} \text{ m}^2 \text{ s}^{-1}$) to be 28 cm. Furthermore, they propose a straightforward method to determine effective transport times from vertical Tn profiles near the ground as:

$$\tau = \ln \left[\frac{C_{Tn_{z_l}}}{C_{Tn_{z_u}}} \right] / \lambda \quad (1)$$

where $C_{Tn_{z_l}}$ and $C_{Tn_{z_u}}$ are the measured Tn concentrations at the lower and upper heights (z_l and z_u).

These authors call this approach a perfect tool for studying near-surface gas transport under stable situations when more conventional micrometeorological methods are not applicable. The Tn tracer technique is independent of any particular transport model and the required physical information is entirely provided by the ‘‘Tn clock’’.

General prerequisites for the application of Lehmann’s method are homogeneity of the Tn emission and a reasonable flatness of the terrain. From the technical point of view the major limitation is the precision of the Tn measurement, which was not investigated under field conditions up to now. Typically, two Tn and Rn monitors (AlphaGuard, Saphymo GmbH, Frankfurt, Germany) were operated in series. Since one AlphaGuard analyzer measures the sum of Tn and Rn, the isotope separation is made by a defined Tn decay volume installed between the two AlphaGuards. The Tn concentration is then obtained by subtraction of the Rn signal (2nd AlphaGuard) from the sum of Tn and Rn (1st AlphaGuard). Gut et al. (2002), Hens (2009) and Nemitz et al. (2009) applied the same technical setup above a rain forest floor, above a spruce forest floor and within a grassland canopy, respectively. However, none of these studies include a determination of systematic errors between the two AlphaGuards, nor do they estimate random concentration errors. Consequently, the uncertainties of the derived τ values in Lehmann et al. (1999), Hens (2009) and Nemitz et al. (2009) are unknown. In addition, the three measurement heights of the profile in these studies were sequentially switched (time resolution: 10 min sampling per hour and height). Thus, the vertical concentration profiles may be prone to non-stationarities.

In this paper, we present a novel automated system for selective Tn and Rn profile measurements consisting of three Tn and Rn monitors. We show measured vertical Tn and Rn concentration profiles

within a grassland canopy. The influence of non-stationarities is minimized by continuous and simultaneous measurements at three heights. For the first time, a rigorous determination of systematic and random uncertainties for Tn and Rn concentrations measured under field conditions is made. Due to the outstanding advantages of using Tn to directly determine τ near the ground (see above), we particularly focus our further analyses on Tn. Transport times are calculated from the vertical Tn concentration profiles and the corresponding random concentration errors are propagated in order to quantify the overall uncertainty of τ . We compare quality assessed τ values with empirical parameterizations used in surface-atmosphere exchange models.

2 Methods

2.1 Radon and Thoron monitor

The concentrations of Tn and Rn were measured with three commercially available radon monitors (RAD7, DurrIDGE, Billerica, USA). The RAD7 uses a solid state alpha detector for alpha particle counting and electronic alpha spectrometry for differentiation between Tn and Rn. In the sample air, alpha particles of different electric charges are emitted as Tn and Rn decay products. The alpha radiation is converted in the RAD7 measurement chamber to an electric signal and its energy is determined. The RAD7 records a spectrum of the incoming alpha particle energies over a chosen integration time and can distinguish Rn from Tn, which is very rare for currently available commercial Rn monitors.

The RAD7 was developed for locating Tn and Rn entry points in basements of buildings and monitoring of mining galleries, i.e. environments with high Tn and Rn concentrations. Our RAD7 monitors were modified in order to meet the requirements of continuous profile measurements in a grass land ecosystem, with relatively low Tn and Rn concentrations. The sensitivity was enhanced by using a high gain modification provided by the manufacturer consisting of a) an increased size of the measurement chambers (0.95 l) and b) alpha detectors with a larger active surface area. In cases when a fast Tn response is required in a standard operation mode, the RAD7 is run in *Sniff mode* with a nominal on-board pump flow rate of 0.65 L min^{-1} . This low flow rate promotes the reduction of the Tn signal due to fast Tn decay during transport from the sampling point to the RAD7 measurement chamber. To diminish this effect we used an external pump and a mass flow controller (MFC) and set the flow rate to 2 L min^{-1} . In addition, precise measurements with a RAD7 require atmospheric pressure conditions and a relative humidity (RH) below 10 % in the measurement chamber.

2.2 System setup and configuration

The automated Tn and Rn profile system (Fig. 1) consists of three identical inlet tubes. The hardware components are described in detail in Table 1. The inlet prevents the aspiration of rain drops and particles into the system and is made of a funnel and a membrane filter (Fig. 2a). Sensitive electronic parts like the RAD7s, pumps, MFCs and data recording units are installed in a rack (Fig. 2b) and protected by a waterproof housing. The air is drawn through PFA tubing ($L = 6 \text{ m}$) from the inlets to the RAD7 monitors in the housing. The tubing is heated above ambient temperature and isolated to avoid con-

densation of water vapor. In-tubing pressures are permanently monitored upstream of the pumps (see Fig. 1). To achieve the required low RH in the RAD7 monitors, Nafion dryers are installed between pumps and MFCs and are operated at high-pressure. Three Nafion dryers are used in parallel for each inlet height. Downstream of the MFCs atmospheric pressure conditions are achieved by using an open bleed line. The drying purge for the Nafions is operated using the highly efficient reflux method. Hence, a part of the previously dried RAD7 exhaust is flushed counter flow back into the under pressurized drying purge (see Fig. 1). The pressure difference between the sample flow/Nafion and the drying purge is about 2000 hPa.

The RAD7 contains an on-board data logger and a RS232 interface. Data are downloaded using the manufacturer software *Capture* on demand. A home-built V25 microprocessor unit collects e.g., the data from the pressure sensors of the Tn and Rn profile system and from a vertical thermocouple profile (ASPTC, Campbell Scientific, Utah, USA). A specially programmed Labview software running on

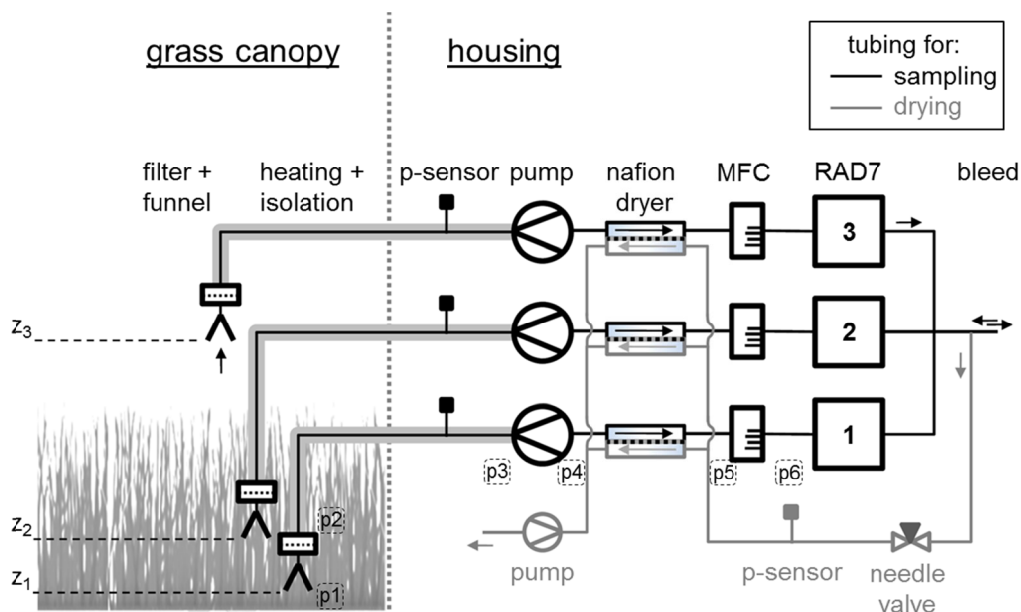


Fig. 1. Simplified gas flow scheme of the automated Tn and Rn profile system. The positions of the pressure measurements (p1 - p6) mentioned in Sect. 2.4.1 are indicated.

a master-PC requests every 10 s the data from the V25 via RS232 connection. The MFC flow rates are monitored periodically with the Labview software.

2.3 Application in the field

The field measurements to test and validate the system were made from July to September 2011 in Rhine Hessen (Germany) at the estate of the Mainz Finthen Airport (49.9685°N, 8.1481°E). The vegetation type is classified as a nutrient poor steppe-like grassland ecosystem with a mean canopy height of 0.6 m. A continuous Tn and Rn profile data set of 51 days is available (06 Aug. – 25 Sep 2011). The integration time of the RAD7 monitors was set to 60 min. The vertical wind speed profile was measured at heights of 0.2 m, 0.8 m, 1.5 m, 2.5 m, 4.0 m (2D ultra sonic anemometer, WS425,

Table 1. Details of the hardware components used for the automated Tn and Rn profile system.

Part	Manufacturer	Specifications
inline filter case	Entegris Inc., USA	Galtek Integral Ferrule in-line filters Zyklon membrane disc filters, model P4PH047, pore size 5 μm , diameter 47 mm
membrane filter	Pall Corporation, USA Saint-Gobain Performance Plastics	
PFA tubing	Isoflour GmbH, Germany	inner diameter (ID) 4 mm, outer diameter 6.35 mm
tube heating	AEG Haustechnik, Germany	heating wire, type SLH 15
pressure sensor	Sensor Technics, Germany	600-1100 hPa, type HDI0611ARY8P5
sample pump	KNF Neuberger, Germany	membrane pump, type DCB24V N86KTDCB
Nafion dryer	Perma Pure, USA	length 3.55 m, ID 2.18 mm, type PPMD-110-144F range 0.05–5 L min ⁻¹ , precision 0.3 %, type Red-y
MFC	Vögtlin, Switzerland	smart controller GSC-B hi-performance
RAD7	DurrIDGE, USA Gardner Denver, Thomas Subdivision,	Tn and Rn monitor, range Rn: 4–400000 Bq m ⁻³
drying pump	USA	type: 607CD22
needle valve	Kurt J. Lesker Company, USA	type: Nupro SS-SS4

Vaisala, Finland). In addition, the three dimensional wind vector and temperature were measured at 20 Hz by a sonic anemometer (CSAT-3, Campbell Scientific) located at 3.0 m above ground and recorded using a data logger (CR3000, Campbell Scientific). The friction velocity (u_*), sensible heat flux (H) and stability parameters were calculated using the Eddy-Covariance Software TK3 (see Mauder and Foken, 2011).

The arrangement of the inlet heights was varied throughout the field experiment (Fig. 3). Although, the vertical inlet separation should be maximal in order to increase the observed vertical concentration differences, this approach is restricted due to the short $T_{0.5}$ of Tn. A more compact inlet arrangement close to the soil (e.g., Fig. 3, block 2) might be favored since all Tn may nearly be decayed just above the canopy.

2.4 System characterization

2.4.1 Tn decay versus system residence time

Due to the short half-life time of Tn the radioactive decay during the residence time of the sample air in the system may significantly reduce the measured Tn concentration. A major prerequisite for reliable simultaneous Tn profile measurements with more than one analyzer is therefore the achievement of identical residence times in all sample lines. A constant flow rate in our setup is maintained by using precise MFCs. Nevertheless, vertical profile measurements can cause inhomogeneous clogging of the membrane filters used in the different sampling heights, which in turn might cause different residence times. To investigate the decrease of the Tn concentration in our system and to characterize the possible effect of filter clogging we proceeded in three steps: i.) pressure characterization with filter

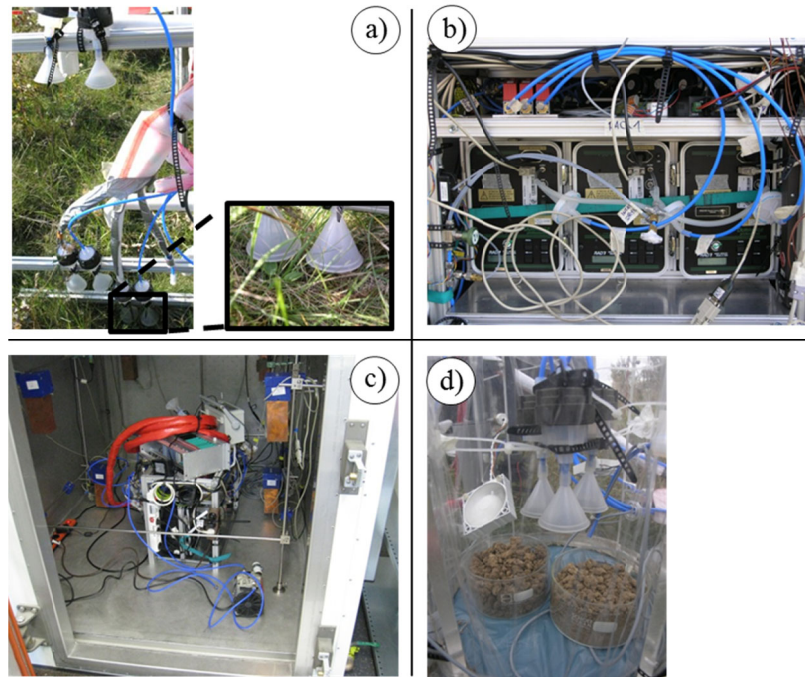


Fig. 2. Setup of the automated Tn and Rn profile system: a) field installation of the inlets, b) rack installation of the system in the housing, c) setup in the Thoron progeny chamber of the PTB in Braunschweig, d) arrangement of inlets and soil samples during the side-by-side measurements in the dynamic chamber.

clogging simulation by using a needle valve, ii.) calculation of residence times from measured flow rates and pressures for laboratory and field conditions, iii.) laboratory measurement of in-situ system residence times.

The pressure in our system was measured at six different positions (p1-p6) indicated in Fig. 1. Initially, pressures were measured at all positions using a clean filter. This procedure was repeated with the filter replaced by a needle valve to simulate the filter clogging states clean ($p_2 = 980 \text{ hPa}$), medium ($p_2 = 960 \text{ hPa}$) and dirty ($p_2 = 920 \text{ hPa}$) in the laboratory. Subsequently, the residence time was calculated for the three filter clogging states based on the continuity equation using the specific dimensions of all hardware components (e.g., tubing length and ID), the in-system pressures (p1-p6) and the volume flow rate at the MFC. In each part of the system the actual volume flow rate was calculated followed by the determination of section specific residence times. The total system residence time was calculated by summing up the individual residence times. The same procedure was applied for the field campaign data set.

The system residence time was measured by replacing the RAD7 with a fast response CO_2 analyzer (LICOR7000, Licor Biosciences, Lincoln, USA). CO_2 data were recorded in 0.5 s intervals. Upstream of the inlet system a three-way valve was installed, which controlled the flushing of the tubes with either zero air (0 ppm CO_2) or ambient air ($\sim 390 \text{ ppm CO}_2$). After flushing the line with zero air for some time, ambient air was sampled for one second, followed by sampling zero air again. The time that has passed between switching to ambient air and the maximum of the recorded CO_2 peak is defined as the residence time with a clean filter.

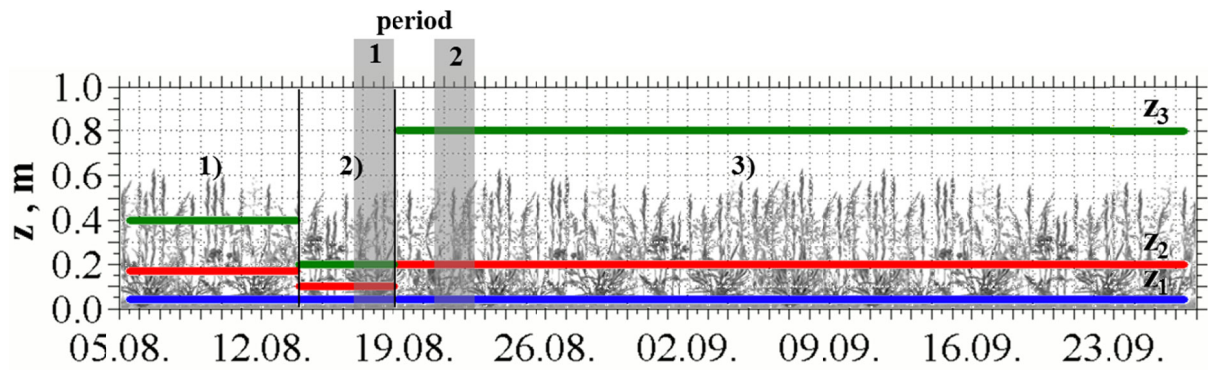


Fig. 3. Arrangement of the inlet heights ($z_1 - z_3$) for the automated Tn and Rn profile measurements with respect to the canopy height h_c . The periods 1 and 2 treated in the data evaluation are indicated. The measurement campaign was divided into three blocks: 1) 05 - 13 Aug.: $z_1 = 0.04$, $z_2 = 0.17$, $z_3 = 0.40$ m; 2) 13 - 18 Aug.: $z_1 = 0.04$, $z_2 = 0.1$ m, $z_3 = 0.20$ m; 3) 18 Aug. - 26 Sep.: $z_1 = 0.04$, $z_2 = 0.20$, $z_3 = 0.80$ m.

The results of the calculations of the residence times under laboratory and field conditions and the in-situ measurement were then compared to quantify the decay of Tn in the system and to evaluate the effect of inhomogeneous filter clogging.

2.4.2 Tn sensitivity

The RAD7 monitors were calibrated by the manufacturer only for Rn. A predefined sensitivity was applied for Tn, which is half of the Rn sensitivity. To ensure the accuracy of the Tn measurements we verified the sensitivity before starting the field measurements. The entire measurement system was set up in the Thoron progeny chamber (Fig. 2c) of the Radon measurement technique group at the Physikalisch-Technische Bundesanstalt (PTB, Braunschweig, Germany). This group at the PTB developed and operates the world's first primary standard for Tn activity concentration in air (Röttger and Honig, 2011). The RAD7 monitors were compared to the reference instrument of the PTB for the concentration range of 0 - 4300 Bq m⁻³.

2.4.3 Side-by-side measurements

Side-by-side (sbs) measurements were performed for sixteen days directly after the campaign under field conditions. The main goals were a) investigation of systematic differences for Tn and Rn between the three RAD7 monitors (accuracy) under realistic conditions and b) determination of the random concentration errors of the RAD7 monitors (precision). First, the RAD7 monitors were directly flushed (without tubing) with zero air for two days. These measurements were used to calculate the limit of detection (LOD) for the automated Tn and Rn system under field conditions according to the recommendations of Currie (1968). For the sbs measurements, we installed the inlets inside the well-mixed headspace of a dynamic chamber system (volume 0.041 m³) (Pape et al., 2009) with an adjustable purging rate of ambient air (0 - 70 L min⁻¹). Two fans guaranteed well-mixed conditions in the chamber. The bottom of the chamber was closed and two bowls with dried soil from the experimental site were placed inside the chamber serving as Tn and Rn source (Fig. 2d). In order to dilute the emitted Tn and Rn with ambient air the chamber purge was adjusted to different flow rates for several

days, these were 70 L min^{-1} , 35 L min^{-1} and 5 L min^{-1} for three, four and seven days, respectively. In contrast to other trace gases, such as O_3 and CO_2 , the fast decay of Tn can cause significant concentration differences even at small horizontal distances of only 15 cm at any time of the day. The application of the well mixed dynamic chamber allowed the performance of reliable sbs measurements under field conditions minimizing the effect of horizontal inlet separation.

2.5 Determination of systematic and random concentration errors

The systematic difference between the RAD7 monitors was determined by plotting the concentrations from the sbs measurements against each other and performing a bivariate weighted linear least-squares fitting regression analysis with the Williamson-York method provided in a Microsoft Excel spreadsheet by Cantrell (2008). The counting statistics of the RAD7 monitors provided the weighting errors. The RAD7 at height z_1 was defined as the reference instrument and the slope and intercept of the regressions were used to correct for the systematic error. The remaining scatter around the 1:1 line is the random error of the concentration difference of two RAD7 monitors ($\sigma\Delta C$) (see Wolff et al., 2010). This error was found to increase with concentration (see below). To quantify the concentration dependence of $\sigma\Delta C$, we plotted the residuals of the corrected fit, binned them, calculated the means and standard deviations of each bin, and made a linear regression (see Wolff et al., 2010). The resulting regression (slope + intercept) was used to calculate $\sigma\Delta C$ as a function of the Tn and Rn concentration. This random error $\sigma\Delta C$ was calculated for the three RAD7s in all six possible combinations by exchanging x and y-axis. Since the air samples at the three heights were measured with RAD7 monitors of identical age and specifications, we assume the random error of each instrument to be the same ($\sigma C_1 = \sigma C_2$). Thus, we calculated an average of $\sigma\Delta C$ for all monitors and computed σC of one concentration measurement required for the error propagation (see below) as:

$$(\sigma\Delta C)^2 = \sigma C_1^2 + \sigma C_2^2 \quad (2)$$

$$\sigma C = \frac{\sigma\Delta C}{\sqrt{2}} \quad (3)$$

2.6 Determination of transport time uncertainties

A measured Tn profile contains information about the average transport time of air molecules between two measurement heights z_l and z_u for the used integration interval. If the difference of the ambient Tn concentrations measured at z_l and z_u can be resolved, the average transport time (s) can be calculated according to Eq. (1). The application of this method is limited by the prevailing ambient Tn concentrations, transport and dilution by atmospheric turbulence, the instrument precision and the instrument sensitivity (LOD).

In order to estimate the uncertainty of the calculated transport times we applied the Gaussian error propagation method (e.g., Taylor, 1997; Staudt et al., 2011)

$$\sigma_{\tau}^2 = \left(\frac{\partial \tau}{\partial C_{Tn_{z_l}}} \cdot \sigma C_{Tn_{z_l}} \right)^2 + \left(\frac{\partial \tau}{\partial C_{Tn_{z_u}}} \cdot \sigma C_{Tn_{z_u}} \right)^2 + 2 \left(\frac{\partial \tau}{\partial C_{Tn_{z_l}}} \cdot \frac{\partial \tau}{\partial C_{Tn_{z_u}}} \cdot \sigma C_{Tn_{z_l}} \cdot \sigma C_{Tn_{z_u}} \cdot r_{(C_{Tn_{z_l}}, C_{Tn_{z_u}})} \right) \quad (4)$$

where $\sigma C_{Tn_{z_l}}$ and $\sigma C_{Tn_{z_u}}$ are the respective concentration errors (see section 2.5), and $r_{(C_{Tn_{z_l}}, C_{Tn_{z_u}})}$ is the correlation coefficient of the measured Tn concentrations. Term C is included since the measured Tn concentrations are dependent on each other. We calculated $r_{(C_{Tn_{z_l}}, C_{Tn_{z_u}})}$ independently for daytime and nighttime as well as for periods with different inlet arrangements (see section 2.3, Fig. 3).

3 Results

3.1 System characterization

3.1.1 Tn recovery

The pressures from p2 to p5 were found to be linearly related for the different filter clogging states (Fig. 4). This enabled us to calculate the pressure at the positions p1-p6 of the system using the reading of the permanently installed pressure sensor at p3 in each sample line (position see Fig. 1). The calculated corresponding residence times from the filter clogging experiment were 10.7 s, 10.4 s, and 10.1 s for the clean, medium and dirty state, respectively (Fig. 5). For comparison, the in-situ measured residence time (maximum of the CO₂ peak) was 11.0 s (Fig. 5). In our experiment (regular filter exchange) the median residence time for each measurement level calculated from the actual volume flows (see section 2.4.1) was 10.4 s (Fig. 5). The results from the filter clogging simulation in the laboratory compare well with the residence times under field conditions. The results imply that nearly 88 % of the Tn concentration at the inlet were recovered inside the measurement system (Fig. 5). If we consider the most extreme residence times during the campaign, the maximal potential Tn difference between the measurement levels was only 0.8 %. Consequently, the Tn concentration differences due to filter clogging were neglected in the further data evaluation.

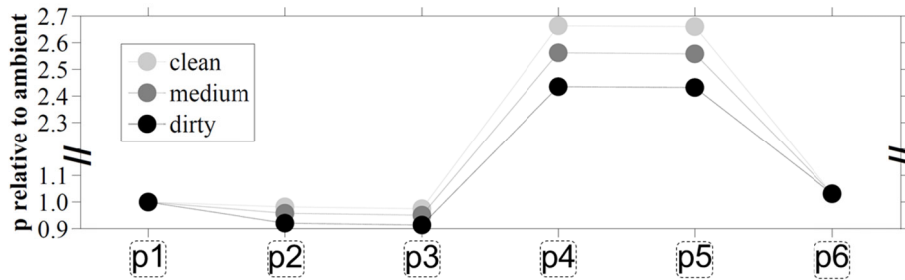


Fig. 4. Pressures measured at positions p1-p6 within the automated Tn and Rn profile system (p1=ambient pressure) during the filter clogging simulation (clean, medium, dirty).

3.1.2 Tn sensitivity

The verification of the sensitivity in the PTB facility revealed that the predefined Tn sensitivity from the manufacturer was very accurate. The sensitivity of the three RAD7 showed a deviation from the reference of less than 8 % within the concentration range of 0 Bq m⁻³ to 4300 Bq m⁻³.

3.1.3 Side-by-side measurements

The regulation of the purging rate in the dynamic chamber allowed us to vary the Tn concentration in the chamber (Fig. 6) to obtain a realistic Tn concentration range (0-300 Bq m⁻³). The highest Tn concentrations were measured with the lowest purging rate. The scatter of the Tn measurements increased with concentration. In contrast, the Rn concentrations could not be adjusted well using the chamber purging rate. Nevertheless, during stable nighttime situations elevated Rn concentrations were recorded. The dissimilarity in the feasibility of the Tn and Rn concentration adjustment by the chamber purge could be attributed to (a) the much smaller Rn emission from the soil at our site compared to Tn (see section 3.3), and (b) the likelihood for an alpha decay of a soil-emitted Tn or Rn nuclide to happen within the dynamic chamber volume. For the three flushing rates 33 %, 52 % and 92 % of the soil-emitted Tn isotopes decayed inside the dynamic chamber volume, whereas for Rn the much longer T_{0.5} caused only <0.04 % of the isotopes to decay within the chamber.

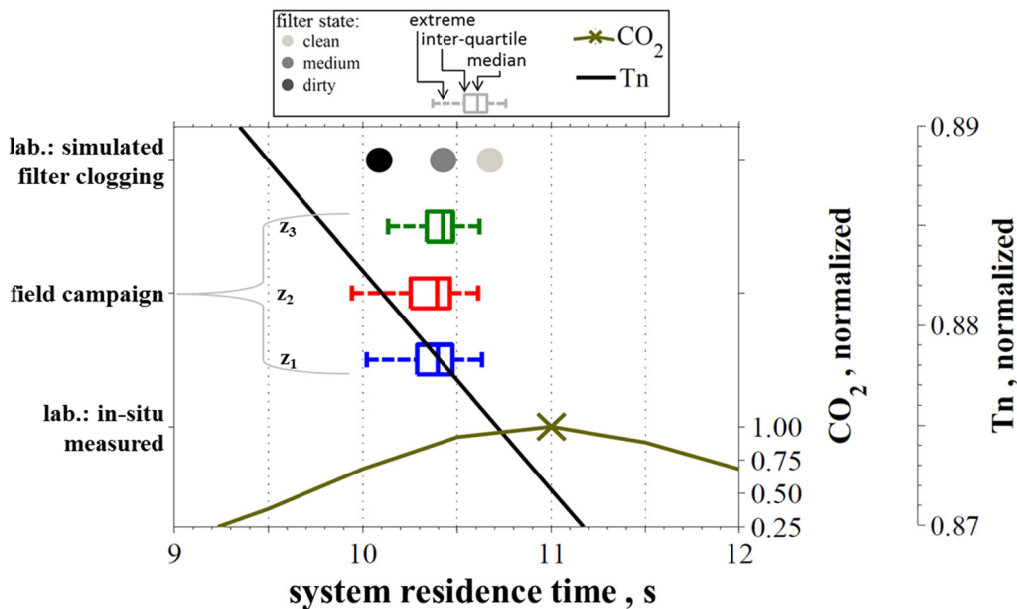


Fig. 5. Comparison of (i.) calculated residence times from the simulated filter clogging experiment in the laboratory (filled circles), (ii.) residence times determined from the field data set (z_1 - z_3 with median, inter-quartile range and extreme values) and (iii.) in-situ measured residence times (CO₂ experiment, green line) with (iv.) the resulting radioactive Tn decay (black line) calculated from Eq. (1).

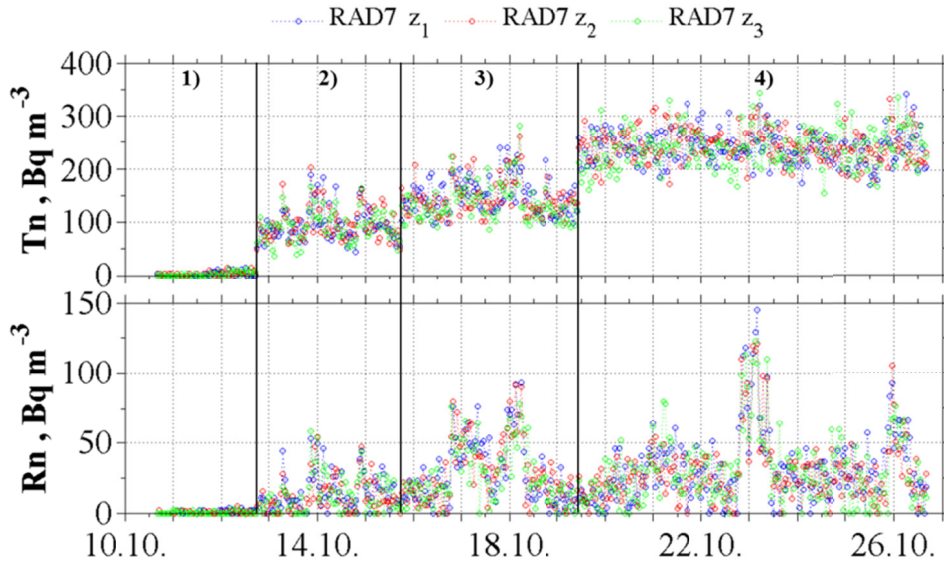


Fig. 6. Time series of Tn and Rn concentrations during sixteen days of side-by-side measurements (10-26 October 2011) measured with the RAD7 monitors (60 min integration time). After the zero air measurement (1) we purged the chamber with 70 L min⁻¹ (2), 35 L min⁻¹ (3), and 5 L min⁻¹ (4).

3.1.4 Limit of detection

The LOD for Tn (LOD_{Tn}) determined under field conditions with a 60 min integration time when purging the instruments with zero air during the sbs measurement varied by $\pm 20\%$ for the different RAD7 monitors. In contrast, the LOD_{Rn} was comparable for all RAD7s (Table 2). The determined LOD_{Tn} of 18.3 Bq m⁻³ for an integration time of 60 min was three times higher than that of Rn.

3.2 Systematic and random errors

Figure 7 shows an example for the determination of the systematic and random errors. The averaged random error $\sigma\Delta C$ for Tn and Rn were $\sigma\Delta C_{Tn} = 0.10 C + 13.2 \text{ Bq m}^{-3}$ and $\sigma\Delta C_{Rn} = 0.19 C + 9.5 \text{ Bq m}^{-3}$, respectively. Hence, the averaged random concentration errors σC (Eq. (3)) for Tn and Rn used for the Gaussian error propagation to estimate σ_τ were $\sigma C_{Tn} = \frac{0.10C + 13.2 \text{ Bq m}^{-3}}{\sqrt{2}}$ and $\sigma C_{Rn} = \frac{0.19C + 9.5 \text{ Bq m}^{-3}}{\sqrt{2}}$. Consequently, the Tn and Rn concentrations where $\sigma C/C = 1$ were 10.0 Bq m⁻³ and 7.8 Bq m⁻³, respectively. The obtained median precisions for three concentration classes ($>100 \text{ Bq m}^{-3}$, $100\text{-}15 \text{ Bq m}^{-3}$, $<15 \text{ Bq m}^{-3}$) were 8.8 %, 23.2 % and 132.1 % for Tn and 16.6 %, 25.0 %, 99.2 % for Rn, respectively.

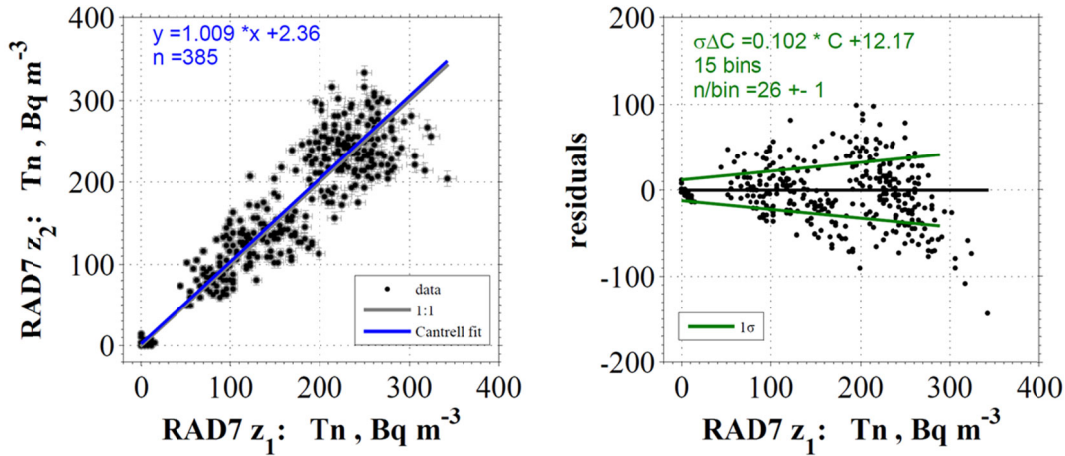


Fig. 7. Example of systematic and random error determination from side-by-side measurements. Left panel: determination of the systematic error of the Tn concentration between the RAD7 at z_1 and z_2 using the bivariate weighted linear least-squares fitting regression analysis by the Williamson-York method (Cantrell, 2008). Error bars represent the uncertainties from counting statistics of the RAD7 ($\sigma = \sqrt{n}$). Right panel: quantification of the random error ($\sigma\Delta C$) from the residuals around the fit (for details see section 2.5 and Wolff et al. (2010)).

3.3 Radon and Thoron concentration profiles

The soil at our measurement site is a much stronger source for Tn than for Rn (median of $C_{Rn}/C_{Tn} = 0.07$ at $z_1 = 0.04$ m). To explain our results, we have selected Tn and Rn concentration measurements of two days in block 2 (period 1) and two days in block 3 (period 2) (Fig. 8a-d) with the respective inlet height arrangements (see section 2.3, Fig. 3). Typical diurnal cycles with higher wind speeds during daytime and lower at nighttime were prevailing during both periods (Fig. 8e-f). The diurnal courses of measured Tn and Rn concentrations mirror the variation of the wind speed, with higher Tn and Rn concentrations during nighttime than during daytime. This is a typical pattern, since stable stratification in the air layer above the canopy top is known to inhibit vertical exchange during nighttime, while during daytime the vertical exchange is driven by turbulent mixing. Our temperature profile measurements (not presented) reveal that the transition from stable to unstable conditions took place after sunrise at around 06:00 LT (CET), and the transition from unstable to stable conditions some hours before sunset (20:00 LT) at around 16:00 to 17:00 LT. Tn concentrations ranged from 0 to 830 Bq m⁻³ and Rn concentrations ranged from 0 to 250 Bq m⁻³, both with highest concentrations close to the ground.

Table 2. Limit of detection (LOD in Bq m⁻³) of the RAD7 monitors (with the system characteristics described in section 2.2) determined under field conditions during the zero air measurements.

RAD7	LOD _{Tn}	mean LOD _{Tn}	LOD _{Rn}	mean LOD _{Rn}
z_1	18.1		5.8	
z_2	22.0	18.3	6.4	6.2
z_3	14.7		6.4	

A pronounced vertical Tn profile was measured during period 1 (Fig. 8a). The measured Tn concentration differences between z_1 and z_3 were about 400 Bq m^{-3} during midnight and about 130 Bq m^{-3} in the early afternoon. These values were typical for period 1 and the precision of the RAD7 monitors was sufficient to resolve significant vertical concentration differences. Obviously, this inlet height arrangement was optimal to determine vertical Tn concentration differences.

In contrast, we found that the inlet arrangement of period 1 was not suitable to measure significant vertical Rn concentration differences between all three heights (Fig. 8c). In particular, the daytime Rn concentrations at z_2 and z_3 were often within the random concentration error (see section 3.2) and the scatter of the concentrations further complicates the determination of significant Rn differences.

After increasing the inlet separation distance (period 2), the Tn concentration differences between z_1 and z_2 (Fig. 8b) are still significantly different from each other. The concentrations at z_1 and z_2 range from daytime values of 100 Bq m^{-3} and $\sim 20 \text{ Bq m}^{-3}$, respectively, to nighttime values of 600 Bq m^{-3} and $100\text{-}300 \text{ Bq m}^{-3}$, respectively. However, the Tn concentrations measured at $z_3 = 80 \text{ cm}$ are always below 30 Bq m^{-3} during period 2 and may occasionally reach the LOD_{Tn} .

The Rn nighttime profile (Fig. 8d) shows substantially higher concentration differences ($25 - 250 \text{ Bq m}^{-3}$) than during period 1. With this inlet arrangement the precision of the RAD7 monitors was sufficient to resolve significant vertical Rn concentration differences during nighttime.

3.4 Calculation of transport times and quality assurance

Since the subject of this paper is the description and evaluation of the novel automated measurement system, we will mainly focus on the data quality, rather than describe and interpret diurnal courses of the transport times. Transport times τ were calculated using the measured Tn concentrations (Fig. 8a,b) using Eq. (1). The propagation of previously determined random concentration errors (σ_C) enabled us to assign each value of τ with an absolute uncertainty (σ_τ) (see Eq. (4)). We assessed the data quality of τ using a classification according to the magnitude of the relative uncertainty. Three data quality classes were introduced ($\frac{\sigma_\tau}{\tau} < 0.5$: good; $0.5 \leq \frac{\sigma_\tau}{\tau} < 1$: adequate; $\frac{\sigma_\tau}{\tau} \geq 1$: inadequate quality).

The calculated transport times for the two investigated periods are shown in Fig. 9. Our setup allowed the calculation of τ for three layers within the canopy. The lower layer was between z_1 and z_2 (Fig. 9a,b), the upper layer between z_2 and z_3 (Fig. 9c,d) and the overall transport time between z_1 and z_3 (Fig. 9e,f). Due to the varying inlet height arrangements in period 1 and 2 the lower and upper layers were not identical. However, the overall transport time during period 1 (Fig. 9e) corresponds to the one of the lower layer in period 2 (Fig. 9b), representing the transport between 0.04 m and 0.20 m.

During period 1, with its more compact inlet arrangement closer to the ground both τ in the lower and in the upper layer ranged between 20 s and 150 s (Fig. 9a,c). The overall transport time of period 1 (Fig. 9e) corresponds to the sum of both other layers and indeed featured a similar diurnal pattern as in the lower layer during period 2 (Fig. 9b). These values were highest from around 06:00 to 12:00 LT ranging from 200 s to 300 s and were lower during nighttime (50 – 150 s). The diurnal course of τ in the upper and lower layer during period 2 were rather different from each other (Fig. 9b,d). In the lower layer τ ranged from nighttime minima of 100 s to midday maxima of about 300 s. In contrast, the τ

values in the upper layer featured maxima during nighttime of up to 350 s and daytime minima ranging from 10 s to 120 s. The overall transport time during period 2 (Fig. 9f) shows the largest values always above 120 s with maxima occasionally exceeding 400 s, which is attributed to the large layer thickness of 0.76 m.

The transport times calculated for period 1 generally show a better data quality than those for period 2 (pie diagrams in Fig. 9). For period 1, 94 %, 88 % and 98 % of the calculated τ values for the lower, upper and overall layer, respectively, are of good data quality. During period 2 the lower and overall layer show a comparably good data quality with 100 % and 94 % of the τ values with good quality, whereas 40 % and 42 % of the τ values in the upper layer are of adequate and inadequate data quality, respectively.

Calculated τ values belonging to the inadequate data quality class can be found at any time of the day and stand in many cases out of the general diurnal course (often as extreme values) in the corresponding plots (e.g., Fig. 9c, d and f).

4 Discussion

4.1 System performance

The presented system for the continuous determination of transport times near the ground is based on vertical Tn profile measurements at three heights using three RAD7 monitors that are selective for Tn and Rn. Although other examples for automated Tn profile measurements can be found in the literature (e.g., Lehmann et al., 1999; Nemitz et al., 2009; Gut et al., 2002; Hens, 2009), the major drawback of these studies is the application of a pair of non-selective monitors to measure a sequentially switched profile. Thus, the measured vertical concentration differences are prone to non-stationarities, particularly for longer integration times. While their method minimizes systematic errors between the measurement heights, the random error of the Tn concentration can be amplified since it is determined from the difference of two signals of non-selective monitors (for details see Lehmann et al., 1999). In contrast, the system of Butterweck et al. (1994), who operated a simultaneous profile consisting of four instruments that are selective for Tn and Rn, is not prone to non-stationarities. Nevertheless, none of the previous studies assessed systematic or random errors of the determined Tn concentration profiles and the calculated τ values. Such an analysis is crucial for applications with multiple analyzers and required for a thorough interpretation of the in-canopy transport.

The overall performance of the novel automated measurement system was satisfying, with a Tn recovery of 88 % that was relatively stable and comparable for all sampling lines. Our setup comprising PFA tubing, pumps, Nafion tubing and MFCs strongly modified the standard setup of the RAD7 monitors. The performance of the Nafion dryers was excellent with an average RH of 4 % in all RAD7 throughout the field experiment.

We found that the signal of the RAD7 at low concentrations is quite noisy. The higher LOD for Tn (18.3 Bq m^{-3}) than for Rn was largely caused by the lower sensitivity of the RAD7 for Tn. The LOD_{Tn} for the setup used e.g., in Lehmann et al. (1999) is not mentioned. Since they determine Tn as the sum of two AlphaGuard signals we assume that the LOD_{Tn} also exceeded LOD_{Rn} for their setup.

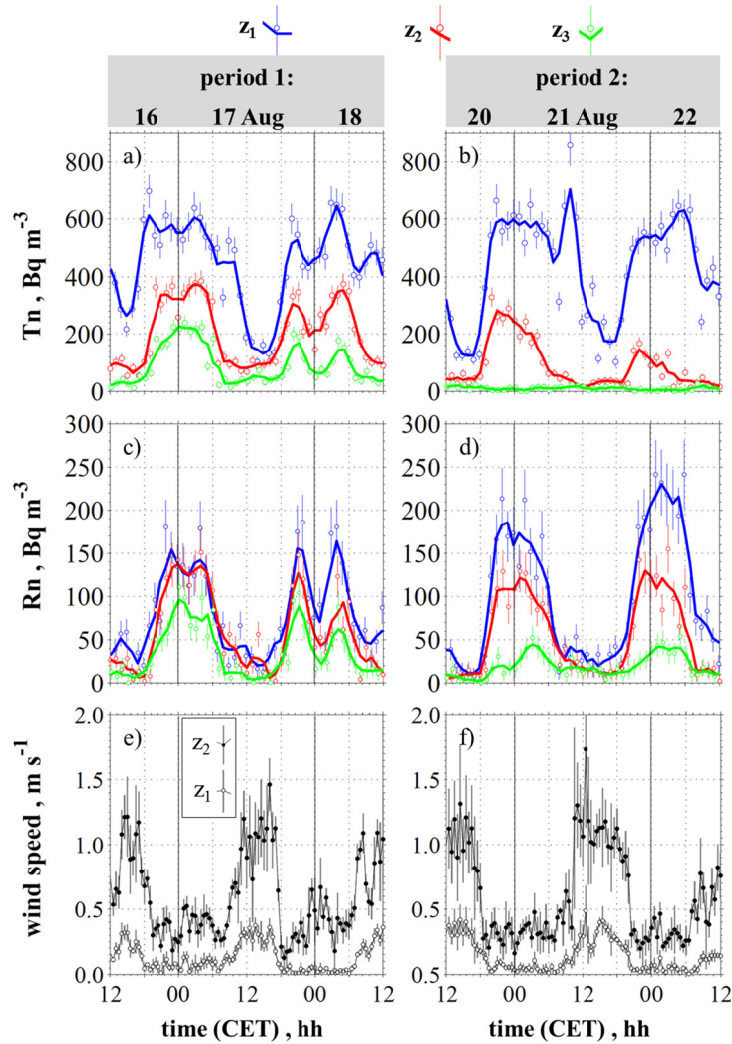


Fig. 8. Tn and Rn concentrations as well as wind speeds ($z_1 = 0.2$ m, $z_2 = 0.8$ m) measured during two periods with different inlet height arrangements (period 1: 16 – 18 Aug., period 2: 20 – 22 Aug., see Fig. 3). Dots with error bars in plots (a)–(d) represent the RAD7 concentration readings (integration time 60 min) and the corresponding random errors (σ_C). The solid lines show the running means (width: 3 hours) of the concentrations. In plots (e) and (f) 30 min averages of the measured wind speed are shown, where error bars represent standard deviations.

The determined mean LOD_{Rn} of 6.2 Bq m^{-3} (see Table 2) is high compared to that of Wada et al. (2010), who developed an electrostatic Rn system with an LOD_{Rn} between 0.16 and 0.2 Bq m^{-3} for 60 min integration time. They achieved this by operating it at a flow rate of 3 L min^{-1} and by using much larger measurement chambers of 32 l and 16.8 l volume, respectively. In contrast, the LOD_{Rn} of the AlphaGuard operated at 10 min integration time, as used in the studies of Lehmann et al. (1999), Nemitz et al. (2009) and Hens (2009), was determined to be 12 Bq m^{-3} by Hens (2009) and, therefore, twice as high as for the RAD7. The LOD comparison with the system used by Butterweck et al. (1994) was not possible due a lack of information on their system configuration.

The systematic error of the RAD7 for Tn determined in the PTB of 6 % to 8 % was somewhat higher than the results from the sbs measurements, which were in the order of 1 % to 3 % (cf. Fig. 7). Since

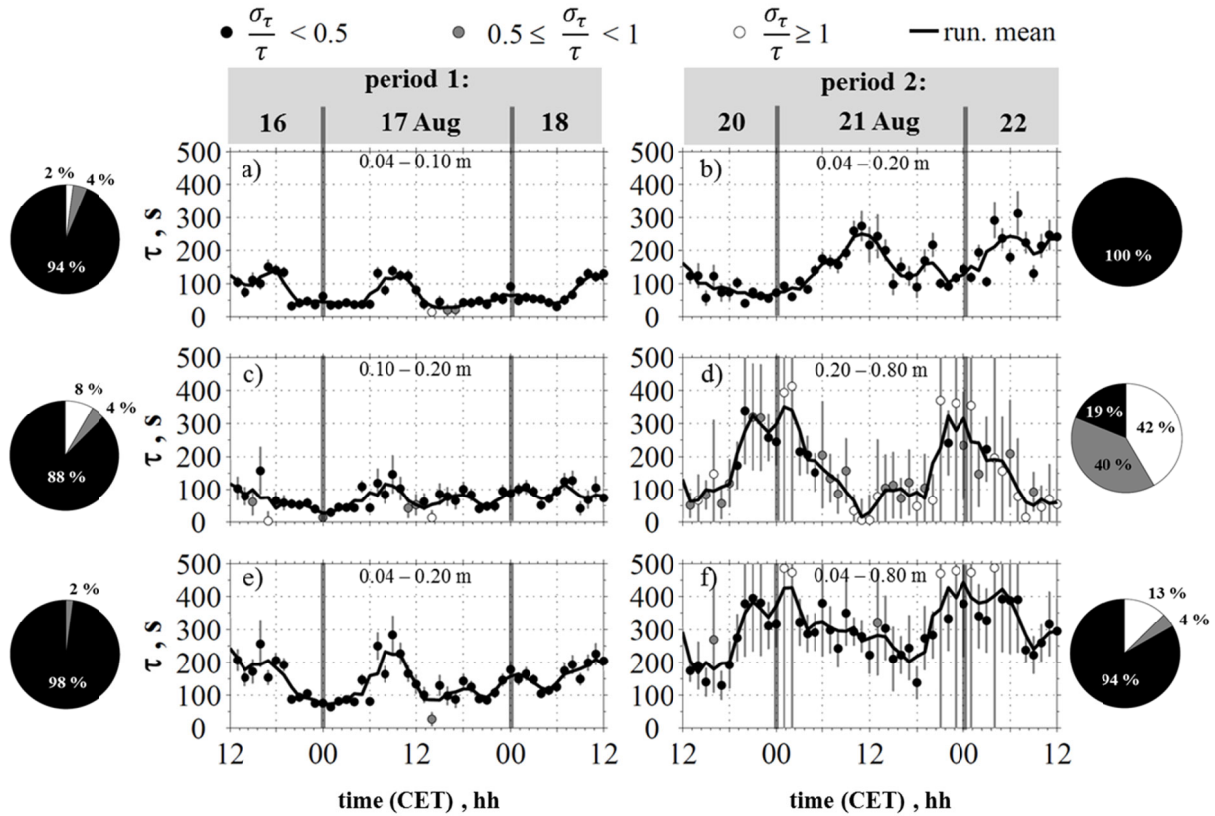


Fig. 9. Calculated transport times τ for three layers (lower (a,b), upper (c,d), and overall (e, f)) classified according to the magnitude of the relative uncertainty for the two selected periods. The error bars represent the absolute uncertainty of τ determined using Gaussian error propagation (Eq. (4)). The pie diagrams represent the percentage of τ in each quality class for the plots shown (black: good, grey: adequate, white: inadequate quality).

75 % of all measured Tn concentrations during the campaign were below 255 Bq m^{-3} , we consider the sbs result as representative for the systematic error of the Tn measurements. The manufacturer provided an Rn error of 2 % on the calibration certificates. The application of the bivariate regression analysis on the sbs data resulted in a systematic error for Rn in the range of 1 % to 6 %, which was corrected for.

The field measurements were conducted under partly harsh field conditions including changing temperatures and RHs for an extended period of two month, which is quite different to standard applications of the RAD7. The monitors proved to be suitable under all conditions at our field site to resolve vertical concentrations differences of Tn and also those of Rn under stable nighttime conditions. These findings, in combination with the comparably low price and the Tn and Rn selectivity of the RAD7 may be convincing arguments for equipping a profile system with these monitors. However, it has to be kept in mind that the analyzer precision is not sufficient for the low Tn and Rn concentrations found at the surface at many sites, and at heights exceeding a few meters above the surface at all sites.

4.2 Comparison of transport times with existing empirical parameterizations

A comparison of our transport times with those of Lehmann et al. (1999) and Nemitz et al. (2009) revealed a reasonable agreement for the lowest layer (0.04-0.2 m), although the canopy structure was probably quite different for all study sites. In addition, we compared our measured and quality controlled transport times with currently existing parameterizations that are used in models such as SURFATM (see Personne et al., 2009). The transport time is expressed as the total resistance multiplied with the layer thickness (h).

$$\tau(\text{surf atm}) = (R_{ac} + R_a(z_{ref})) \cdot h \quad (5)$$

where R_{ac} is the in-canopy and R_a the aerodynamic resistance (Thom, 1975) at the reference height ($z_{ref} = 0.8$ m). We calculated $\tau(\text{surf atm})$ for our overall layer (z_1 - z_3) and for data from block 3 according to Personne et al. (2009) (equations modified):

$$R_{ac} = \frac{h_c \cdot \exp(\alpha_u)}{\alpha_u \cdot K_m(h_c)} \cdot \left\{ \exp\left(\frac{-\alpha_u \cdot z_{0s}}{h_c}\right) - \exp\left(\frac{\alpha_u \cdot (d+z_0)}{h_c}\right) \right\} \quad (6)$$

$$R_a(z_{ref}) = \frac{1}{\kappa^2 \cdot u(z_{ref})} \cdot \left\{ \ln\left[\frac{Z}{z_0}\right] - \Psi_H(Z/L) \right\} \cdot \left\{ \ln\left[\frac{Z}{z_0}\right] - \Psi_M(Z/L) \right\} \quad (7)$$

where h_c is the canopy height, α_u ($= 4.2$) the attenuation coefficient for the decrease of the wind speed inside the plant cover, z_{0s} the ground surface roughness length, d the displacement height, z_0 the canopy roughness height, $K_m(h_c)$ the eddy diffusivity coefficient at h_c ($K_m = \kappa \cdot u_* \cdot (h_c - d)$), κ the von-kàrmàn constant, $u(z_{ref})$ the horizontal wind speed at z_{ref} , $Z = z_{ref} - d$, L the Monin-Obukhov length and Ψ_H and Ψ_M are the stability correction functions for heat and momentum, respectively. Furthermore, we compared our transport times with an empirical approach provided by van Pul and Jacobs (1994) used e.g., in the STOCHEM model (Sanderson et al., 2003), where the transport time is expressed as:

$$\tau(\text{vanPul}) = \left(\frac{13.9 \cdot LAI \cdot h_c^2}{u_*} \right) \quad (8)$$

where LAI is the single sided leaf area index. For our study, the LAI was 4.8 as determined by biomass harvest and photographic imagery of subsamples (harvested area: 0.29 m²) close to the inlets after the experiment. The values of u_* , z_{0s} , z_0 , d , L , Ψ_H , Ψ_M were estimated using standard micrometeorological methods (Foken, 2008).

Measured median transport times (τ) between z_1 and z_3 for all data from block 3 range between 350 s during nighttime to 220-290 s during daytime (Fig. 10). The values are in very good agreement with $\tau(\text{surf atm})$ during daytime from around 09:00 to 18:00 LT. However, nighttime values of $\tau(\text{surf atm})$ are significantly higher than the measured τ values and range between 700 s and 900 s. Although the transport in the layer just above the canopy is expressed by R_a , the value of $\tau(\text{surf atm})$ mainly depends on R_{ac} since the contribution of R_a is below 3 % at any time of the day. This reveals that the parameterization of R_{ac} by Personne et al. (2009) is not suitable to accurately calculate the in-canopy transport times during nighttime in this canopy. The reason for the much lower measured nighttime values of τ is the presence of unstable conditions and convective transport in the lowest part of the canopy, which was confirmed by measured temperature profiles (not shown). In contrast, $\tau(\text{vanPul})$ compares well with the measured τ values during nighttime, but is significantly lower during daytime with values of around 100 s. Since both parameterizations require u_* as input, which

typically features very high uncertainties during prevailing low wind speeds (mainly at nighttime), the contrasting results are remarkable. In addition, the Tn method showed a much smaller scatter than transport times derived from empirical parameterizations, as indicated by the inter-quartile range in Fig. 10.

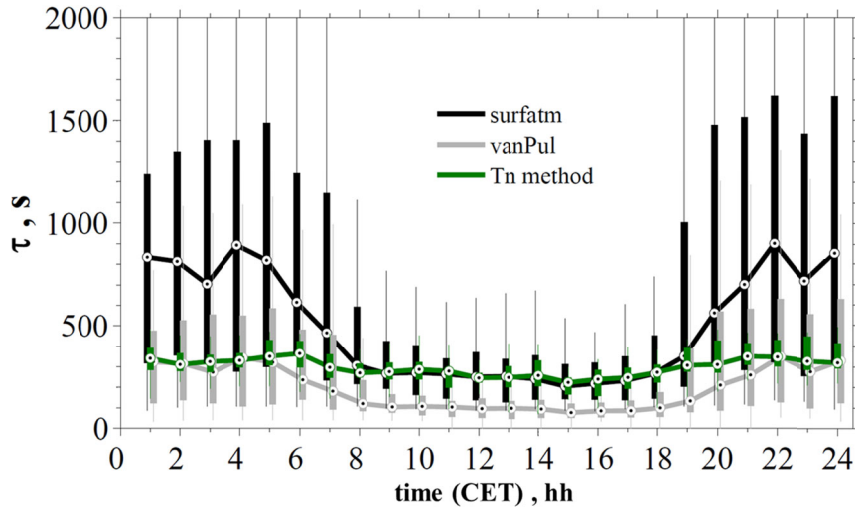


Fig. 10. Median diurnal course of measured transport times between 0.04 and 0.8 m using the Tn method (values of inadequate quality were rejected) compared to existing empirical parameterizations for all data from block 3 for the natural grassland site. The statistical distribution of the data sets is represented by hourly boxplots. The dots indicate the medians, the filled boxes cover the inter-quartile range and the whiskers represent the extreme data points.

4.3 Transport time uncertainty

Since during our experiment transport times of good quality and those of inadequate quality with high uncertainties were present, we conducted a detailed analysis to identify the inlet height arrangement with the optimal performance for the determination of transport times using the Tn method. The comparison of the τ values of inadequate quality with the measured Tn concentration profiles (Fig. 8) indicates that inadequate quality may occur when (a) the concentration differences are very small (e.g., Fig. 8a and Fig. 9c (z_2 and z_3)), or (b) the Tn concentration at the upper of both inlet heights (z_u) is very low (see Fig. 8b and Fig. 9d).

To investigate (a), we plotted the σ_τ values as a function of the measured Tn gradient for the entire Tn profile data set (51 days) including all inlet height arrangements (block 1 - 3) and heights (z_1 , z_2 , z_3), and found a strong exponential relationship (Fig. 11). Obviously, at high absolute gradients the uncertainty of the transport time is lowest and the uncertainty increases significantly with decreasing gradients. In order to obtain reliable values for the transport times with $\frac{\sigma_\tau}{\tau} < 0.5$ an absolute gradient of at least $1000 \text{ Bq m}^{-3} \text{ m}^{-1}$ is desirable. In the intermediate Tn gradient range between 1000 and $350 \text{ Bq m}^{-3} \text{ m}^{-1}$ the values of $\frac{\sigma_\tau}{\tau}$ range from 0.3 to 0.6 . To obtain τ values with $\frac{\sigma_\tau}{\tau}$ smaller than unity the

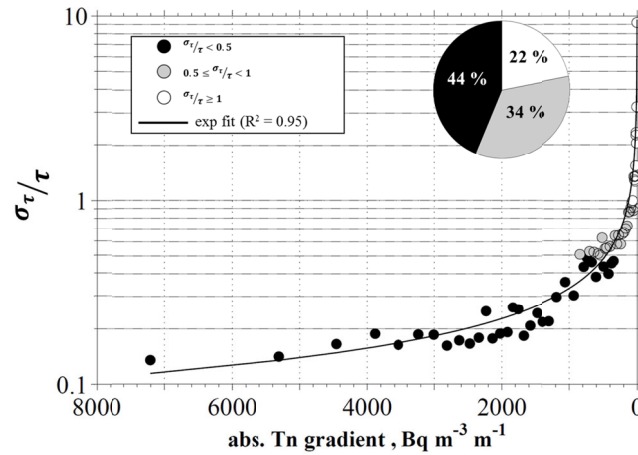


Fig. 11. Dependency of the relative uncertainty of the transport time (σ_τ/τ) on the absolute Tn gradient for the entire data set (51 days) including all inlet height arrangements (block 1 - 3) and heights (z_1, z_2, z_3). The data were sorted by the magnitude of the Tn gradient and averages of bins ($n = 50$) were calculated before the exponential fit was made. The pie diagram summarizes the fraction of τ values in each quality class (black: good, grey: adequate, white: inadequate quality (for details see text)).

gradient should not be $< 70 \text{ Bq m}^{-3} \text{ m}^{-1}$. Using the findings from Fig. 11 we are able to deduce a minimal Tn concentration difference that has to be measured between two inlet heights in order to determine transport times of good quality. For example during period 1 between z_1 and z_2 (0.04 m and 0.1 m) this value is 60 Bq m^{-3} , which is prevailing at any time. Additionally, the dependency of $\frac{\sigma_\tau}{\tau}$ on the Tn gradient underlines the importance of a careful choice of the inlet heights.

Of all determined τ values (block 1 - 3, z_1, z_2, z_3), 44 % are of good quality (pie diagram in Fig. 11), followed by 34 % and 22 % in the adequate and inadequate quality class, respectively. The data quality of the τ values presented for period 1 and 2 (pie diagrams in Fig. 9) is higher than the overall data quality, except for the upper layer during period 2 (Fig. 9d). Period 2 represents the inlet height arrangement during block 3 (Fig. 3), which is the longest of the three blocks and lowers the overall data quality mainly due to the low data quality in the upper layer. This can be explained by (b) the influence of the measured Tn concentration at the upper inlet height ($C_{Tn_{z_u}}$ in Eq. (1)) on σ_τ , which we compare with the effect of the Tn concentration at the lower inlet height ($C_{Tn_{z_l}}$) on σ_τ (shown using the values measured at z_2 and z_1 (Fig. 12)). While the values of $C_{Tn_{z_u}}$ were found to have a strong influence on the magnitude of σ_τ (following a power function), the values of $C_{Tn_{z_l}}$ showed only a weak impact. Higher values of $C_{Tn_{z_u}}$ result in low absolute σ_τ values and lower $C_{Tn_{z_u}}$ values cause a substantial increase of σ_τ . Since the soil is the Tn source and z_u is located at a higher distance from the ground than z_l , lower Tn concentrations are expected to be measured at z_u . This fact automatically increases the probability that $C_{Tn_{z_u}}$ is close to or below the LOD, where the relative value of $\sigma C_{Tn_{z_u}}$ can be close to or even higher than unity. Since $\sigma C_{Tn_{z_u}}$ is propagated it may cause very high values of

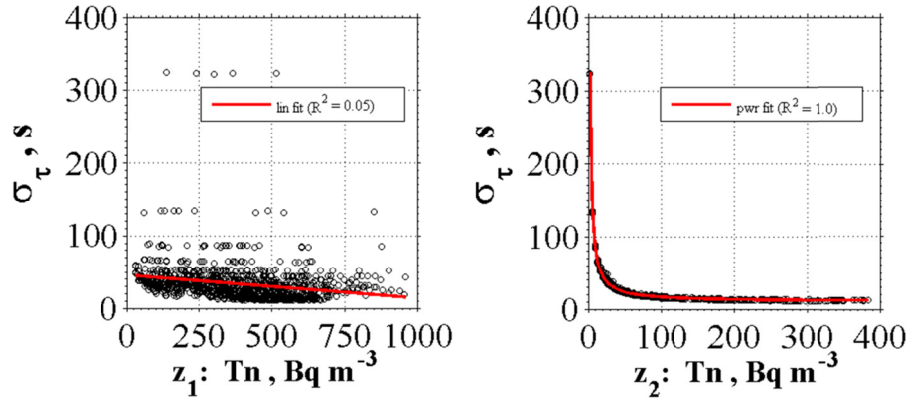


Fig. 12. Dependency of the absolute uncertainty of the transport time (σ_t) on the Tn concentrations measured at the lower ($C_{Tn_{z_l}}$) and upper ($C_{Tn_{z_u}}$) inlet positions using the data from z_1 (left panel) and z_2 (right panel) for the entire data set (51 days) including all inlet height arrangements (block 1 - 3).

σ_t . Furthermore, $C_{Tn_{z_u}}$ is the denominator in Eq. (1) and thus strongly impacts τ . Consequently, a more compact vertical inlet height arrangement will provide more reliable τ values. The vertical limit of the inlet height separation for our system at any site can be assessed by applying the results in Fig. 11.

4.4 Contribution of individual error propagation terms

We additionally quantified the contribution of the individual error propagation terms A, B and C (Eq. (4)) to the total transport time uncertainty σ_t . Note that the sum of error terms A and B can be reduced by term C (cf. Eq. 4). Figure 13 presents the error partitioning as a function of the $C_{Tn_{z_l}}/C_{Tn_{z_u}}$ ratio for our entire Tn dataset. Generally, terms A and B contribute with up to 50 % and 50-100 % to the overall uncertainty σ_t , respectively. This highlights the strong impact of $C_{Tn_{z_u}}$ on σ_t . Term A shows a tendency to shift from 0 % to 50 % with a decreasing Tn concentration ratio $C_{Tn_{z_l}}/C_{Tn_{z_u}}$ (Fig. 13). For example, during periods with $C_{Tn_{z_l}}/C_{Tn_{z_u}}$ ratios below 2.5 the terms A and B contribute to the total uncertainty with about 30-50 % and 70-50 %, respectively. In contrast, under conditions when the $C_{Tn_{z_l}}/C_{Tn_{z_u}}$ ratio is higher than 2.5, term B can account for up to 100 % to the total uncertainty. In other words, in cases when the Tn concentration at the upper measurement height is very small, the error in the calculated value of τ is dominated by errors in the upper measurement height. We found that term C can reduce the sum of term A and B by 0-43 % for our dataset (not shown), and strongly depends on the correlation coefficient $r_{(C_{Tn_{z_l}}, C_{Tn_{z_u}})}$ of the measured Tn concentrations at the two heights.

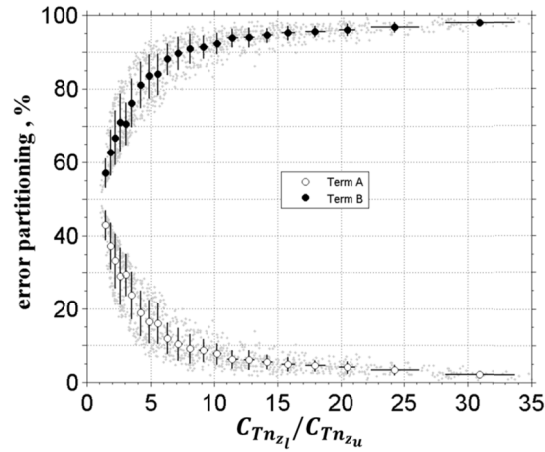


Fig. 13. The error partitioning of Term A and B in Eq. (4) as a function of the $C_{Tn_{z_1}}/C_{Tn_{z_u}}$ ratio for the entire data set (51 days) including all inlet height arrangements (block 1 - 3) and heights (z_1, z_2, z_3).

5 Summary and conclusions

We present and characterize a novel automated system for the measurement of vertical Tn and Rn profiles near the ground. In contrast to most previous studies, we perform continuous measurements with one single instrument per inlet height using commercially available monitors (RAD7) that are selective for Tn and Rn. Hence, the major progress of the system is its suitability for the direct determination of the in-canopy transport time from vertical Tn concentration differences. We found that the system, including optimized chambers, alpha detectors and flows, is suitable to detect vertical differences of Tn and also those of Rn close to a relatively strong source (e.g., in low canopies). The performance of the system was investigated by considering (a) residence times of the air in the system, including the effect of filter clogging, (b) validation of the Tn sensitivity using a primary standard, (c) determination of the limits of detection, and (d) a rigorous determination of systematic and random errors for Tn concentrations measured under field conditions. These achievements were the prerequisite to analyze the inlet height arrangements required to obtain a high data quality. The system was operated during an intensive field campaign for two months at a natural grassland ecosystem. Vertical concentration profiles of Tn and Rn for two periods with different inlet height arrangements are presented. For the first time, we calculate transport times (τ) directly from selectively measured Tn concentration profiles and propagate the uncertainty of the in-canopy transport time (σ_τ) from the random Tn concentration errors (σC_{Tn}). The averaged σC for Tn and Rn was determined to be $\sigma C_{Tn} = \frac{0.10C + 13.2 \text{ Bq m}^{-3}}{\sqrt{2}}$ and $\sigma C_{Rn} = \frac{0.19C + 9.5 \text{ Bq m}^{-3}}{\sqrt{2}}$. A quality assessment of the transport times revealed a good data quality with relative uncertainties below 50 % for 44 % of all determined transport times during the field experiment. The occasional occurrence of transport time uncertainties higher than 100 % are related to measured absolute Tn gradients below 70 Bq m⁻³ m⁻¹ and occur for 22 % of all calculated transport times. Large gradients cause smaller relative transport time errors. In addition, the

method appears highly sensitive to the Tn concentration measured in the upper height ($C_{Tn_{z_u}}$). Low values of $C_{Tn_{z_u}}$ result in high absolute values of σ_τ . An analysis of the contribution of individual error propagation terms to σ_τ underlines these findings. It should be noted that to obtain large gradients it is preferable to increase the vertical separation of the measurement heights. For Rn, this is possible to some extent since $C_{Rn_{z_u}}$ decreases only as a result of dilution by turbulence. However, the vertical inlet separation is much more limited for the determination of the transport time by the fast Tn decay due to sharply decreasing values of C_{Tn} with height. Consequently, the analyzer with the best precision should always be placed in the uppermost height, whose position has to be chosen very carefully. The major requirement for the future is the improvement of the RAD7 precision at low concentrations, which implies a decrease of the LOD. This might be achieved by further increasing the size of the measurement chamber as well as the active surface area of the alpha detectors.

Our setup allows the quantification of τ within the grass canopy for different layers. The transport times may subsequently be converted into a vertical profile of bulk diffusion coefficients. Our results provide an excellent basis for a reliable investigation of turbulence-chemistry interactions (e.g., Damköhler number) in canopies. The uncertainties of τ values determined with the Tn or Rn method should be considered for the interpretation of results in further studies.

Acknowledgements

This project was funded by the Max Planck Society. We are grateful to H. Gross for the electrical installations at the field site and for logistical support. We thank D. Lane-Smith for discussing the setup of the system and M. Flanz at the electronic department of MPIC for support with the data acquisition. We are indebted to A. Röttger at the Physikalisch-Technische Bundesanstalt (PTB, Braunschweig, Germany) for her help to validate the sensitivity of the RAD7 monitors for Thoron.

References

- Brost, R.A. and Chatfield, R.B.: Transport of radon in a 3-dimensional, subhemispheric model. *Journal of Geophysical Research-Atmospheres*, 94(D4): 5095-5119, Doi 10.1029/Jd094id04p05095, 1989
- Butterweck, G., Reineking, A., Kesten, J. and Porstendörfer, J.: The Use of the natural radioactive noble-gases radon and thoron as tracers for the study of turbulent exchange in the atmospheric boundary-layer - case-study in and above a wheat field. *Atmospheric Environment*, 28(12): 1963-1969, 1994
- Cantrell, C.A.: Technical note: review of methods for linear least-squares fitting of data and application to atmospheric chemistry problems. *Atmos Chem Phys*, 8(17): 5477-5487, 2008
- Currie, L.A.: Limits for qualitative detection and quantitative determination - application to radiochemistry. *Anal Chem*, 40(3): 586-593, 10.1021/ac60259a007, 1968
- De Arellano, J., Duynkerke, P.G. and Builtjes, P.J.H.: The divergence of the turbulent-diffusion flux in the surface-layer due to chemical-reactions - the NO-O₃-NO₂ System. *Tellus Series B-Chemical and Physical Meteorology*, 45(1): 23-33, DOI 10.1034/j.1600-0889.1993.00002.x, 1993
- Denmead, O.T. and Bradley, E.F.: Flux-gradient relationships in a forest canopy. In: B.A. Hutchinson and B.B. Hicks (Editors), *The Forest-Atmosphere Interaction*. Reidel, Dordrecht, pp. 421 1985.
- Dlugi, R. et al.: Turbulent exchange and segregation of HO_(x) radicals and volatile organic compounds above a deciduous forest. *Atmos Chem Phys*, 10(13): 6215-6235, DOI 10.5194/acp-10-6215-2010, 2010

- Dorr, H., Kromer, B., Levin, I., Munnich, K.O. and Volpp, H.J.: CO₂ and radon 222 as tracers for atmospheric transport. *J Geophys Res-Oc Atm*, 88(Nc2): 1309-1313, 1983
- Finnigan, J.: Turbulence in plant canopies. *Annu Rev Fluid Mech*, 32: 519-571, DOI 10.1146/annurev.fluid.32.1.519, 2000
- Foken, T., *Micrometeorology*. Springer, Berlin, Heidelberg 306 pp., 2008.
- Gut, A. et al.: Exchange fluxes of NO₂ and O₃ at soil and leaf surfaces in an Amazonian rain forest. *Journal of Geophysical Research-Atmospheres*, 107(D20): LBA 27-1–LBA 27-15, DOI: 10.1029/2001JD000654, 2002
- Hänsel, H. and Neumann, W., 1995. *Physik*. Spectrum, Akad. Verl., Heidelberg, Berlin, Oxford.
- Hens, K.: Der bodennahe, vertikale, turbulente Transport von ²²²Rn, ²²⁰Rn und anderen Spurengasen im Stammraum eines Fichtenbestandes, Johannes Gutenberg - Universität, Mainz, 93 pp 2009 (in German).
- Ikebe, Y. and Shimo, M.: Estimation of vertical turbulent diffusivity from thoron profiles. *Tellus*, 24(1): 29-37, 10.1111/j.2153-3490.1972.tb01530.x, 1972
- Israel, G.W.: Thoron (Rn220) measurements in the atmosphere and their application in meteorology. *Tellus Series B-Chemical and Physical Meteorology*, 17(3): 383-388, 1965
- Lehmann, B.E., Lehmann, M., Neftel, A., Gut, A. and Tarakanov, S.V.: Radon-220 calibration of near-surface turbulent gas transport. *Geophysical Research Letters*, 26(5): 607-610, 1999
- Lide, D.R., 2004. *CRC handbook of chemistry and physics : a ready-reference book of chemical and physical data*. CRC Press, Boca Raton, 2589 pp.
- Liu, S.C., McAfee, J.R. and Cicerone, R.J.: Radon 222 and tropospheric vertical transport. *J Geophys Res*, 89(D5): 7291-7297, 1984
- Martens, C.S. et al.: Radon fluxes in tropical forest ecosystems of Brazilian Amazonia: night-time CO₂ net ecosystem exchange derived from radon and eddy covariance methods. *Global Change Biology*, 10(5): 618-629, 2004
- Mauder, M. and Foken, T.: Documentation and instruction manual of the eddy-covariance software package TK3. *Arbeitsergebnisse Nr. 46(46)*, 2011
- Nemitz, E. et al.: Turbulence characteristics in grassland canopies and implications for tracer transport. *Biogeosciences*, 6(8): 1519-1537, 2009
- Pape, L., Ammann, C., Nyfeler-Brunner, A., Spirig, C., Hens, K. and Meixner, F.X.: An automated dynamic chamber system for surface exchange measurement of non-reactive and reactive trace gases of grassland ecosystems. *Biogeosciences*, 6(3): 405-429, DOI 10.5194/bg-6-405-2009, 2009
- Personne, E. et al.: SURFATM-NH3: a model combining the surface energy balance and bi-directional exchanges of ammonia applied at the field scale. *Biogeosciences*, 6(8): 1371-1388, DOI 10.5194/bg-6-1371-2009, 2009
- Röttger, A. and Honig, A.: Recent developments in radon metrology: new aspects in the calibration of radon, thoron and progeny devices. *Radiation Protection Dosimetry*, 145(2-3): 260-266, Doi 10.1093/Rpd/Ncr047, 2011
- Sanderson, M.G., Collins, W.J., Derwent, R.G. and Johnson, C.E.: Simulation of global hydrogen levels using a lagrangian three-dimensional model. *J Atmos Chem*, 46(1): 15-28, Doi 10.1023/A:1024824223232, 2003
- Simon, E. et al.: Lagrangian dispersion of Rn-222, H₂O and CO₂ within Amazonian rain forest. *Agricultural and Forest Meteorology*, 132(3-4): 286-304, 2005
- Staudt, K., Serafimovich, A., Siebicke, L., Pyles, R.D. and Falge, E.: Vertical structure of evapotranspiration at a forest site (a case study). *Agricultural and Forest Meteorology*, 151(6): 709-729, DOI 10.1016/j.agrformet.2010.10.009, 2011
- Taylor, J.R., 1997. *An introduction to error analysis. The study of uncertainties in physical measurements*. University Science Books, Sausalito, California.

- Thom, A.S.: Momentum, mass and heat exchange of plant communities. In: J.L. Monteith (Editor), *Vegetation and the Atmosphere*. Academic Press, London, pp. 57-109 1975.
- Trumbore, S.E., Keller, M., Wofsy, S.C. and Dacosta, J.M.: Measurements of soil and canopy exchange-rates in the Amazon rain-forest using Rn-222. *Journal of Geophysical Research-Atmospheres*, 95(D10): 16865-16873, 1990
- Ussler, W., Chanton, J.P., Kelley, C.A. and Martens, C.S.: Radon-222 tracing of soil and forest canopy trace gas-exchange in an open canopy boreal forest. *Journal of Geophysical Research-Atmospheres*, 99(D1): 1953-1963, 1994
- van Pul, W.A.J. and Jacobs, A.F.G.: The conductance of a maize crop and the underlying soil to ozone under various environmental-conditions. *Boundary-Layer Meteorology*, 69(1-2): 83-99, 1994
- Wada, A., Murayama, S., Kondo, H., Matsueda, H., Sawa, Y. and Tsuboi, K.: Development of a compact and sensitive electrostatic radon-222 measuring system for use in atmospheric observation. *J Meteorol Soc Jpn*, 88(2): 123-134, DOI 10.2151/jmsj.2010-202, 2010
- Wolff, V., Trebs, I., Ammann, C. and Meixner, F.X.: Aerodynamic gradient measurements of the NH₃-HNO₃-NH₄NO₃ triad using a wet chemical instrument: an analysis of precision requirements and flux errors. *Atmos Meas Tech*, 3(1): 187-208, 2010
- Yienger, J.J. and Levy, H.: Empirical-model of global soil-biogenic NO_x emissions. *Journal of Geophysical Research-Atmospheres*, 100(D6): 11447-11464, DOI 10.1029/95jd00370, 1995
- Zahorowski, W., Chambers, S.D. and Henderson-Sellers, A.: Ground based radon-222 observations and their application to atmospheric studies. *Journal of Environmental Radioactivity*, 76(1-2): 3-33, 2004
- Zhang, K., Wan, H., Zhang, M. and Wang, B.: Evaluation of the atmospheric transport in a GCM using radon measurements: sensitivity to cumulus convection parameterization. *Atmos Chem Phys*, 8(10): 2811-2832, 2008

APPENDIX C

Comparison of ozone deposition measured with the dynamic chamber and the eddy covariance method

D. Plake¹, P. Stella^{1*}, A. Moravek¹, J.-C. Mayer^{1**}, C. Ammann², A. Held³
and I. Trebs^{1***}

[1] Max Planck Institute for Chemistry, Biogeochemistry Department, P. O. Box 3060, 55020 Mainz, Germany.

[2] Agroscope Research Station, Climate and Air Pollution Group, 8046 Zürich, Switzerland.

[3] University of Bayreuth, Junior Professorship in Atmospheric Chemistry, Bayreuth, Germany.

* now at: AgroParisTech, UMR INRA/ AgroParisTech SAD-APT, Paris, France

** now at: Hessian Agency for the Environment and Geology, 65203 Wiesbaden, Germany.

*** now at: Centre de Recherche Public - Gabriel Lippmann, Department Environment and Agro-biotechnologies, 41 rue du Brill, L-4422 Belvaux, Luxembourg

Correspondence to: D. Plake (daniel.plake@mpic.de)

Submitted to Agricultural and Forest Meteorology: 16 January 2014

Abstract

Nowadays, eddy covariance is the state-of-the-art method to quantify turbulent exchange fluxes in the surface boundary layer. In the absence of instruments suitable for high-frequency measurements, fluxes can also be determined using e.g., chamber techniques. However, up to date fluxes of depositing compounds were rarely determined using chamber techniques, mainly due to a modification of the aerodynamic conditions for the trace gas transport within the chamber. In this study, we present ozone (O_3) deposition fluxes measured by the dynamic chamber technique and validate them against the eddy covariance (*EC*) method for a natural grassland site in Germany. The chamber system presented in Pape et al. (2009) was used and optimized to (i) reduce the likelihood of non-stationarities, (ii) yield 30 min averages of flux measurements and (iii) supply simultaneous profile measurements. The raw O_3 fluxes of the dynamic chamber were corrected for gas-phase chemistry in the chamber volume and for the modification of the aerodynamic resistances. Simultaneously measured carbon dioxide and

water vapor fluxes by both methods compared well during daytime documenting an equal vegetation activity inside and outside the chambers. The final corrected O₃ deposition fluxes of both methods deviated on average by only 11 % during daytime. The findings demonstrate the capability of the dynamic chamber method to capture representative O₃ deposition fluxes for grassland ecosystems, even when the canopy height is similar to the chamber height. The canopy resistance to O₃ was assessed by both methods and showed a characteristic diurnal cycle with minimum hourly median values of 180 s m⁻¹ (chambers) and 150 s m⁻¹ (*EC*) before noon. During nighttime the flux and resistance results showed a higher uncertainty for both methods due to frequent low wind associated with non-stationary conditions at the experimental site. Canopy resistances for nitrogen dioxide (NO₂) deposition were determined analogously with the chambers and showed on average 86 % higher values than for O₃.

Keywords: Ozone flux, eddy covariance, dynamic chamber, dry deposition, canopy resistance, flux partitioning

1 Introduction

Tropospheric ozone (O₃) is a well-known greenhouse gas, accounting for 25 % of the net radiative forcing attributed to human activities since the beginning of the industrial era and is among the largest contributors to radiative forcing (Forster et al., 2007). Since the pre-industrial era, mean annual O₃ concentrations have increased due to human activities from 10 ppb to between 20 and 45 ppb depending on the geographical location (Vingarzan, 2004). O₃ concentrations will probably continue to rise in the next century: according to Meehl et al. (2007), mean global O₃ concentration could increase by 20–25 % between 2015 and 2050. Because of its oxidative capacity, O₃ is also a widespread air pollutant and is responsible for damages to plants. In this way it is causing a reduction of the CO₂ sink of terrestrial ecosystems and, thus, also indirectly contributing to global warming (e.g., Felzer et al., 2007; Sitch et al., 2007). Consequently, control strategies based on flux-oriented dose-response relationships are crucial to protect vegetation as well as to mitigate climate change effects, and they require O₃ flux measurements for representative ecosystems as scientific base (Grünhage et al., 2000).

O₃ removal from the troposphere predominantly occurs through dry deposition to the Earth's surface. Since O₃ is hardly soluble in water, it is deposited mainly to terrestrial ecosystems (Fowler et al., 2009). Since the terrestrial deposition depends on vegetation and soil characteristics that vary in space and time, the quantitative description of processes governing O₃ deposition is still poor, and, therefore, the estimation of the current tropospheric O₃ budget as well as the projections of future climate are limited (Wild, 2007). Hence, the accurate quantification of O₃ exchange fluxes between the atmosphere and the biosphere (including a large variety of ecosystems) is a major challenge in current atmospheric research.

Large efforts have been made during the last decades to develop methodologies to quantify the surface-atmosphere exchanges of trace gases such as O₃. The most commonly applied methods are (i) micrometeorological approaches like eddy covariance (*EC*) and profile methods (Foken, 2008), and (ii) enclosure techniques using static or dynamic chambers (Denmead, 2008). While micrometeorolog-

ical methods allow measurements at the landscape scale (from about one hectare to several square kilometers), chambers represent much smaller spatial scales (around 1 m²).

The *EC* technique is the most direct and sophisticated method often used as a reference for the measurement of surface-atmosphere exchange fluxes of greenhouse gases. This was favored by the development of sonic anemometers and fast response trace gas analyzers. The method is extensively used in CO₂ and energy flux measurement networks such as CarboEuroFlux, (Aubinet et al., 2000), AmeriFlux (Running et al., 1999), Fluxnet (Baldocchi et al., 2001), and CarboEurope (Dolman et al., 2006). However, for other trace gases like O₃ fast response trace gas sensors are not always available or might be too expensive. Moreover, micrometeorological methods can be mathematically complex and expensive. In contrast, chambers offer low-cost and spatially/temporally flexible measurements of exchange fluxes based on a relatively simple operating principle (Denmead, 2008). In contrast to micrometeorological methods, they can be used to investigate small vegetation plots e.g. in multiple factor experiments or to investigate spatial heterogeneity effects. When applied on larger ecosystems, the small spatial scale of an individual chamber has to be compensated by operating several chambers simultaneously (e.g., Laville et al., 2009; Pape et al., 2009).

A variety of studies have used dynamic chambers to measure emission fluxes of reactive trace gases like nitric oxide (NO) (e.g., Gut et al., 2002b; Pape et al., 2009), ammonia (Amon et al., 2006) or volatile organic compounds (VOCs) (e.g., Bourtsoukidis et al., 2012; Kesselmeier et al., 1998; Pape et al., 2009) from soils, plants or other surfaces. However, only few studies used this technique to determine deposition fluxes of compounds like O₃ (e.g., Gut et al., 2002a). This is mainly due to difficulties associated with the application of the chamber itself, which modifies the aerodynamic and boundary layer resistances above the surface and, consequently, also the deposition flux (Pape et al., 2009).

NO, O₃ and nitrogen dioxide (NO₂) constitute a triad that undergoes fast chemical reactions. Thus, experiments investigating at least one member of the triad often measure all three compounds simultaneously to correct for chemical reactions. This is true, e.g., for dynamic chamber experiments that investigate biogenic NO soil emissions (see literature survey in Pape et al., 2009). Such dynamic chamber experiments could be used to improve the coverage of deposition flux observations if the difficulties mentioned above can be overcome.

In this study, we investigate the comparability of fluxes measured simultaneously by dynamic chambers and *EC* at a natural grassland ecosystem in Germany. After examining the fluxes of the non-reactive trace gases CO₂ and H₂O for comparability of vegetation activity in the footprint, the study focuses on the O₃ flux measurements with both techniques. The O₃ chamber fluxes were corrected for chemical reactions and for modified turbulence in the chambers and are compared to *EC* fluxes, which serve as a reference. In addition, the partitioning of observed O₃ fluxes into stomatal and non-stomatal uptake and the application of the chamber method for NO₂ deposition measurements are illustrated.

2 Material and Methods

2.1 Site description

An intensive field campaign was performed from July to September 2011 at a natural nutrient-poor steppe-like grassland ecosystem on the estate of the Mainz-Finthen Airport in Rhineland-Palatinate, Germany (49.9685°N, 8.1481°E). The grassland ecosystem had only occasionally been subject to management activities such as e.g., sheep grazing in the past. The site was topographically situated on a plateau besides the Rhine valley and located about 9 km south-west of the city center of Mainz. Smaller villages and motorways surrounded the site in a distance of 2 to 6 km and 4 to 15 km, respectively. The largest fetch without significant anthropogenic pollution sources was in the south-western sector of the site. The mean canopy height (h_c) during the field campaign was 0.6 m. A leaf area index (*LAI*) profile including three heights (0.05 m, 0.07 m, 0.20 m) was determined with an *LAI*-meter (*LAI*-2000, Licor Bioscience, Lincoln, USA) near the dynamic chambers on 18 August 2011. Additionally, the plant species enclosed by the dynamic chambers were determined. The *LAI* for green and brown leaves in each chamber was assessed by biomass harvest and photographic imagery of subsamples using the software ImageJ (National Institute of Health, Bethesda, USA).

2.2 Meteorological parameters

Standard meteorological parameters were measured at a tripod mast (Fig. 1) and recorded by a data logger (CR3000, Campbell Scientific Inc., USA) every 10 s. Global radiation and NO₂ photolysis frequency (j_{NO_2}) were measured at a height of 2.5 m with a net radiometer (CNR1, Kipp&Zonen, Delft, Netherlands) and a filter radiometer (Meteorology Consult GmbH, Glashütten, Germany), respectively. Gaps in the j_{NO_2} time series were filled by using a parameterization based on global radiation (Trebs et al., 2009). Rainfall was recorded at 1 m height by a rain gauge (AGR100, Environmental Measurements, North Shields, UK). Temperature and relative humidity (*RH*) were measured at 2.5 m height using a combined transmitter (HMT337, Vaisala, Helsinki, Finland) located in a ventilated housing. Wind speed was measured at 2.5 m height by a 2D ultra sonic anemometer (WS425, Vaisala, Helsinki, Finland).

2.3 Eddy covariance measurements

The *EC* technique is the most direct approach for the measurement of turbulent exchange fluxes in the surface boundary layer and has been extensively used during the last decades. The method and its theoretical background are well described in the literature (e.g., Foken et al., 2012) and will not be detailed hereafter.

The three-dimensional wind and temperature fluctuations were measured at the *EC* mast (Fig. 1) at 3.0 m above ground by a sonic anemometer (CSAT-3, Campbell Scientific Inc., Logan, USA). CO₂ and H₂O fluctuations were detected by a fast response open-path CO₂/H₂O infrared gas analyzer (IR-GA LI-7500A, LI-COR, USA) installed in a lateral distance of 0.25 m to the sonic path. Highly time-resolved O₃ concentrations were measured by a high-frequency, dry chemiluminescence O₃ detector

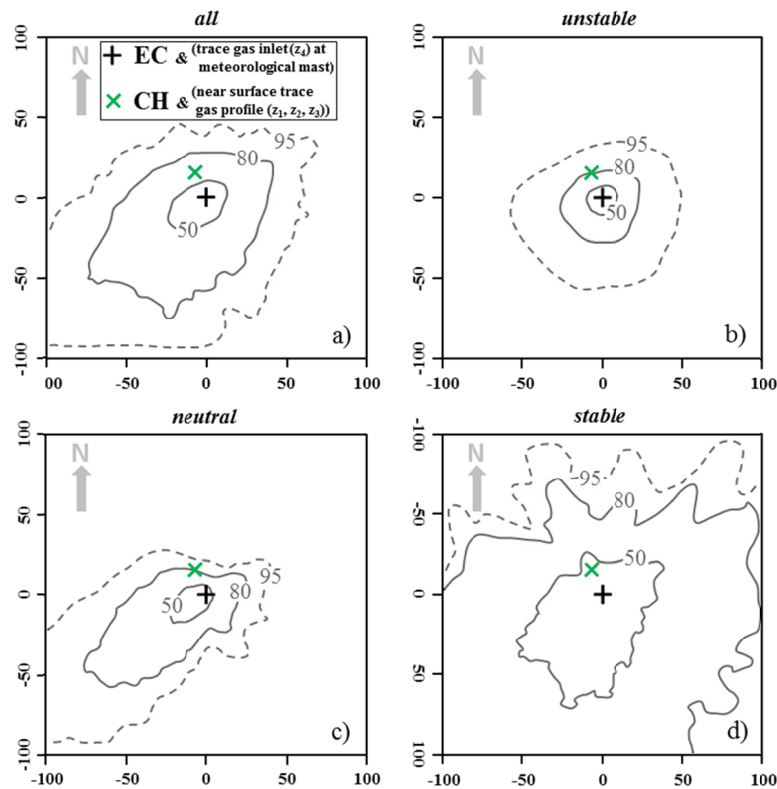


Fig. 1. Simplified sketch showing the positions of the EC system with the trace gas inlet ($z_4 = 4$ m) at the meteorological tripod mast, and the CH system with the combined near surface trace gas profile ($z_1 = 0.04$ m, $z_2 = 0.2$ m, $z_3 = 0.8$ m) at the Mainz-Finthen grassland site. Averaged cumulative footprint contours indicating the footprint areas for 50 % (solid line), 80 % (solid line) and 95 % (dotted line) of the total flux measured by eddy covariance for (a) all, (b) unstable, (c) neutral, and (d) stable conditions for the period from 4 August–26 September 2011 are also shown. The x-axis and y-axis are distances (in m).

(Enviscope GmbH, Frankfurt, Germany) (Zahn et al., 2012) with its 2.5 m long inlet tube positioned at the same lateral distance as the IRGA to the sonic path. The high-frequency signals were recorded at 20 Hz by a CR3000 data logger. The sensor discs required for the chemiluminescence reaction in the high-frequency O_3 detector were prepared as described in Ermel et al. (2013) and replaced every five to eight days.

Turbulent fluxes were computed using the TK3 software (see Mauder and Foken, 2011). The EC high-frequency data set was despiked and the wind vector was rotated using the planar fit method (Wilczak et al., 2001). The high-frequency CO_2 , H_2O and O_3 time series were time lag corrected using the cross correlation method. The data were averaged for 30 min intervals and the fluxes were corrected for high-frequency attenuation (Moore, 1986). In addition, CO_2 and H_2O fluxes were also corrected for density fluctuations due to temperature and water vapor (Massman, 2004; Webb et al., 1980). In addition, the corresponding random flux errors (Mauder et al., 2013) and standard micrometeorological parameters like the friction velocity (u_*) or stability parameter (z/L) were evaluated using TK3.

Because the fast response O_3 detector showed a considerable drift in sensitivity, the turbulent fluxes of O_3 were calculated using the so-called ratio method (Muller et al., 2010). Owing to the generally very

small offset of the O₃ detector, the O₃ deposition velocities $v_d(z_{ref})$ (in m s⁻¹) could be derived using the uncalibrated fast O₃ signal s_{O_3} as the ratio of the respective eddy covariance $\overline{w's_{O_3}'}$ (in V m s⁻¹) and the mean O₃ signal $\overline{s_{O_3}}$ (in V) over 30 min intervals:

$$v_d(z_{ref}) = -\frac{\overline{w's_{O_3}'}}{\overline{s_{O_3}}} \quad (1)$$

The calibrated eddy covariance trace gas fluxes (F_{EC}) were then calculated as:

$$F_{EC} = -v_d(z_{ref}) \cdot \overline{\mu_{O_3}}(z_{ref}) \cdot \rho_d \quad (2)$$

where ρ_d denotes the molar density of dry air (mol m⁻³) and $\overline{\mu_{O_3}}$ the 30 min average of the reference O₃ mixing ratio (in ppb) measured by a slow response UV-absorption analyzer (TEI-49i, Thermo Scientific, Waltham, USA) at a height of 4 m. The TEI-49i was operated in a nearby air-conditioned container and was calibrated every two weeks using the gas-phase titration (GPT) method (Rehme et al., 1974) with a GPT unit (SYCOS K-GPT, Ansyco GmbH, Karlsruhe, Germany) and a 50 ppm NO standard (Air Liquide, Germany). The inlet was installed at a trace gas mast next to the *EC* station (Fig. 1). The 30 m long inlet line was made of PFA and was heated above ambient temperature to avoid condensation in the tubing. A Teflon coated sample pump (N840FT.18, KNF Neuberger GmbH, Freiburg, Germany), operated at a flow rate of 8 L min⁻¹, flushed the sample air to the TEI-49i, where an overflow guaranteed ambient pressure conditions. The sampling error of the *EC* fluxes was estimated based on the statistical variance of $\overline{w's_{O_3}'}$ as described by Finkelstein and Sims (2001), which is derived from both the auto- and the covariance terms of w and s_{O_3} . A footprint analysis and site specific characterization approach (Göckede et al., 2004; 2006) was conducted, utilizing the Lagrangian forward stochastic model by Rannik et al. (2000).

2.4 Dynamic chamber measurements

2.4.1 Chamber system

The dynamic chamber system consisted of three dynamic chambers (henceforth abbreviated as $CH_{\#1-\#3}$), which are identical with those described in detail by Pape et al. (2009). $CH_{\#1-\#3}$ were set up approximately 15 m north-west of the *EC* station (Fig. 1) and placed in a triangular configuration with a mutual distance of smaller than 3.5 m. Mixing ratios of CO₂ and H₂O at the chamber inlet and outlet (see below) were measured using an IR-absorption analyzer (LI-840, Licor Bioscience, USA), those of NO with the chemiluminescence technique (TEI-42iTL Thermo Scientific, Waltham, USA), and to measure NO₂ the TEI-42iTL was equipped with a Blue Light Converter (BLC, Droplet Measurement Technologies, Boulder, USA). The O₃ mixing ratios at the chamber inlet and outlet were measured with a TEI-49i (see above). The trace gas analyzers were located in the air-conditioned container.

The dynamic chamber system was operated in combination with an adjacently installed near surface trace gas profile (see Fig. 1) consisting of three inlets ($z_1 = 0.04$ m, $z_2 = 0.2$ m, $z_3 = 0.8$ m). An additional inlet was installed at 4 m height and sampled side by side (*sbs*) with the O₃ analyzer serving as a reference for the *EC* system (see Sect. 2.3). In this way, potential systematic errors between the two independent systems (air humidity effect) could be accounted for. The 30 m long inlet lines (ID:

4 mm) from $CH_{\#1-\#3}$ and the profile system were made of PFA and were heated above ambient temperature to avoid condensation in the tubing. Teflon coated solenoid valves (Entegris Inc., USA) enabled the sequential sampling of either the profile heights z_1-z_3 or the inlet/outlet of $CH_{\#1-\#3}$. The air was drawn through the corresponding inlet by a Teflon coated sample pump (N840FT.18, KNF Neuberger GmbH) at a flow rate of 8 L min^{-1} resulting in a tube residence time below 2 s. To guarantee fresh sample air throughout the switching sequence a bypass permanently flushed the tubing not in use. A Nafion dryer (PP-MD-110-144F, Perma Pure, Toms River, USA) was installed directly upstream the TEI-42iTL analyzer inlet to prevent a potential water vapor quenching effect on the chemiluminescence reaction in the instrument (Matthews et al., 1977). A second Nafion dryer was placed in front of the TEI-49i to avoid O_3 reading biases caused by step changes in RH (Wilson and Birks, 2006), which are unavoidable in a profile system. The trace gas instruments were calibrated every two weeks. The LI-840 was calibrated using standards of 350, 450, 550 and 650 ppm CO_2 (Air Liquide, Germany) and a dew point generator for H_2O (LI-610, Licor Bioscience, USA). The calibrations of the NO , NO_2 and O_3 analyzers were performed together with the reference TEI49i for the EC measurement (see Sect. 2.3). A self-programmed LABVIEW software installed on a PC controlled the chamber and the profile system and logged the data every 10 s.

2.4.2 Sampling schedule

The measurement cycle of an individual chamber consisted of three consecutive trace gas mixing ratio measurement modes: (i) sampling at the chamber inlet (μ_{IN}), (ii) sampling at the chamber outlet (μ_{OUT}) and (iii) a repeated sampling of μ_{IN} (see Pape et al., 2009). We optimized the sampling schedule to get at least one flux estimate for each chamber within a 30 min interval. The optimization was based on response time tests at the field site for the individual trace gases (NO , NO_2 , O_3 , CO_2) and resulted in the measurement cycle of the dynamic chamber system combined with the near surface trace gas profile presented in Fig. 2a. The optimal duration of a single mode was found to be 150 s. After each valve switching the data of the initial flushing phase (NO : 40 s, NO_2 : 80 s, O_3 : 70 s, $\text{CO}_2/\text{H}_2\text{O}$: 30 s) were left out from further analysis (cf. Fig. 2b). An additional optimization was achieved by generally omitting mode (iii) and by using mode (i) of the subsequent chamber instead. For $CH_{\#3}$ the nearby installed z_2 of the trace gas profile (equal height as chamber inlet ($z = 0.2 \text{ m}$)) was used for μ_{IN} of mode (iii).

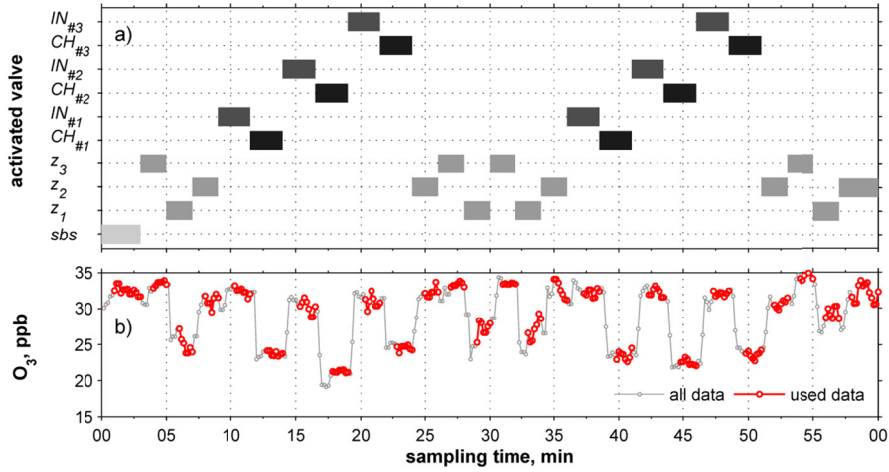


Fig. 2. (a) Hourly sampling cycle of the dynamic chamber system combined with the near surface trace gas profile. Each chamber was sampled at the inlet ($IN_{\#1-\#3}$) and inside the chamber volume ($CH_{\#1-\#3}$) and the near surface trace gas profile at the three heights (z_{1-3}). The sampling time of the activated valve is indicated by the shaded boxes. At the beginning of each hour a side by side measurement (*sbs*) with the *EC* reference system was automatically performed. (b) The O_3 time series demonstrates the difference between the recorded and the used data (see text for details).

2.4.3 Theory

From *EC* fluxes of depositing compounds like O_3 the canopy resistance R_c is calculated as:

$$R_c = \frac{1}{v_d(z_{ref})} - R_a(z_{ref}) - R_b = \left[-\frac{\mu_{z_{ref}} \cdot \rho_d}{F} \right] - R_a(z_{ref}) - R_b \quad (3)$$

where $R_a(z_{ref})$ and R_b are the aerodynamic and quasi-laminar boundary layer resistances (cf. Fig. 3), respectively, that can be calculated based on results from *EC* measurements, such as u_* , z/L or wind speed u (e.g., according to Hicks et al., 1987).

In case of the dynamic chamber method (*CH*) a flux of an inert trace gas between the plant-soil system and the chamber air can be computed as (Pape et al., 2009):

$$F_{CH} = \frac{Q}{A} \cdot \rho_d \cdot [\mu_{OUT} - \mu_{IN}] \quad (4)$$

where Q is the volumetric purging flow rate (set to $60 \text{ L min}^{-1} = 6 \cdot 10^{-3} \text{ m}^3 \text{ s}^{-1}$) and A the soil surface area (0.096 m^2) enclosed by the chamber. μ_{IN} is the mean of the trace gas mixing ratios measured in mode i and iii (see above) and μ_{OUT} is the corresponding mean measured in mode ii. For reactive trace gases such as the NO - NO_2 - O_3 triad that undergo chemical transformations on timescales of seconds to minutes, net chemical gas-phase sources and sinks in the chamber volume (S_{gp}) have to be accounted for (Pape et al., 2009):

$$S_{gp} = V \cdot [j_{NO_2} \cdot \mu_{OUT}(NO_2) - k \cdot \mu_{OUT}(NO) \cdot \mu_{OUT}(O_3)] \quad (5)$$

where V denotes the chamber headspace volume (0.041 m^3), j_{NO_2} the NO_2 photolysis frequency (in s^{-1}) and k (in $\text{ppb}^{-1} \text{ s}^{-1}$) the first order reaction rate constant of the reaction $NO + O_3 \rightarrow NO_2 + O_2$ (see Atkinson et al., 2004). Trace gas fluxes of the NO - NO_2 - O_3 triad corrected for gas-phase chemistry can then be computed as:

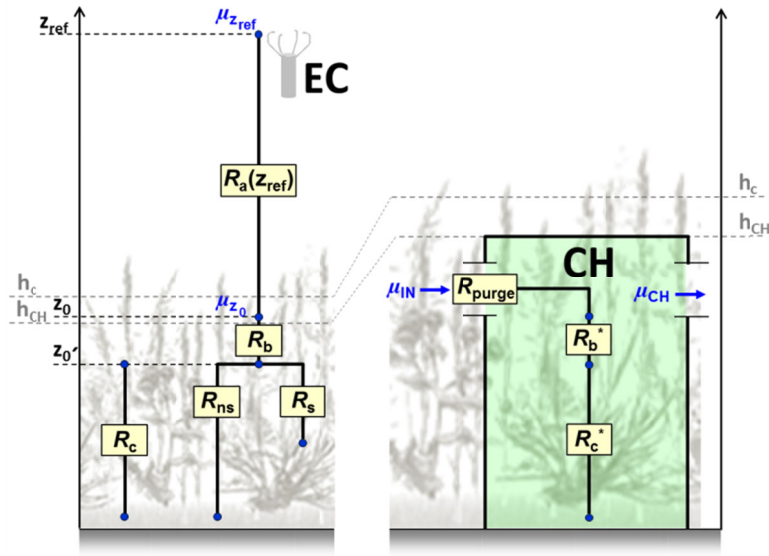


Fig. 3. Resistive scheme used for the determination of representative deposition fluxes of depositing compounds such as O_3 . The left panel represents the resistive concept valid for *EC* measurements. $R_a(z_{ref})$, R_b , R_s , R_{ns} and R_c are the aerodynamic resistance above the canopy, the quasi-laminar boundary layer resistance, the stomatal resistance, the non-stomatal and the canopy resistance, respectively. z_{ref} , z_0 and z_0' indicate the reference height, the canopy roughness height for momentum and the canopy roughness height for the scalar, respectively. $\mu_{z_{ref}}$ and μ_{z_0} represent the corresponding trace gas mixing ratios. h_c and h_{CH} indicate the canopy and chamber height. The resistive scheme of Pape et al. (2009) for the *CH* method is shown on the right panel. R_{purge} , R_b^* and R_c^* are the purging resistance, the quasi-laminar boundary layer resistance within the chamber and the canopy resistance within the chamber. μ_{IN} and μ_{OUT} represent the trace gas mixing ratios entering and leaving the chamber, respectively.

$$F_{CH_{gp}} = \frac{Q}{A} \cdot \rho_d \cdot [\mu_{OUT} - \mu_{IN}] - \frac{1}{A} \cdot \rho_d \cdot S_{gp} \quad (6)$$

The uncertainty of the calculated trace gas fluxes (σF_{CH}) is mainly determined by the non-stationarity (temporal variation) of the ambient mixing ratio during the chamber measurement cycle. Therefore, it is estimated as the flux error induced by using either only mode i (beginning of cycle) or mode iii (end of cycle) for μ_{IN} instead of the average:

$$\sigma F_{CH} = 0.5 \cdot \frac{Q}{A} \cdot \rho_d \cdot |\mu_{IN_i} - \mu_{IN_{iii}}| \quad (7)$$

The application of a dynamic chamber leads to a modification of the aerodynamic and diffusive transport (turbulent resistive scheme) (see Eq. 3), which results in modified trace gas mixing ratios within the chamber headspace. For the quantification of fluxes of soil-emitted compounds, such as NO , the modification of the aerodynamic transport by the dynamic chamber is of minor importance. This is because the emission flux is hardly influenced by (moderate) changes in the aboveground gas concentration and aerodynamic conditions. However, for deposited trace gases, such as O_3 , the modification of the turbulent resistive scheme is highly important as the deposition flux depends on the mixing ratio and is often limited by the turbulent transport. Thus, for a reliable quantification of deposition fluxes using the dynamic chamber method, the modified resistive scheme has to be quantified and corrected for. Pape et al. (2009) presented a corresponding correction using a common bulk re-

sistance model (see Fig. 3). The correction is based on the assumption that the canopy resistance for deposited compounds inside the dynamic chamber (R_c^*) is equal to the corresponding canopy resistance R_c outside (Eq. 3) if the canopy itself remains unchanged and an appropriate chamber design is used. Under these conditions R_c^* can be computed according to Pape et al. (2009) as:

$$R_c^* = \left[-\frac{\mu_{IN} \rho_d}{F_{CHgp}} \right] - R_b^*(LAI) - R_{purge} - R_{mix} \quad (8)$$

where R_{purge} is defined by the purging flow rate ($R_{purge} = A/Q = 100 \text{ s m}^{-1}$) and R_{mix} is the internal mixing resistance in the chamber that was quantified by Pape et al. (2009) to be close to zero and is therefore neglected. R_b^* was semi-empirically parameterized as a function of the LAI . Then the undisturbed deposition flux F_{CHcor} (for ambient aerodynamic conditions) can be calculated from R_c^* by rearranging Eq. 3:

$$F_{CHcor} = \frac{\mu_{zref}}{R_a(z_{ref}) + R_b + R_c^*} \quad (9)$$

The combination of Eq. 8 with Eq. 9 gives the resulting flux correction ratio:

$$\frac{F_{CHgp}}{F_{CHcor}} = \frac{R_a(z_{ref}) + R_b + R_c^*}{R_{purge} + R_{mix} + R_b^* + R_c^*} \cdot \frac{\mu_{IN}}{\mu_{zref}} \quad (10)$$

Compared to the relationship given in Pape et al. (2009), Eq. 10 is extended by the ratio of the trace gas mixing ratios (μ_{IN}/μ_{zref}). This was necessary because the grassland canopy at the study site slightly exceeded the chamber height $h_{CH} = 0.43 \text{ m}$ (cf. Fig. 3), and therefore the height for the reference mixing ratio μ_{zref} had to be chosen higher up than the height of the chamber inlet (μ_{IN}).

2.5 Stomatal conductance for O_3 and flux partitioning

H_2O flux measurements can be used to derive the stomatal conductance (g_s) for O_3 . This can be done in a three-step procedure in accordance with e.g., Lamaud et al. (2009) and Stella et al. (2011b), where in the first step a preliminary stomatal conductance (g_{SPM}) is derived by inverting the Penman-Monteith equation and adding the ratio of molecular diffusivities between O_3 and H_2O :

$$g_{SPM} = \frac{D_{O_3}}{D_{H_2O}} \cdot \frac{\frac{E}{\delta_w}}{1 + \frac{E}{\delta_w} (R_a + R_b) \left(\frac{\beta s}{\gamma} - 1 \right)} \quad (11)$$

where D_{O_3} and D_{H_2O} are the molecular diffusivities for O_3 and H_2O (in $\text{m}^2 \text{ s}^{-1}$), respectively, E is the H_2O evapotranspiration flux (in $\text{kg m}^{-2} \text{ s}^{-1}$), δ_w the water vapor density saturation deficit (in kg m^{-3}), β is the Bowen ratio, s the slope of the saturation curve (in Pa K^{-1}) and γ the psychrometric constant (in Pa K^{-1}).

The H_2O flux E represents the sum of the plant transpiration and evaporation from different compartments of an ecosystem such as soil pores and liquid water on diverse surfaces. Hence, to estimate a representative stomatal conductance E should be plant transpiration only and the estimate resulting from Eq. 11 has to be corrected in the second step. As proposed by Lamaud et al. (2009) only dry conditions with $RH < 60 \%$ were used to compute g_{SPM} , a threshold for which liquid water on surfaces is assumed to be fully evaporated. In the third step, the stomatal conductance is then corrected for soil evaporation by plotting g_{SPM} against Gross Primary Production (estimated according to Kowalski et

al. (2003)) (for further details, see Lamaud et al. (2009), Stella et al. (2011a; 2013b) The stomatal O₃ flux (F_s) can be calculated as:

$$F_s = g_s \cdot \mu_{O_3}(z'_0 + d) \cdot \rho_d \quad (12)$$

where $\mu_{O_3}(z'_0 + d)$ is the O₃ mixing ratio (in ppb) at the leaf surface and is calculated from the Ohm's analogy using the *EC* flux measurements as:

$$\mu_{O_3}(z'_0 + d) = -v_{d_{O_3}}(z_{ref}) \cdot \mu_{O_3}(z_{ref}) \cdot (R_a(z_{ref}) + R_b) + \mu_{O_3}(z_{ref}) \quad (13)$$

3 Results

3.1 Overview

3.1.1 Characterization of the grass canopy

The plant species identified in $CH_{\#1-\#3}$ are listed in Table 1. The list contains species that are typical for dry and nutrient poor Arrhenatheretum elatoris plant societies. As described above (see Sect. 2.1) individual *LAI*s (in m² m⁻², henceforth omitted) for green alive (LAI_g) and brown dead (LAI_b) plant biomass were determined for each chamber and subsequently summed up to the total leaf area index (LAI_{tot}). The *LAI* results in Table 2 reveal that the three chambers showed some variability of LAI_g , while LAI_b was more uniformly distributed. The average LAI_{tot} was 4.8.

Table 1. List of plant species determined inside the three dynamic chambers ($CH_{\#1-\#3}$) at the Mainz-Finthen grassland site on 26 September 2011.

$CH_{\#1}$	$CH_{\#2}$	$CH_{\#3}$
Elytrigia repens	Arrhenatherum elatius	Daucus carota
Eryngium campestre	Daucus carota	Elytrigia repens
Festuca rubra	Leucanthemum ircutianum	Festuca rubra
Helictotrichon pubescens	Poa angustifolia	Latyrus pratensis
Latyrus pratensis	Trifolium campestre	Poa angustifolia
Poa angustifolia	Trisetum flavescens	

The composite vertical *LAI* profile in Fig. 4 demonstrates the consistency of the *LAI* determination from the two independent methods (*LAI* meter and photographic imagery, see Sect. 2.1). The observed shape and the total *LAI* are very similar to those presented in Jäggi et al. (2006) for the beginning of their experiment at an intensively managed grassland site with a total *LAI* around 4.5 ($h_c = 0.4$ m). In both cases, the *LAI* profile shows the highest biomass density below 0.2 m which is typical for grassland sites. During an average daytime situation the lowest measurement levels $z_1 = 0.04$ m and $z_2 = 0.2$ m were exposed to 70 and 90 % of the O₃ mixing ratios prevailing at $z_4 = 4.0$ m. The nighttime profiles were much steeper with z_1 and z_2 encountering only 25 and 60 % of the O₃ levels at z_4 . In comparison, the reduction between z_4 and z_3 was only around 3 and 13 % during daytime and nighttime, respectively. Hence, the largest O₃ gradients were observed in the lower canopy between z_1

Table 2. Individual single sided leaf area indexes of alive green (LAI_g) and dead brown (LAI_b) biomass for each chamber ($CH_{\#1-\#3}$) and their averages ($AVG(CH_{\#1-\#3})$) as well as the total leaf area index (LAI_{tot}) defined as the sum of LAI_g and LAI_b for the three chambers at the Mainz-Finthen grassland site.

	$CH_{\#1}$	$CH_{\#2}$	$CH_{\#3}$	$AVG(CH_{\#1-\#3})$
LAI_g	2.8	3.5	2.1	2.8
LAI_b	1.9	1.9	2.3	2.0
LAI_{tot}	4.7	5.3	4.4	4.8

and z_2 during any time of day. This is in accordance with Jäggi et al. (2006), although they report a stronger O_3 reduction within the canopy (64 % of reference concentration) at a height corresponding to our z_2 . While the grass vegetation of the present study was already in the mature and partly senescing state, the one in Jäggi et al. (2006) was in the growing state characterized by a LAI increase from 4.7 to 6.8, which may explain the deviation in the averaged profiles.

3.1.2 Meteorological conditions, mixing ratios and fluxes

The time series presented in Fig. 5 comprise 54 measurement days with contrasting meteorological and air chemistry characteristics. The five day extract highlighted in gray contains such differing conditions, which will be exemplarily discussed below. Daytime maxima of global radiation (Fig. 5a) ranged between 250 and 930 $W m^{-2}$. During the campaign sunrise was around 06:00 CET (= UTC+1), sunset at 19:00 CET and the global radiation maximum between 12:30 and 13:30 CET. Henceforth in this manuscript, daytime values refer to global radiation $> 10 W m^{-2}$. The maximum of the 24 h rainfall sums (Fig. 5a) was 3.6 mm and was as well as other rainfall events directly linked to summer thunderstorms. Air temperature ranged from 6 to 33 °C with corresponding anti-correlated RH between 100 and 30 % (Fig. 5b). The horizontal wind speed u was generally higher during daytime than during nighttime and ranged between 0.07 and 5.8 $m s^{-1}$ (Fig. 5c). The friction velocity u_* was closely linked to u and ranged between around 0.1 and 0.7 $m s^{-1}$ (Fig. 5c). At least four distinct periods with persistently higher u and u_* values (during day and night) could be identified. One of these events was found in the first half of the five day period highlighted in gray. However, the last two days of the highlighted period featured a contrasting situation with horizontal wind speeds below 1.8 $m s^{-1}$. A strong temperature inversion (not shown) prevailed during calm nights at the site, which limited vertical mixing and led to high CO_2 mixing ratios and near zero O_3 mixing ratios.

NO and NO_2 mixing ratios (Fig. 5e) ranged from nearly zero up to 26 and 40 ppb, respectively. Relatively clean air masses (NO and NO_2 below 2 and 5 ppb, respectively) arrived at the site with higher wind speeds from the south-westerly direction (not shown) during 52 % of the time, as e.g., in the first part of the gray highlighted period. On the other hand, advective transport of NO_x (sum of NO and NO_2), attributed to anthropogenic emissions from neighbored motorways, villages and the city of Mainz, typically caused the NO_x mixing ratios to peak between 06:00 and 10:00 CET. This pattern was particularly evident during periods with low wind speeds from the north-eastern direction, which

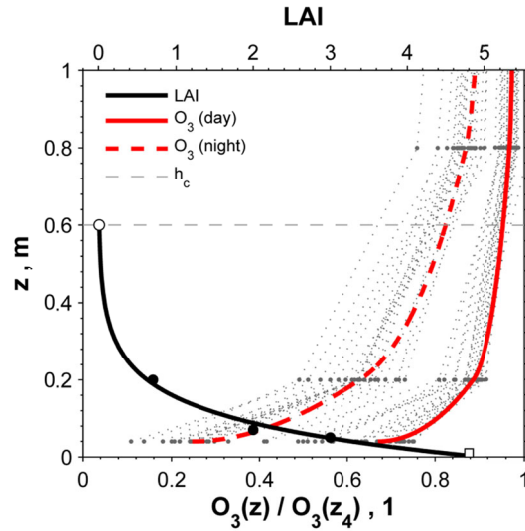


Fig. 4. Vertical *LAI* profile composite of (i) three points (filled circles) measured with an *LAI* meter (0.05 m, 0.07 m, 0.20 m) on 18 August 2011 and (ii) the LAI_{tot} (hollow square) at $z = 0$ m determined by biomass harvest inside the dynamic chamber at 26 September 2011 (see Sect. 2.1 for details) and (iii) the *LAI* at $z = h_c$ set to zero (hollow circle). Median vertical O_3 profiles scaled to $\mu_{O_3}(z_4)$ for each 30 min interval of the data set from 04 August–26 September 2011 (gray lines and dots) and corresponding day and nighttime fits through the median profiles. The O_3 profiles are composites from measurements of (i) the near surface trace gas profile (z_{1-3}) and (ii) the O_3 mixing ratio measured at z_4 of the meteorological tripod mast (see Fig. 1).

were observed during 15 % of the time. During the night of 09–10 September 2011, an extreme situation with high NO and NO_2 mixing ratios was observed. Within thirteen hours (19:00 to 08:00 CET) the high NO probably entirely titrated the ambient O_3 (Fig. 5e). Otherwise, the O_3 mixing ratios featured a typical diurnal cycle and ranged between minima of 2 ppb in the early morning and diurnal maxima of 30 to 67 ppb in the afternoon. Generally, the diurnal O_3 amplitude was larger during periods with lower wind speeds.

The *EC* fluxes of H_2O and CO_2 showed typical diurnal cycles related to the vegetation activity and the meteorological conditions (Fig. 5f). The measured O_3 deposition fluxes showed a distinct diurnal cycle. The daytime O_3 deposition fluxes (Fig. 5g) reached their diurnal maxima (-4 to -7 $nmol\ m^{-2}\ s^{-1}$) during a time window of about four hours centered around 14:00 CET. This maximum occurred one or two hours earlier than the diurnal O_3 mixing ratio peak (see above). Stronger O_3 deposition fluxes up to -13 $nmol\ m^{-2}\ s^{-1}$ were also observed. Generally, high O_3 deposition fluxes were related to high O_3 mixing ratios and high u_* (Fig. 5c). Daytime deposition fluxes slightly decreased towards the end of the experiment. Nighttime fluxes of O_3 were mostly between -0.5 to -3 $nmol\ m^{-2}\ s^{-1}$ and were larger during periods with elevated wind speeds. The median random flux error of the *EC* method (Mauder et al., 2013) was quantified for CO_2 , H_2O and O_3 to be 11, 12 and 12 %, respectively, during daytime and to be 29, 15 and 15 %, respectively, during nighttime.

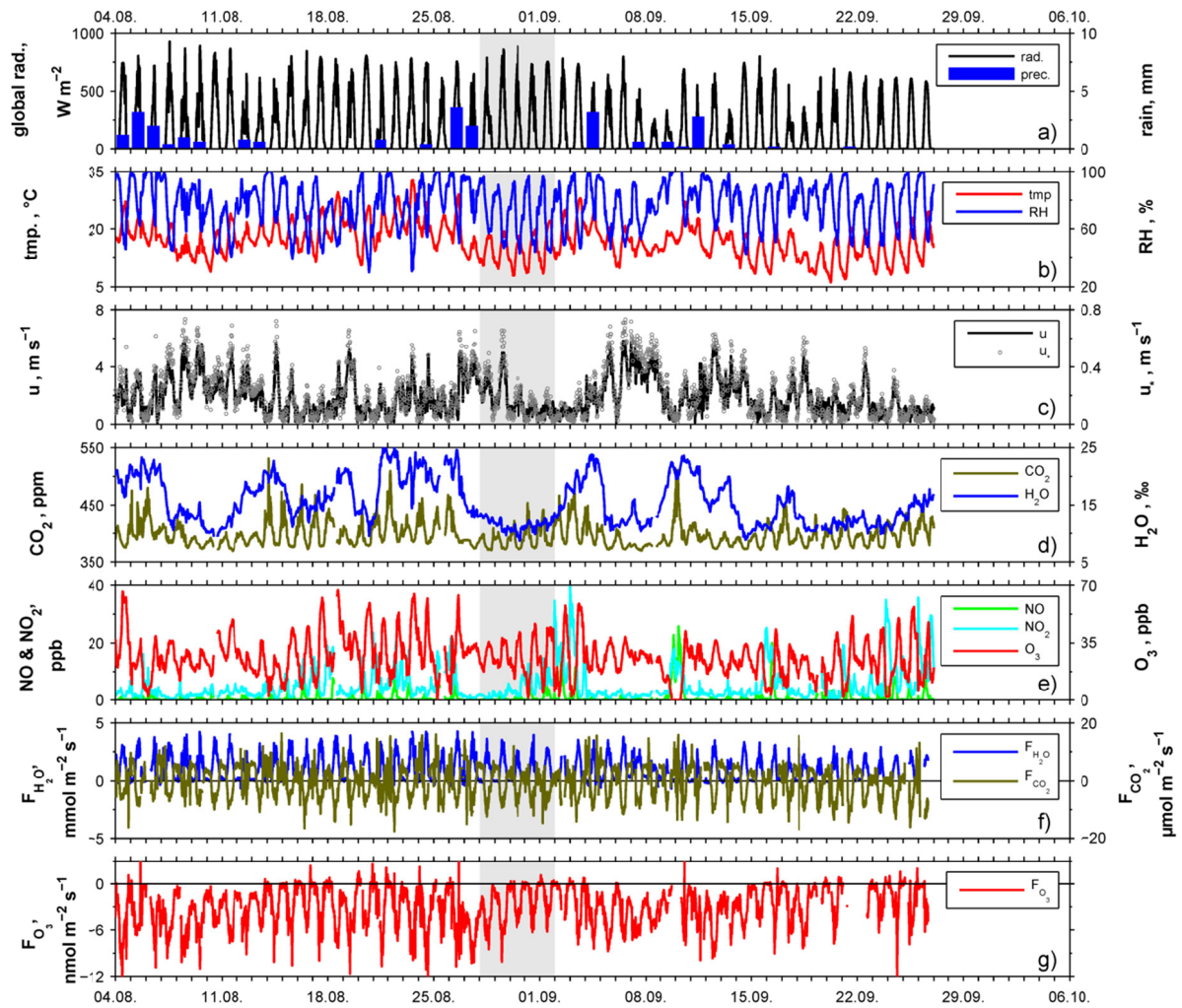


Fig. 5. Time series measured during 54 days (04 August–26 September 2011) at the Mainz-Finthen grassland site: (a) global radiation and 24-hourly integrated rainfall, (b) temperature (tmp) and relative humidity (RH), (c) horizontal wind speed (u) and friction velocity (u_*), (d) mixing ratios of CO_2 and H_2O at $z_4 = 4.0$ m, (e) mixing ratios of NO , NO_2 and O_3 at $z_4 = 4.0$ m, (f) turbulent fluxes of H_2O and CO_2 and (g) turbulent fluxes of O_3 . All fluxes were determined using the EC method. All presented values are 30 min averages, except for the 24 h precipitation sums. The grey-shaded period from 28 August–02 September 2011 is presented in more detail in Fig. 11.

3.2 Comparison of fluxes measured by EC and dynamic chambers

3.2.1 Non-reactive trace gases

As shown in Fig. 6a, the CO_2 fluxes of both, EC and CH method, featured a larger scatter during nighttime than during daytime. This was especially true for the CO_2 fluxes resulting from the CH method as indicated by the large number of outliers (black dots, partly out of axis range) determined by the box plot statistics. However, during daytime from 10:00 to 15:00 CET a very good agreement of the hourly medians and the interquartile ranges (25th to 75th percentiles) was observed between EC

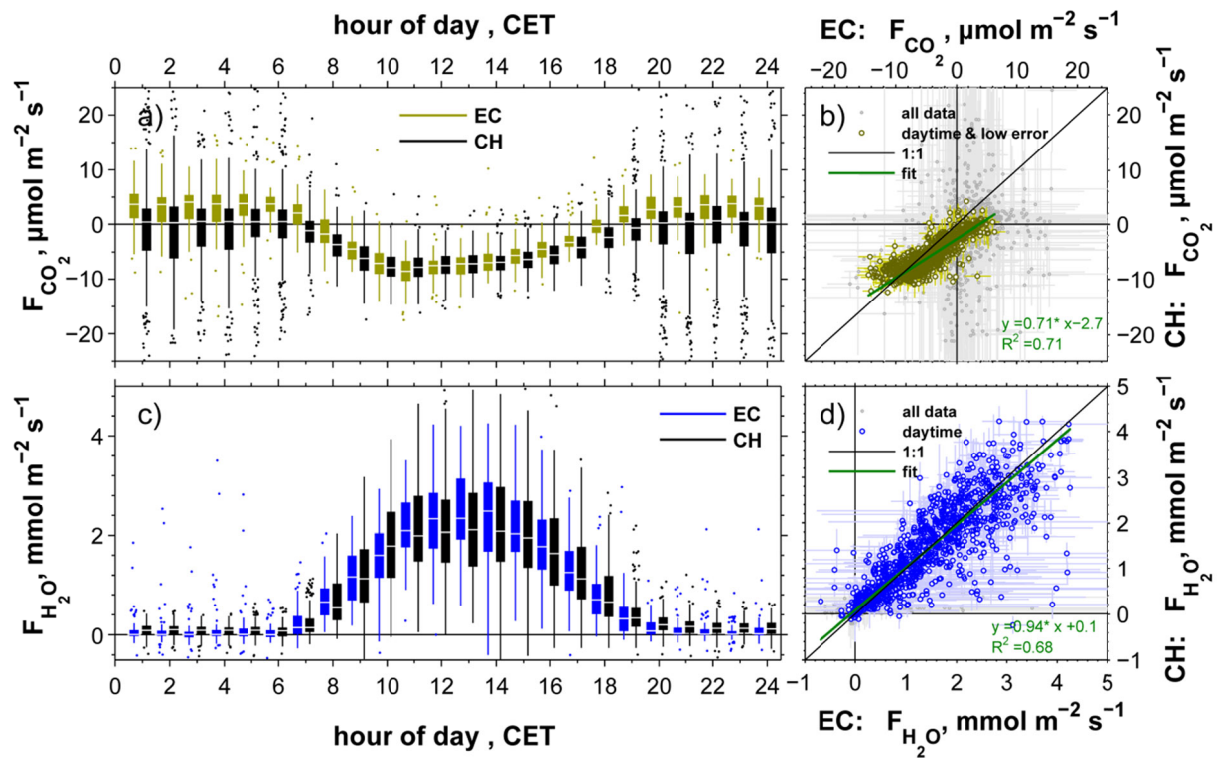


Fig. 6. Comparison of fluxes determined by *EC* and *CH* methods for CO_2 and H_2O presented as diurnal cycles using hourly box plot statistics (a), (c) and scatter plots (b), (d). All data from 04 August–26 September 2011 are included. Daytime values refer to global radiation $> 10 \text{ W m}^{-2}$. The fluxes determined from the individual $\text{CH}_{\#1-\#3}$ were averaged for 30 min intervals matching the results from *EC* measurements. The corresponding flux errors were determined according to Mauder et al. (2013) and Eq. 7 for the *EC* and *CH* method, respectively. Values identified as outliers by the standard box plot statistics, are indicated in grey in the scatterplot and were rejected for the fitting procedure. The bivariate weighted least-squares fitting by the Williamson-York method (Cantrell, 2008) was used for the regression analysis.

and *CH* with the medians deviating by only 0 to 13 %. A systematic separation of the median CO_2 fluxes of *EC* and *CH* was observed after 16:00 CET. Median *EC* fluxes were then considerably higher than *CH* fluxes with nighttime median values in the order of $3.5 \mu\text{mol m}^{-2} \text{ s}^{-1}$, while the *CH* fluxes exhibited medians of around $0.5 \mu\text{mol m}^{-2} \text{ s}^{-1}$.

Very large errors were determined for nighttime CO_2 fluxes near or above zero for both methods; these were particularly pronounced for the *CH* results. A linear regression analysis by the bivariate weighted least-squares fitting with the Williamson-York method (Cantrell, 2008), excluding data points with extremely high errors (outlier definition by the standard box plot statistics), was performed on the remaining daytime fluxes (see Fig. 6b). The resulting fit had a slope of 0.71 and an offset of $-2.7 \mu\text{mol m}^{-2} \text{ s}^{-1}$ mainly caused by the systematic difference in the nighttime fluxes. In the range of -5 to $-10 \mu\text{mol m}^{-2} \text{ s}^{-1}$ the daytime *EC* and *CH* fluxes exhibited small errors and scattered around the 1:1 line. A median overall comparison of the daytime CO_2 fluxes revealed that the *CH* results were only 10 % higher than those by the *EC* method.

Diurnal H₂O fluxes determined by the *EC* and *CH* methods (Fig. 6c) generally displayed a very good agreement of both methods throughout the entire day. The nighttime H₂O fluxes were close to zero for both methods, but the scatter of the *EC* fluxes was much higher than for the *CH* method, as illustrated by the outliers of the box plot statistics. The linear regression analysis for the daytime values (Fig. 6d) confirmed the good agreement (slope = 0.94, offset = 0.1 mmol m⁻² s⁻¹). However, significant random-like scatter around the 1:1 line is visible. A median overall comparison revealed that the daytime H₂O fluxes determined by the *CH* method were 1 % smaller than those by the *EC* method.

3.2.2 Ozone

Fig. 7a presents the mean diurnal course of O₃ deposition fluxes determined by *EC* and *CH* measurements. For the *CH* method, the preliminary fluxes corrected only for gas-phase chemistry (*CH_{gp}*, Eq. 6) as well as the finally corrected fluxes (*CH_{cor}*, Eq. 9) are shown. Nighttime fluxes were generally weak and mostly ranged between -0.5 and -3 nmol m⁻² s⁻¹ and the *CH_{cor}* flux agreed well with the *EC* measurements. During daytime the *EC* fluxes were in the range between -2 to -7 nmol m⁻² s⁻¹, and the median *CH_{cor}* fluxes revealed a slight underestimation (0 to 1 nmol m⁻² s⁻¹). The scatter in the *CH_{cor}* data was higher than in the *EC* data, as indicated by the length of the whiskers and the numbers of outliers.

The *CH_{gp}* flux (without correction for modified resistances in the chamber) showed generally lower values compared to the final corrected fluxes and the *EC* method (Fig. 7a). The effect of the resistance correction for the chamber fluxes is also illustrated in the scatter plots of Fig. 7b,c. The systematic deviation of the *CH_{gp}* fluxes from the *EC* fluxes is reflected by the slope of 0.55 in Fig. 7b resulting from the bivariate linear regression analysis. In contrast, the *CH_{cor}* fluxes (Fig. 7c) showed no systematic deviation from the 1:1 line (slope of 0.98). The binned median indicated only a small underestimation of the very large fluxes.

While the *EC* method directly yields O₃ fluxes, the *CH* method more directly quantifies the respective canopy resistance, which is also used in deposition modeling schemes. Fig. 8 compares *R_c* estimated from the *EC* measurements (Eq. 3) with *R_c^{*}* derived from the *CH* method (Eq. 8). The comparison of the diurnal courses (Fig. 8a) reveals a good agreement during daytime from 07:00 to 18:00 CET with only minor differences in the hourly medians. At this time, median *R_c* and *R_c^{*}* values ranged from 150 to 320 s m⁻¹ and from 180 to 370 s m⁻¹, respectively. Between 08:00 and 13:00 CET the distribution of the *R_c* values from the *EC* method was narrower than for the *CH* method. During nighttime the canopy resistances from the two methods revealed a considerable deviation. The estimates from the *EC* method were systematically higher (by around 150 s m⁻¹) with a much larger scatter than the ones determined by the *CH* method.

Fig. 8b shows a scatter plot of the *R_c* and *R_c^{*}* estimates of both methods, illustrating a substantial scatter around the 1:1 line. Because the canopy resistance is a ratio of concentration over flux, it can get a very high uncertainty when the flux (denominator) is close to zero (mainly during night). The linear regression resulted in a slope of 1.04.

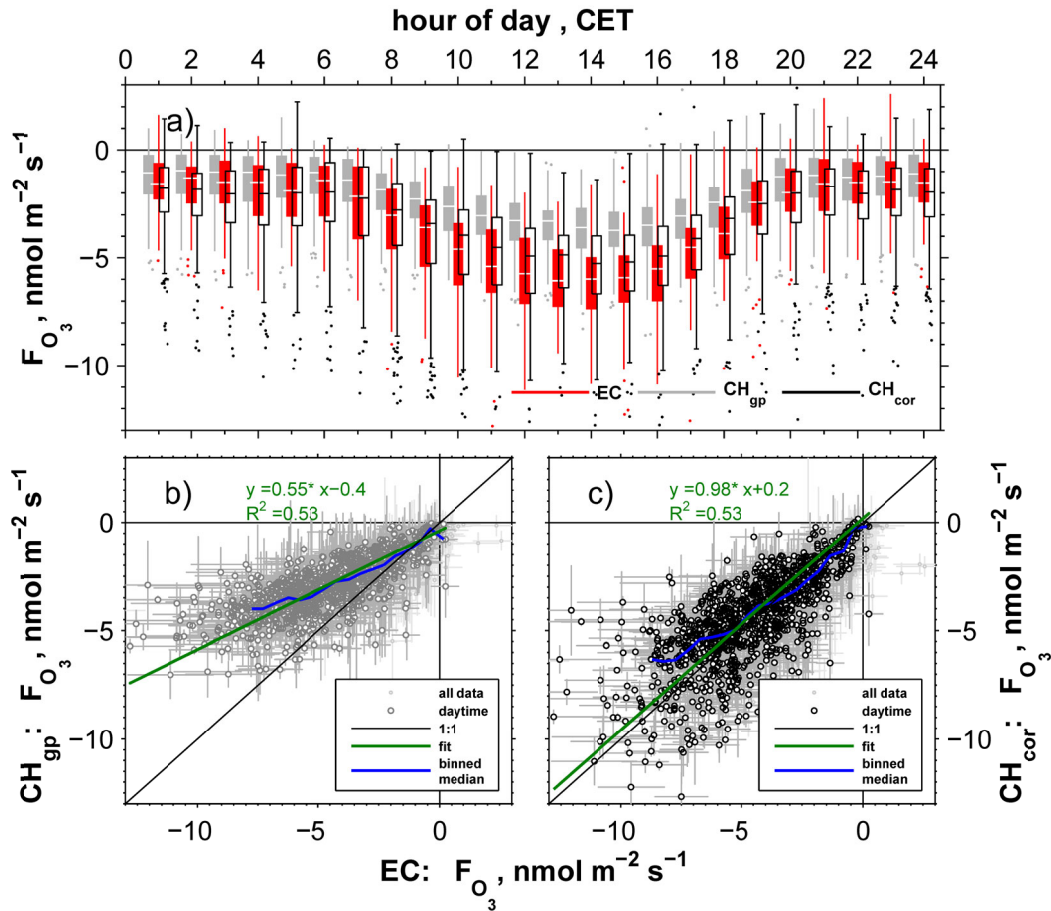


Fig. 7. Comparison of O₃ fluxes determined by EC and CH methods presented as diurnal cycles using hourly box plot statistics (a) and scatter plots (b), (c). All data from 04 August–26 September 2011 are included. Daytime values refer to global radiation > 10 W m⁻². O₃ fluxes determined by the CH method are shown in (b) as gas-phase chemistry-corrected (CH_{gp}, Eq. 6) and in (c) as finally corrected (CH_{cor}, Eq. 9). The corresponding flux errors were determined according to Mauder et al. (2013) and Eq. 7 for the EC and CH method, respectively. The bivariate weighted least-squares fitting by the Williamson-York method (Cantrell, 2008) was used for the regression analysis. A binned median (step width = 0.5 nmol m⁻² s⁻¹) illustrates deviations from the fit.

3.2.3 Dependence of dynamic chamber flux quality on environmental conditions

Significantly changing ambient trace gas mixing ratios (non-stationarities) during the measurement cycle of one single chamber (modes i–iii, cf. Sect. 2.4.2) can lead to bias the measured flux (Eqs. 6, 8) due to the high flow of ambient air through the chamber. Usually, stationary situations are more likely under turbulent conditions since they provide well-mixed air masses. The turbulence intensity can be addressed by the friction velocity (u_*). Eq. 7 provides a measure of the CH flux error due to non-stationarities. Fig. 9a displays binned median σF_{O_3} and σF_{CO_2} as functions of u_* during daytime. Both σF_{O_3} and σF_{CO_2} increased with decreasing u_* . For u_* below 0.15 m s⁻¹, a contrasting behavior of σF_{O_3} and σF_{CO_2} became obvious: while σF_{CO_2} further increased, σF_{O_3} started to decrease again with declining u_* . This can be attributed to the contrasting source and sink behavior of CO₂ and O₃. Under low

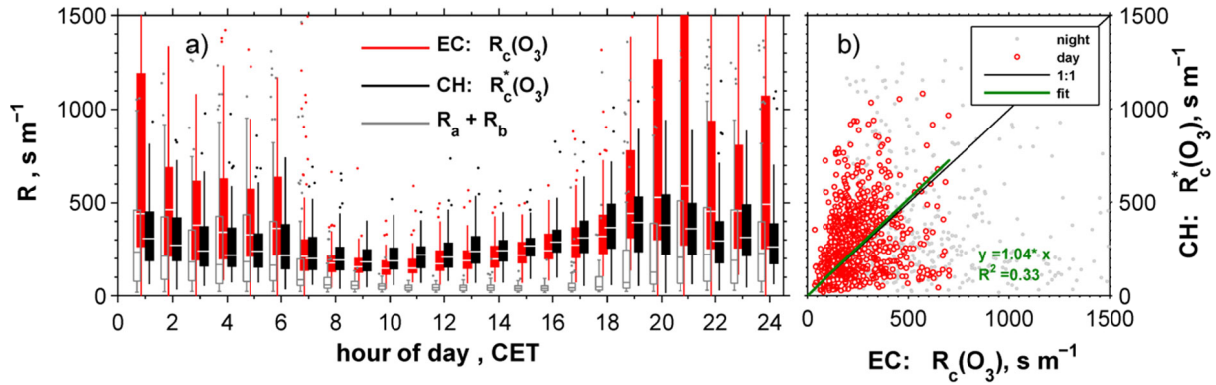


Fig. 8. (a) Diurnal comparison of the canopy resistances for O₃ determined by EC (R_c) and CH method (R_c^*) and the total aerodynamic resistance ($R_a(z_{ref}) + R_b$) using hourly box plot statistics; (b) scatter plot of R_c against R_c^* and the resulting linear fit; all data from 04 August–26 September 2011 are included; Daytime values refer to global radiation $> 10 \text{ W m}^{-2}$. Extreme outliers were identified using the extreme outlier definition of the box plot statistics, and rejected from the fitting procedure.

turbulent conditions (mostly stable stratification), the vertical exchange and the air renewal in the canopy was generally limited. These also strongly limited the O₃ deposition (cf. Fig. 7a) by reducing the mixing ratio, as well as the deposition velocity. Consequently, σF_{O_3} declined together with the O₃ flux. CO₂, in contrast, was emitted by the soil without limitation by the low turbulence but was accumulated in the canopy layer. Fig. 9 excludes nighttime, but includes the respective transition periods, during which photosynthesis and turbulence were on average weak. Thus, the CO₂ exchange was connected with significant non-stationary conditions causing high σF_{CO_2} values.

In contrast to the absolute errors, the relative CH flux errors (Fig. 9b) showed a general decrease with increasing turbulence for both O₃ and CO₂ over the entire u_* range. Relative CO₂ and O₃ flux errors were to a large extent found below 25 % when u_* was above 0.16 m s^{-1} and 0.22 m s^{-1} , respectively. For lower u_* values much higher relative errors, often above 100 %, were found.

The median σF_{CH} was quantified for CO₂, H₂O and O₃ to be 18, 24 and 32 %, respectively, for daytime and 301, 134 and 58 %, respectively, for nighttime. The values represent random-like errors but are not fully comparable to the random EC error given above due to different calculations. The variability between $\text{CH}_{\#1-\#3}$ was within 30 %, 20 %, 20 % during daytime and 45 %, 50 %, 15 % during nighttime for the CO₂, H₂O and O₃ fluxes, respectively. In general, the highest O₃ deposition fluxes were observed for $\text{CH}_{\#2}$, which exhibited the highest LAI.

3.3 Partitioning of O₃ fluxes between stomatal and non-stomatal pathways

Distinct median diurnal cycles of the canopy (g_c), stomatal (g_s) and non-stomatal (g_{ns}) conductances derived from the measured EC fluxes are presented in Fig. 10a. The canopy conductance for O₃ exhibited a diurnal pattern with nighttime values of $0.15\text{--}0.25 \text{ cm s}^{-1}$ and maximum values of 0.7 cm s^{-1} in the morning between 09:00 and 11:00 CET. From 11:00–19:00 CET, g_c continuously decreased again towards nighttime values. The stomatal conductance g_s exhibited nighttime values of zero due to sto-

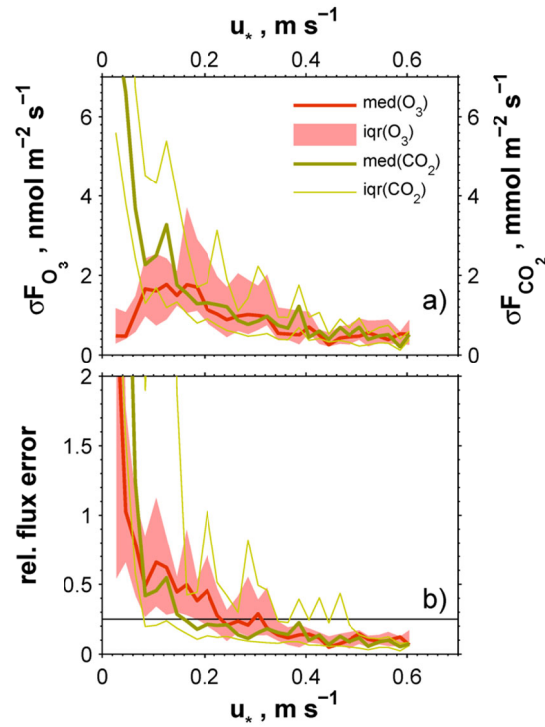


Fig. 9. a) Binned medians (med) and corresponding interquartile ranges (iqr) of the absolute CH flux errors (Eq. 7) for O_3 and CO_2 as function of u_* during daytime. b) Binned medians and corresponding interquartile ranges of the relative flux errors of the CH method for O_3 and CO_2 as function of u_* during daytime. The black line represents a 25 % relative error.

mata closure. The daytime pattern of g_s generally followed that of global radiation, featuring a bell-shaped curve with values above zero between 06:00 and 19:00 CET. g_s reached a maximum of 0.4 cm s^{-1} at 11:00 CET. The non-stomatal conductance g_{ns} equaled g_c during nighttime until stomata opening at 06:00 CET. Thereafter, g_{ns} showed its diurnal maximum between 07:00 and 11:00 CET with $0.3\text{--}0.4 \text{ cm s}^{-1}$. From 12:00 CET onwards g_{ns} reached the nighttime values again. The relative partitioning of g_c indicated the dominance of g_s between 10:00 and 16:00 CET, with a maximal contribution of 71 % at 13:00 CET.

Fig. 10b shows median diurnal cycles of total O_3 fluxes measured by the EC method (F_{EC}) with estimated flux contributions by the stomatal (F_s) and non-stomatal (F_{ns}) pathways. The dominant contribution of F_s at midday when F_{EC} values were highest resulted in a median F_s maximum of around $-4.7 \text{ nmol m}^{-2} \text{ s}^{-1}$ from 13:00–14:00 CET. The course of F_s symmetrically followed the one of F_{EC} . F_{ns} approached around -2.5 and $-1.5 \text{ nmol m}^{-2} \text{ s}^{-1}$ during daytime and nighttime, respectively.

4 Discussion

4.1 Reliability and pathway attribution of the reference EC flux

4.1.1 EC flux, corrections and uncertainties

For the *EC* measurements that served as a flux reference, the impact of the vertical inlet separation of the $v_d(z_{ref})$ and $\overline{\mu_{O_3}}(z_{ref})$ measured at 3 m and 4 m height, respectively, was of minor importance (on average 1 % for daytime and 9 % for nighttime determined from accompanying profile records, not shown).

The fast chemiluminescence O_3 detector was equipped with 2.5 m inlet tubing (OD: 3/8"), which resulted in a high-frequency (hf) damping effect that was corrected after Leuning and King (1992). The corresponding correction was typically 17 % and 12 % during daytime and nighttime, respectively. These values compared well with results from Moravek et al. (2013), who simulated the effect of different low pass-filter strengths on *EC* fluxes of different scalars at the Mainz-Finthen site. In comparison to the effect of the inlet tubing, the individual hf-damping correction accounting for the sensor separation (Moore, 1986) was 8 and 15 % during daytime and nighttime, respectively. The total combined hf-damping correction was quantified to be on average 20 % during daytime and 24 % during nighttime. The relatively large hf-correction lowered to some extent the reliability of the *EC* method as reference for the O_3 flux comparison, because the correction factor was not measured but estimated based on common knowledge concerning turbulent cospectra and spectral attenuation functions. In retrospect, the use of inlet tubing with a smaller inner diameter might have favored a less pronounced hf-attenuation by increasing the flow speed. The hf-damping due to the tube sampling was much higher than the damping caused by the lateral sensor separation during daytime when the fluxes were of largest magnitude. In conclusion one should minimize the tube residence time for *EC* flux measurements as far as possible.

In some experiments reported in the literature, a vertical chemical divergence was observed resulting in a net loss of O_3 in the air column beneath the *EC* measurement. Reasons were the reactions of O_3 with NO (e.g., Dorsey et al., 2004) or VOCs (e.g., Kurpius and Goldstein, 2003) emitted by soil or plants, respectively. NO soil emissions at the nutrient-poor Mainz-Finthen site were too small to be detected by the *CH* system and VOC emissions by the vegetation were most likely also small as shown in previous studies for undisturbed mature grasslands (see literature survey in Ruuskanen et al., 2011). This was confirmed by the low VOC levels measured at the site (e.g., isoprene < 0.7 ppb, monoterpene < 0.3 ppb, J. Kesselmeier, personal communication). However, the regularly elevated NO_x mixing ratios during the morning hours led to an investigation on potential flux divergence. The net effect between O_3 loss ($O_3 + NO \rightarrow NO_2 + O_2$) and production ($NO_2 + j_{NO_2} \rightarrow NO + O$) was quantified according to Rummel et al. (2007). The results revealed a median net chemical O_3 production flux of $0.6 \text{ nmol m}^{-2} \text{ s}^{-1}$ during daytime and a corresponding loss of $-0.05 \text{ nmol m}^{-2} \text{ s}^{-1}$ during nighttime. Hence, the day and nighttime O_3 deposition would increase and decrease by around 10 and 3 %, respectively. However, the fluxes were not corrected for this effect since the estimation method is prone

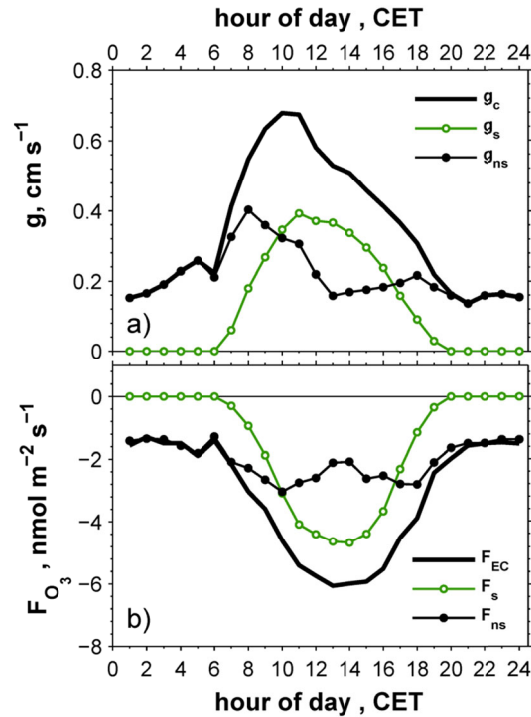


Fig. 10. Hourly median diurnal courses of (a) the canopy ($g_c = 1/R_c$) and stomatal (g_s) conductance (cf. Sect. 2.5) and the difference of both ($g_{ns} = g_c - g_s$) representing the non-stomatal conductance and (b) contribution of the stomatal (F_s) and non-stomatal ($F_{ns} = F_{EC} - F_s$) O_3 fluxes to the total O_3 deposition flux. All data from 04 August–26 September 2011 at the Mainz-Finthen grassland site are included.

to high uncertainties, caused by (i) calculation of the net effect as a difference of two counteracting chemical reactions and (ii) not involving all chemical reactions important for O_3 .

Massman et al. (2000) presented a helpful overview of studies on daytime O_3 fluxes above a variety of ecosystems. They reported on various grassland sites, some with large O_3 fluxes of -12 to -29 $\text{nmol m}^{-2} \text{s}^{-1}$ (e.g., Delany et al., 1986; Massman, 1993), others with fluxes in a mid-range of -6 to -13 $\text{nmol m}^{-2} \text{s}^{-1}$ (Grünhage et al., 1994), and also those with relatively low O_3 fluxes of -2 to -8 $\text{nmol m}^{-2} \text{s}^{-1}$ (Massman et al., 1994; Pio et al., 2000). The latter ones were in line with the O_3 fluxes determined by the *EC* method at the Mainz-Finthen site (Sect. 3.2.2, Fig. 7a). They also matched the daytime O_3 fluxes of -3 to -8 $\text{nmol m}^{-2} \text{s}^{-1}$ given in Meszaros et al. (2009) for a grassland site in Germany during late spring time ($LAI > 3$). Nevertheless, the nighttime O_3 fluxes of -1 $\text{nmol m}^{-2} \text{s}^{-1}$ given in Meszaros et al. (2009) were at the lower limit of the corresponding fluxes at our site.

4.1.2 Ozone flux partitioning

During the 54 measurement days daily averages of F_s and F_{ns} contributed 27 and 73 %, respectively, to the total O_3 deposition flux. Thus, the stomatal O_3 flux contribution at the natural grassland site in this study was lower compared to Stella et al. (2013b) who reported a contribution of F_s around 40 % and of F_{ns} around 60% for winter-wheat and maize crops at maturity, or Bassin et al. (2004) who

found similar partitioning results for both spring wheat crop in Italy and intensively managed grassland in Germany. In the present study, the average partitioning during daytime was almost equal between F_s and F_{ns} with 47 and 53 %, respectively. In comparison, Meszaros et al. (2009) reported a daytime partitioning of the total O_3 flux in F_s and F_{ns} by 84 and 16 %, respectively.

One explanation for the high contribution of F_{ns} to the daily averages in Mainz-Finthen were several nights with high wind speeds (cf. Fig. 5c). Those exhibited relatively high nighttime O_3 fluxes (cf. Fig. 5g), which entirely contributed to the non-stomatal O_3 deposition. In addition, Lamaud et al. (2009) reported a strong dependency of the partitioning on RH for a maize crop. They found F_{ns} for $RH > 60$ % but F_s for $RH < 60$ % to provide the dominating portion of the total O_3 deposition flux. They attributed this to (i) a decrease of g_s under high RH (e.g., Emberson et al., 2000) and (ii) an increase in cuticular deposition with RH (e.g., Altimir et al., 2004; 2006). During our campaign the median diurnal RH just above the canopy ($z = 0.8$ m) was below 60 % only for about three hours per day (15:00–17:00 CET; not shown), which would explain the relatively high non-stomatal O_3 deposition during daytime. Furthermore, the proportion of biologically inactive brown leaves found at the natural grassland site in Mainz-Finthen (> 40 %, cf. Table 2) was much higher than e.g., for intensive managed grassland ecosystems with regular cuts. These leaves did not contribute to stomatal O_3 uptake, but may have been involved in O_3 destruction by offering sufficient surface for water vapor condensation and heterogeneous surface reactions of O_3 .

Beside destruction of O_3 on outer plant and soil surfaces, the non-stomatal deposition has been attributed to chemical reactions of O_3 within and above the canopy. For example, Kurpius and Goldstein (2003) observed a chemically induced flux during summer for a ponderosa pine forest, that contributed 51 % to the total O_3 flux during daytime. In their study, the chemical reaction of O_3 with emitted VOCs resulted consequently in a F_{ns} contribution of 70 % during daytime. In contrast, Galmarini et al. (1997) found for a peat grassland that the O_3 flux was not affected by chemical reactions. As the NO and VOC emission fluxes at the Mainz-Finthen site were negligibly small (see above), the gas-phase chemical reactions of O_3 could not account for the high non-stomatal O_3 deposition. A consideration of the unusual O_3 production above the canopy (cf. Sect. 4.1.1) would have conversely led to an even higher non-stomatal O_3 flux.

4.2 Intercomparison of chamber and EC method

4.2.1 Method comparison for CO_2 and H_2O fluxes

A good comparability of the vegetation structure and activity covered by the *EC* and *CH* methods were prerequisite to compare the O_3 deposition fluxes from both methods. This was investigated by measuring the biologically relevant CO_2 and H_2O exchange with both methods. The good comparability of the H_2O fluxes throughout the day and of the CO_2 fluxes during daytime between 10:00 and 15:00 CET clearly indicated a reliable functioning of the chambers and no major disturbance of the plant activity within the chambers. In addition, the selected chamber plots appeared to be representative for the *EC* footprint area displayed in Fig. 1.

The generally high scatter and uncertainty of the CO_2 fluxes at low u^* (Fig. 6 and 9) mainly between late afternoon and morning is attributed to the initiation of stable stratification near the surface in the late afternoon, induced by cooling due to evaporation and simultaneously weakening of incoming short wave radiation (cf. also Riederer et al., 2013). Consequently, the vertical exchange was suppressed, which should be visible in the vertical CO_2 gradient. Fig. 11 shows a median diurnal course of vertical CO_2 profile measurements. A strong negative CO_2 gradient predominated during nighttime, which resulted from a temperature inversion inside the canopy (not shown), suppressing the exchange with the above-canopy layer. The emission from soil enriched the in-canopy air with CO_2 . The strong CO_2 gradients started to build up at 15:30 CET (Fig. 11b) with decreasing global radiation and lasted until 10:00 CET. The CH fluxes (Eq. 4) were based on sequentially measured trace gas mixing ratio differences between the well-mixed air in the chamber and the air at the chamber inlet in 0.2 m height. The assumption of stationarity was obviously violated for CO_2 under nighttime conditions due to the prevailing strong CO_2 gradients. Under these conditions, weak movements of the stably stratified air around the chamber inlet resulted in strongly fluctuating CO_2 mixing ratio with time. Consequently, the determined CO_2 fluxes from the CH method at 16:00–10:00 CET were highly uncertain. The results of the flux comparison for H_2O and CO_2 were in good agreement with other studies at low vegetation ecosystems, where often a slight underestimation of both fluxes by the CH method was reported (e.g., Graf et al., 2013; Oechel et al., 1998).

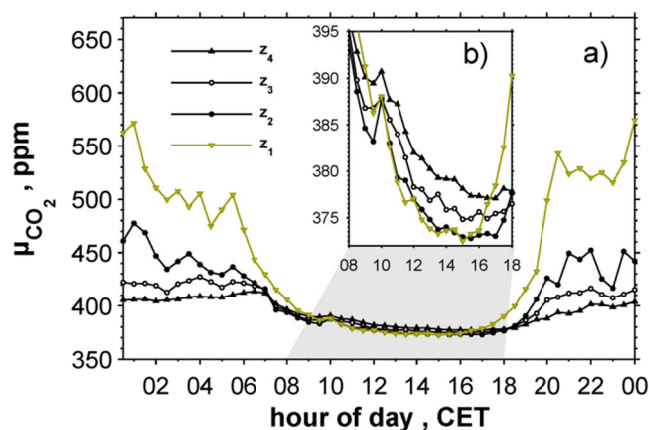


Fig. 11. Hourly median diurnal course of the vertical CO_2 mixing ratio profile (a) consisting of four heights (z_{1-4}) for the entire measurement campaign (04 August–27 September 2011) and (b) a zoom in for daytime.

4.2.2 Method comparison for O_3 flux and canopy resistance

The direct comparison of the (final corrected) EC and CH fluxes for O_3 showed a good agreement. Overall, the CH method underestimated the EC flux by only 11 % during daytime and overestimated it by 26 % during nighttime. The results clearly revealed the capability of the dynamic chamber method to capture representative diurnal cycles of O_3 deposition fluxes. Furthermore, the extract of the O_3 flux time series in Fig. 12a demonstrates that the method also allows a reliable determination of O_3 fluxes

for 30 min averaging intervals. The agreement was especially good, when u_* ranged between 0.15 and 0.3 m s⁻¹ (daytime of 30 Aug–01 Sep in Fig. 12a,b). During periods of higher u_* (28–29 Aug in Fig. 12b) the *EC* fluxes clearly exceeded the *CH* method and showed an unplausibly high peak. The discrepancy might have resulted from the hf-correction accounting for the tubing (Sect. 4.1.1), which most affected the *EC* fluxes during daytime as it is a function of wind speed.

For the correct estimation of deposition fluxes to ecosystems using e.g., big leaf dry deposition models with single (Hicks et al., 1987) or multiple vegetation layers (Baldochi, 1988), the canopy resistance R_c for the corresponding compound has to be quantified. According to Pape et al. (2009) and Eq. 10, the correction involves chamber characteristic resistances (R_{purge} , R_{mix} , R_b^*) and is fundamentally based on the assumption that the canopy resistance outside the chamber R_c (Eq. 3) is equal to the one inside R_c^* (Eq. 8). The good agreement of R_c and R_c^* suggests that this assumption was mostly fulfilled (Fig. 8a) as the daytime medians differed by only 25 % and taking into account that R_c and R_c^* were derived independently. Thus, they were prone to different sources of uncertainty. The uncertainty of the *EC* derived R_c depends on the errors of $R_a(z_{ref})$ and R_b (Eq. 3). They are both functions of the friction velocity u_* , which exhibits higher relative uncertainties for weak wind conditions (e.g., Stella et al., 2012). In addition, $R_a(z_{ref})$ is dependent on the stability parameter (z/L), which is prone to uncertainties especially during stable nighttime conditions (e.g., Geissbühler et al., 2000). This might explain the large scatter in the R_c values during nighttime. Furthermore, as discussed in the last paragraph, a strong nighttime inversion prevailed during several nights at the site, separating the in-canopy air layer from above. The corresponding decoupling effect might have been underestimated by the calculated $R_a(z_{ref})$. Consequently, the nighttime R_c values might have been overestimated, resulting in higher median values of R_c compared to R_c^* in Fig. 8a.

The daytime canopy resistances for O₃ measured at the natural grassland ecosystem in Mainz-Finthen were in the upper range of those reported for low vegetation ecosystems in the literature. Pleijel (1998) reported a median daytime R_c of 80 s m⁻¹ for a dense oat crop ($h_c = 1$ m) for spring and summer measurements. The dependence of the canopy resistance on maturation and senescence was illustrated in Gerosa et al. (2003), who found mean diurnal minima for R_c of 80 s m⁻¹ and 160 s m⁻¹ for fully developed and senescent wheat crops, respectively, in Italy. De Miguel and Bilbao (1999) reported mean daytime R_c of 100–150 s m⁻¹ for a Spanish green grassland in early summer. For an already harvested wheat field, Pilegaard et al. (1998) determined daytime R_c of 200 s m⁻¹. Hence, the comparatively high canopy resistances at our site was most likely caused by the high portion of senescent plant material during the summer-autumn transition (see Sect. 3.1.1 and 4.1.2) and the insignificant biogenic emissions (NO, VOCs) (see Sect. 4.1.1).

Previous studies rarely discussed the comparison of O₃ flux measurement methods. They mainly focused on the comparison of *EC* and aerodynamic gradient method (*AGM*) and reported contradictory results. For instance, Keronen et al. (2003) and Stella et al. (2012) found an agreement of both methods for O₃ flux measurements, whereas Muller et al. (2009) and Loubet et al. (2013) reported large discrepancies between *AGM* and *EC* methods. The present study is, to our knowledge, the first to report a direct comparison of *EC* and dynamic chamber measurements of O₃ ecosystem fluxes and canopy resistances.

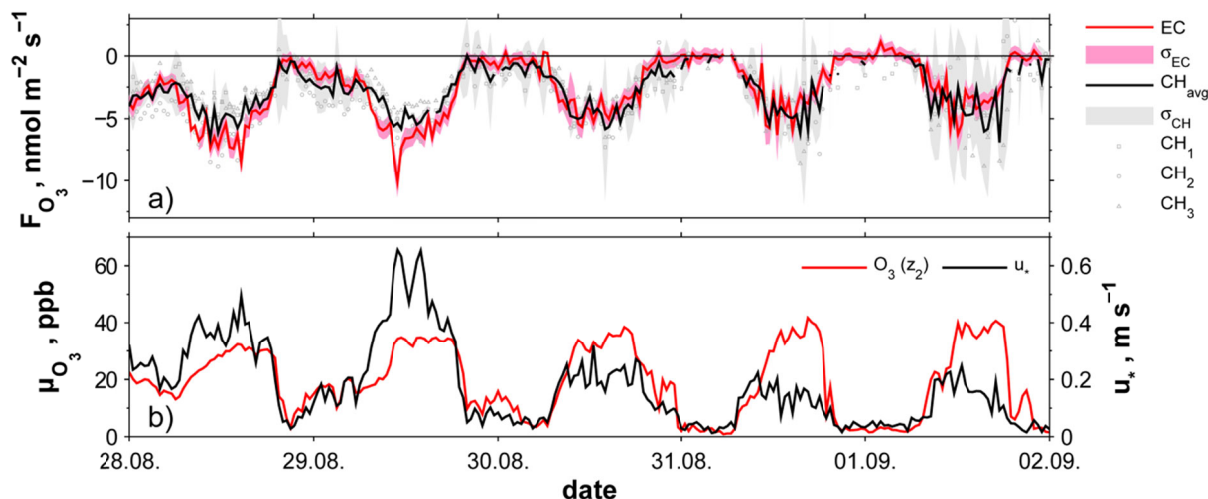


Fig. 12. Five days extract (28 August–02 September 2011) from the 30 min averaged time series of (a) O_3 fluxes determined by the *EC* and *CH* methods the Mainz-Finthen grassland site. The individual fluxes determined the dynamic chambers $CH_{\#1-\#3}$ are displayed along with the *CH* fluxes (CH_{avg}). *EC* flux errors determined by the TK3 software (Mauder et al., 2013) are shown (σ_{EC}) as well as the propagated error estimates (Eq. 7) for the fluxes determined by the *CH* method (σ_{CH}). In (b) the corresponding mixing ratios at $z_2 = 0.2$ m and u_* determined from the *EC* measurements are shown.

4.3 Characteristics and uncertainties of the dynamic chamber method

The good agreement of the final corrected chamber fluxes with the reference *EC* flux validated the applied chamber system and flux evaluation method including the used corrections. The chemically induced O_3 deposition flux within the *CH* volume (S_{gp} in Eq. 5) was on average below 1 % of the estimated O_3 flux throughout the campaign. Pape et al. (2009) demonstrated that for high NO soil emission and relatively low ambient O_3 mixing ratios S_{gp} could affect the determined O_3 flux by 25–100 %. However, due to the insignificant NO soil emissions at the Mainz-Finthen grassland site, S_{gp} was very low as well.

Much more relevant for the quantification of the true deposition flux was the correction of the modified aerodynamic conditions by the chambers (Eq. 10). It resulted in $F_{CH_{cor}}$ to be 33 % higher during daytime and 41 % higher during nighttime than $F_{CH_{gp}}$. For our setup and measurement conditions, the chamber fluxes would be strongly underestimated without this correction (Fig. 7b). Yet the effect can be different for other chamber operation characteristics and/or aerodynamic conditions.

The possibility of representative deposition measurements can be highly interesting for operators of dynamic chamber systems that are designed to measure biogenic soil NO emissions, as these systems often operate O_3 instruments simultaneously to account for chemical reactions in the chamber headspace. This implies that O_3 fluxes can be determined as a complementary component of standard NO flux measurements solely by installing one additional 3D ultra sonic anemometer for the quantification of R_a and R_b , which are required for the flux correction (Eqs. 9, 10). For cases with higher canopies,

such as in this study (see Fig. 3), an additional O_3 mixing ratio measurement above the canopy is needed as reference level (z_{ref}) for the ambient resistive scheme.

For the dynamic chamber system the chosen measurement cycle represented an optimized compromise between several requirements and aims: (a) a limitation of instationarities (for details see Sect. 2.4.2); (b) a sufficient time resolution, even in combination with the near surface trace gas profile (Fig. 2a), to yield one flux estimate per CH within 30 min; (c) representative rainfall amounts and soil moisture in the CH as a result of long open phases during 90 % of the day and (d) useful additional information due to the combination with the near surface trace gas profile. Furthermore, water vapor interference in the trace gas detection was eliminated by using Nafion dryers for the NO , NO_2 and O_3 measurements, which is particularly important for sequentially switched sampling in and outside of soil chambers associated with large humidity differences. Nevertheless, the fluxes determined with the CH method were based on much worse statistics than those from the EC method, which was mainly due to the much lower sampling frequency and the switching between different inlets. Thus, the error of the chamber fluxes σF_{CH} was clearly dominated by the effect of non-stationarity (quantified by Eq. 7).

4.4 Application of the chamber method for other trace gases

The suitability of the dynamic chamber method for deposition flux measurements has been verified here for ozone. However, the method may be equally applied for other depositing trace gases. We show exemplary results for NO_2 that was measured simultaneously in the present study (Sect. 2.4.1). The canopy resistance (R_c^*) for NO_2 was calculated from the CH measurements according to Eq. 8 assuming pure deposition with a zero compensation point. The resulting diurnal cycle presented in Fig. 13 shows a distinct pattern with minimum hourly medians of around 270 s m^{-1} in the morning hours. After that, the $R_c^*(NO_2)$ medians start to rise until they reach their maximal values around 560 s m^{-1} in the evening.

The median diurnal course of the canopy resistance for NO_2 was similar to the one for O_3 determined by the CH method (cf. Fig. 8a) but $R_c^*(NO_2)$ was on average 86 % higher than for O_3 . A direct interpretation and partitioning is more difficult for NO_2 , because of the potential existence of an internal leaf resistance in addition to the stomatal resistance as found in other studies (e.g., Eller and Sparks, 2006; Gut et al., 2002a; Stella et al., 2013a). The results indicate that the CH method is a useful tool to determine deposition fluxes and characteristic resistances for ecosystems with low vegetation.

5 Conclusion

Eddy covariance is the state-of-the-art method for trace gas flux measurements between the surface and the atmosphere. Nevertheless, there are arguments favoring the dynamic chamber against the eddy covariance method for certain applications. Among these are (i) applicability of chamber methods on small plots for investigations on gas exchange of different vegetation species and management forms, (ii) a more direct determination of canopy resistances that are required as input parameters for process and modeling studies, (iii) well defined gas-phase chemistry corrections for reactive compounds under the well-mixed chamber conditions. Thus, for fluxes of compounds emitted by soils or plants, such as

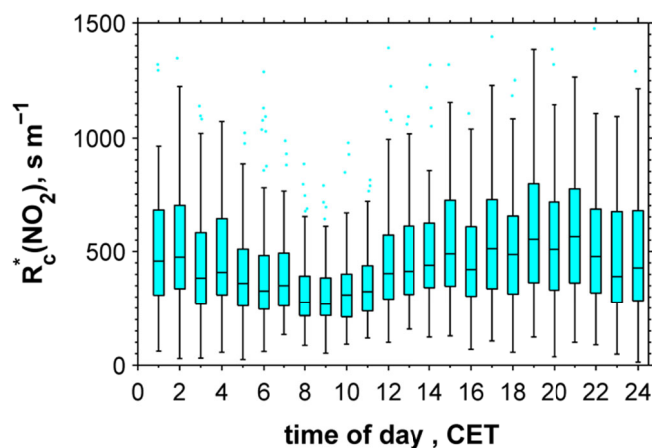


Fig. 13. Diurnal cycles based on hourly box plot statistics of the canopy resistance (R_c^*) for NO_2 determined by the *CH* method (Eq. 8) for the entire measurement campaign (04 August–27 September 2011) at the Mainz-Finthen grassland site.

CO_2 , H_2O , NO , ammonia or VOCs, the application of the dynamic chamber method is a commonly and widely used approach.

In this manuscript we demonstrated that the dynamic chamber method is also a suitable technique to determine O_3 deposition fluxes for grassland ecosystems. Our results are based on 54 continuous measurement days on a natural, nutrient-poor grassland site in Germany. Prerequisites for the O_3 flux comparison were a similar vegetation structure and activity within the (mostly overlapping) footprint of both methods. A good daytime agreement of CO_2 and H_2O fluxes (deviations only 10 and 1 %, respectively) and a footprint analysis confirmed these prerequisites to be fulfilled.

Since deposition fluxes strongly depend on the turbulent resistances and a dynamic chamber itself modifies the resistive scheme, a correction of the measured deposition flux has to be applied. The correction depends on chamber characteristics (chamber height, flow rate, mixing inside the chamber) and on the ambient turbulence conditions. For quantifying the latter, a sonic anemometer is needed in addition to the chamber measurements. In cases when the canopy height is similar to the chamber height, a reference O_3 mixing ratio has to be measured above the canopy. This can be significantly different from the O_3 mixing ratio at the chamber inlet.

In our study, the corrected O_3 deposition flux resulting from the dynamic chamber method agreed well with the fluxes determined with the *EC* method (within 11 and 26 % during day and nighttime, respectively). Even short term variations in the time series of the half-hourly eddy covariance fluxes can be retraced by the dynamic chamber method. The investigation on the dynamic chamber flux quality revealed a strong u_* dependence of the relative flux error. For CO_2 and O_3 the relative half-hourly flux sampling error was mostly below 25 % when u_* was above 0.16 m s^{-1} and 0.22 m s^{-1} , respectively. In contrast, lower u_* values were connected with much higher relative errors. On the other hand, some systematic disagreement between the O_3 fluxes was also observed during phases of very strong wind speed and turbulence. The partitioning of the total O_3 deposition flux revealed that O_3 was predominantly deposited through a non-stomatal pathway considering the daily total. During daytime the sto-

matal and non-stomatal pathways both contributed about 50 % to the O₃ deposition. Since the contribution of gas phase chemical reactions to the (apparent) non-stomatal O₃ deposition was of minor importance in the present study, ozone destruction processes at the plant and soil surfaces must have played a major role.

The present findings may be especially useful for operators of dynamic chamber systems for the determination of NO soil emission fluxes. These systems generally run simultaneous O₃ mixing ratio measurements for gas-phase chemistry corrections. Such systems can easily be used for continuous O₃ and NO₂ flux measurements in order to extend the knowledge on the deposition of these gases and on the underlying processes for a large range of ecosystems.

Acknowledgements

This project was funded by the Max Planck Society. We are grateful to H. Gross for the electrical installations at the field site and for logistical support. We are indebted to E. Falge for support in determining the plant species and the leaf area index.

References

- Altimir, N. et al., 2006. Foliage surface ozone deposition: a role for surface moisture? *Biogeosciences*, 3(2): 209-228.
- Altimir, N., Tuovinen, J.P., Vesala, T., Kulmala, M. and Hari, P., 2004. Measurements of ozone removal by Scots pine shoots: calibration of a stomatal uptake model including the non-stomatal component. *Atmospheric Environment*, 38(15): 2387-2398.
- Amon, B., Kryvoruchko, V., Amon, T. and Zechmeister-Boltenstern, S., 2006. Methane, nitrous oxide and ammonia emissions during storage and after application of dairy cattle slurry and influence of slurry treatment. *Agriculture Ecosystems & Environment*, 112(2-3): 153-162.
- Atkinson, R. et al., 2004. Evaluated kinetic and photochemical data for atmospheric chemistry: Volume I - gas phase reactions of O_(x), HO_(x), NO_(x) and SO_(x) species. *Atmospheric Chemistry and Physics*, 4: 1461-1738.
- Aubinet, M. et al., 2000. Estimates of the annual net carbon and water exchange of forests: The EUROFLUX methodology. *Advances in Ecological Research*, Vol 30, 30: 113-175.
- Baldocchi, D., 1988. A multi-layer model for estimating sulfur-dioxide deposition to a deciduous oak forest canopy. *Atmospheric Environment*, 22(5): 869-884.
- Baldocchi, D. et al., 2001. FLUXNET: A new tool to study the temporal and spatial variability of ecosystem-scale carbon dioxide, water vapor, and energy flux densities. *Bulletin of the American Meteorological Society*, 82(11): 2415-2434.
- Bassin, S., Calanca, P., Weidinger, T., Gerosa, G. and Fuhrer, E., 2004. Modeling seasonal ozone fluxes to grassland and wheat: model improvement, testing, and application. *Atmospheric Environment*, 38(15): 2349-2359.
- Bourtsoukidis, E. et al., 2012. Ozone stress as a driving force of sesquiterpene emissions: a suggested parameterisation. *Biogeosciences*, 9(11): 4337-4352.
- Cantrell, C.A., 2008. Technical note: review of methods for linear least-squares fitting of data and application to atmospheric chemistry problems. *Atmospheric Chemistry and Physics*, 8(17): 5477-5487.
- De Miguel, A. and Bilbao, J., 1999. Ozone dry deposition and resistances onto green grassland in summer in central Spain. *Journal of Atmospheric Chemistry*, 34(3): 321-338.

- Delany, A.C. et al., 1986. Direct measurements of nitrogen-oxides and ozone fluxes over grassland. *Journal of Atmospheric Chemistry*, 4(4): 429-444.
- Denmead, O.T., 2008. Approaches to measuring fluxes of methane and nitrous oxide between landscapes and the atmosphere. *Plant and Soil*, 309(1-2): 5-24.
- Dolman, A.J. et al., 2006. The CarboEurope regional experiment strategy. *Bulletin of the American Meteorological Society*, 87(10): 1367-1379.
- Dorsey, J.R. et al., 2004. Oxidized nitrogen and ozone interaction with forests. I: Experimental observations and analysis of exchange with Douglas fir. *Quarterly Journal of the Royal Meteorological Society*, 130(600): 1941-1955.
- Eller, A.S.D. and Sparks, J.P., 2006. Predicting leaf-level fluxes of O₃ and NO₂: the relative roles of diffusion and biochemical processes. *Plant Cell and Environment*, 29(9): 1742-1750.
- Emberson, L.D., Wieser, G. and Ashmore, M.R., 2000. Modelling of stomatal conductance and ozone flux of Norway spruce: comparison with field data. *Environmental Pollution*, 109(3): 393-402.
- Ermel, M. et al., 2013. Preparation methods to optimize the performance of sensor discs for fast chemiluminescence ozone analyzers. *Environmental Science & Technology*, 47(4): 1930-1936.
- Felzer, B.S., Cronin, T., Reilly, J.M., Melillo, J.M. and Wang, X.D., 2007. Impacts of ozone on trees and crops. *Comptes Rendus Geoscience*, 339(11-12): 784-798.
- Finkelstein, P.L. and Sims, P.F., 2001. Sampling error in eddy correlation flux measurements. *Journal of Geophysical Research-Atmospheres*, 106(D4): 3503-3509.
- Foken, T., 2008. *Micrometeorology*. Springer, Berlin, Heidelberg 306 pp.
- Foken, T., Aubinet, M. and Leuning, R., 2012. The eddy covariance method. In: M. Aubinet, T. Vesala and D. Papale (Editors), *Eddy covariance*. Springer, Dordrecht, Heidelberg, London, New York, pp. 438.
- Forster, P. et al., 2007. Changes in atmospheric constituents and in radiative forcing. In: S. Solomon et al. (Editors), *Climate change 2007: the physical basis. contribution of working group I to fourth assessment report of IPCC on climate change*. Cambridge University Press, Cambridge, UK/ NY, USA.
- Fowler, D. et al., 2009. Atmospheric composition change: ecosystems-atmosphere interactions. *Atmospheric Environment*, 43(33): 5193-5267.
- Galmarini, S., DeArellano, J.V.G. and Duyzer, J., 1997. Fluxes of chemically reactive species inferred from mean concentration measurements. *Atmospheric Environment*, 31(15): 2371-2374.
- Geissbühler, P., Siegwolf, R. and Eugster, W., 2000. Eddy covariance measurements on mountain slopes: The advantage of surface-normal sensor orientation over a vertical set-up. *Boundary-Layer Meteorology*, 96(3): 371-392.
- Gerosa, G., Cieslik, S. and Ballarin-Denti, A., 2003. Micrometeorological determination of time-integrated stomatal ozone fluxes over wheat: a case study in Northern Italy. *Atmospheric Environment*, 37(6): 777-788.
- Göckede, M., Markkanen, T., Hasager, C.B. and Foken, T., 2006. Update of a footprint-based approach for the characterisation of complex measurement sites. *Boundary-Layer Meteorology*, 118(3): 635-655.
- Göckede, M., Rebmann, C. and Foken, T., 2004. A combination of quality assessment tools for eddy covariance measurements with footprint modelling for the characterisation of complex sites. *Agricultural and Forest Meteorology*, 127(3-4): 175-188.
- Graf, A. et al., 2013. Validation of a minimum microclimate disturbance chamber for net ecosystem flux measurements. *Agricultural and Forest Meteorology*, 174: 1-14.
- Grünhage, L., Dammgen, U., Haenel, H.D. and Jäger, H.J., 1994. Response of a grassland ecosystem to air-pollutants. 3. The chemical climate - Vertical flux densities of gaseous species in the atmosphere near the ground. *Environmental Pollution*, 85(1): 43-49.
- Grünhage, L., Haenel, H.D. and Jäger, H.J., 2000. The exchange of ozone between vegetation and atmosphere: micrometeorological measurement techniques and models. *Environmental Pollution*, 109(3): 373-392.

- Gut, A. et al., 2002a. Exchange fluxes of NO₂ and O₃ at soil and leaf surfaces in an Amazonian rain forest. *Journal of Geophysical Research-Atmospheres*, 107(D20): LBA 27-1–LBA 27-15.
- Gut, A. et al., 2002b. NO emission from an Amazonian rain forest soil: Continuous measurements of NO flux and soil concentration. *Journal of Geophysical Research-Atmospheres*, 107(D20): LBA 24-1–LBA 24-10.
- Hicks, B.B., Baldocchi, D.D., Meyers, T.P., Hosker, R.P. and Matt, D.R., 1987. A preliminary multiple resistance routine for deriving dry deposition velocities from measured quantities. *Water Air and Soil Pollution*, 36(3-4): 311-330.
- Jäggi, M., Ammann, C., Neftel, A. and Fuhrer, J., 2006. Environmental control of profiles of ozone concentration in a grassland canopy. *Atmospheric Environment*, 40(28): 5496-5507.
- Keronen, P. et al., 2003. Ozone flux measurements over a scots pine forest using eddy covariance method: performance evaluation and comparison with flux-profile method. *Boreal Environment Research*, 8(4): 425-443.
- Kesselmeier, J., Bode, K., Gerlach, C. and Jork, E.M., 1998. Exchange of atmospheric formic and acetic acids with trees and crop plants under controlled chamber and purified air conditions. *Atmospheric Environment*, 32(10): 1765-1775.
- Kowalski, S., Sartore, M., Burlett, R., Berbigier, P. and Loustau, D., 2003. The annual carbon budget of a French pine forest (*Pinus pinaster*) following harvest. *Global Change Biology*, 9(7): 1051-1065.
- Kurpius, M.R. and Goldstein, A.H., 2003. Gas-phase chemistry dominates O₃ loss to a forest, implying a source of aerosols and hydroxyl radicals to the atmosphere. *Geophysical Research Letters*, 30(7).
- Lamaud, E. et al., 2009. Partitioning of ozone deposition over a developed maize crop between stomatal and non-stomatal uptakes, using eddy-covariance flux measurements and modelling. *Agricultural and Forest Meteorology*, 149(9): 1385-1396.
- Laville, P. et al., 2009. Characterisation of soil emissions of nitric oxide at field and laboratory scale using high resolution method. *Atmospheric Environment*, 43(16): 2648-2658.
- Leuning, R. and King, K.M., 1992. Comparison of eddy-covariance measurements of CO₂ fluxes by open-path and closed-path CO₂ analyzers. *Boundary-Layer Meteorology*, 59(3): 297-311.
- Loubet, B. et al., 2013. Investigating discrepancies in heat, CO₂ fluxes and O₃ deposition velocity over maize as measured by the eddy-covariance and the aerodynamic gradient methods. *Agricultural and Forest Meteorology*, 169: 35-50.
- Massman, W., 2004. Concerning the measurement of atmospheric trace gas fluxes with open- and closed-path eddy covariance systems: the WPL terms and spectral attenuation. In: X. Lee, W. Massman and B. Law (Editors), *Handbook of micrometeorology*. Kluwer, New York, Boston, Dordrecht, London, Moscow, pp. 250.
- Massman, W.J., 1993. Partitioning ozone fluxes to sparse grass and soil and the inferred resistances to dry deposition. *Atmospheric Environment Part a-General Topics*, 27(2): 167-174.
- Massman, W.J., Musselman, R.C. and Lefohn, A.S., 2000. A conceptual ozone dose-response model to develop a standard to protect vegetation. *Atmospheric Environment*, 34(5): 745-759.
- Massman, W.J. et al., 1994. An evaluation of the regional acid deposition model surface module for ozone uptake at 3 sites in the San-Joaquin Valley of California. *Journal of Geophysical Research-Atmospheres*, 99(D4): 8281-8294.
- Matthews, R.D., Sawyer, R.F. and Schefer, R.W., 1977. Interferences in chemiluminescent measurement of NO and NO₂ emissions from combustion systems. *Environmental Science & Technology*, 11(12): 1092-1096.
- Mauder, M. et al., 2013. A strategy for quality and uncertainty assessment of long-term eddy-covariance measurements. *Agricultural and Forest Meteorology*, 169: 122-135.
- Mauder, M. and Foken, T., 2011. Documentation and instruction manual of the eddy-covariance software package TK3. *Arbeitsergebnisse Nr. 46(46)*.

- Meehl, G.A. et al., 2007. Global climate projections. In: S. Solomon et al. (Editors), *Climate change 2007: the physical basis. Contribution of working group I to fourth assessment report of IPCC on climate change*. Cambridge University Press, Cambridge, UK/NY, USA.
- Meszaros, R. et al., 2009. Measurement and modelling ozone fluxes over a cut and fertilized grassland. *Biogeosciences*, 6(10): 1987-1999.
- Moore, C.J., 1986. Frequency-response corrections for eddy-correlation systems. *Boundary-Layer Meteorology*, 37(1-2): 17-35.
- Moravek, A., Trebs, I. and Foken, T., 2013. Effect of imprecise lag time and high-frequency attenuation on surface-atmosphere exchange fluxes determined with the relaxed eddy accumulation method. *Journal of Geophysical Research-Atmospheres*, 118(17): 10210-10224.
- Muller, J.B.A. et al., 2009. Comparison of ozone fluxes over grassland by gradient and eddy covariance technique. *Atmospheric Science Letters*, 10(3): 164-169.
- Muller, J.B.A. et al., 2010. Sources of uncertainty in eddy covariance ozone flux measurements made by dry chemiluminescence fast response analysers. *Atmos. Meas. Tech.*, 3(1): 163-176.
- Oechel, W.C., Vourlitis, G.L., Brooks, S., Crawford, T.L. and Dumas, E., 1998. Intercomparison among chamber, tower, and aircraft net CO₂ and energy fluxes measured during the Arctic System Science Land-Atmosphere-Ice Interactions (ARCSS-LAII) Flux Study. *Journal of Geophysical Research-Atmospheres*, 103(D22): 28993-29003.
- Pape, L. et al., 2009. An automated dynamic chamber system for surface exchange measurement of non-reactive and reactive trace gases of grassland ecosystems. *Biogeosciences*, 6(3): 405-429.
- Pilegaard, K., Hummelshoj, P. and Jensen, N.O., 1998. Fluxes of ozone and nitrogen dioxide measured by eddy correlation over a harvested wheat field. *Atmospheric Environment*, 32(7): 1167-1177.
- Pio, C.A., Feliciano, M.S., Vermeulen, A.T. and Sousa, E.C., 2000. Seasonal variability of ozone dry deposition under southern European climate conditions, in Portugal. *Atmospheric Environment*, 34(2): 195-205.
- Pleijel, H., 1998. A suggestion of a simple transfer function for the use of ozone monitoring data in dose-response relationships obtained using open-top chambers. *Water Air and Soil Pollution*, 102(1-2): 61-74.
- Rannik, U. et al., 2000. Footprint analysis for measurements over a heterogeneous forest. *Boundary-Layer Meteorology*, 97(1): 137-166.
- Rehme, K.A., Martin, B.E. and Hodgeson, J.A., 1974. Tentative method for the calibration of nitric oxide, nitrogen dioxide and ozone analyzers by gas phase titration, U.S. Environmental Protection Agency, Research Triangle Park, NC, USA.
- Riederer, M., Serafimovich, A. and Foken, T., 2013. Net ecosystem CO₂ exchange measurements by the closed chamber method and the eddy covariance technique and their dependence on atmospheric conditions - a case study. *Atmos. Meas. Tech. Discuss.*, 6(5): 8783-8805.
- Rummel, U. et al., 2007. Seasonal variation of ozone deposition to a tropical rain forest in southwest Amazonia. *Atmospheric Chemistry and Physics*, 7(20): 5415-5435.
- Running, S.W. et al., 1999. A global terrestrial monitoring network integrating tower fluxes, flask sampling, ecosystem modeling and EOS satellite data. *Remote Sensing of Environment*, 70(1): 108-127.
- Ruuskanen, T.M. et al., 2011. Eddy covariance VOC emission and deposition fluxes above grassland using PTR-TOF. *Atmospheric Chemistry and Physics*, 11(2): 611-625.
- Sitch, S., Cox, P.M., Collins, W.J. and Huntingford, C., 2007. Indirect radiative forcing of climate change through ozone effects on the land-carbon sink. *Nature*, 448(7155): 791-U4.
- Stella, P. et al., 2013a. Measurements of nitrogen oxides and ozone fluxes by eddy covariance at a meadow: evidence for an internal leaf resistance to NO₂. *Biogeosciences*, 10(9): 5997-6017.
- Stella, P., Loubet, B., Lamaud, E., Laville, P. and Cellier, P., 2011a. Ozone deposition onto bare soil: a new parameterisation. *Agricultural and Forest Meteorology*, 151(6): 669-681.

- Stella, P. et al., 2012. Comparison of methods for the determination of NO-O₃-NO₂ fluxes and chemical interactions over a bare soil. *Atmospheric Measurement Techniques*, 5(6): 1241-1257.
- Stella, P. et al., 2013b. Assessment of the total, stomatal, cuticular, and soil 2 year ozone budgets of an agricultural field with winter wheat and maize crops. *Journal of Geophysical Research: Biogeosciences*: 1120-1132.
- Stella, P. et al., 2011b. Predicting and partitioning ozone fluxes to maize crops from sowing to harvest: the Surf atm-O₃ model. *Biogeosciences*, 8(10): 2869-2886.
- Trebs, I. et al., 2009. Relationship between the NO₂ photolysis frequency and the solar global irradiance. *Atmospheric Measurement Techniques*, 2(2): 725-739.
- Vingarzan, R., 2004. A review of surface ozone background levels and trends. *Atmospheric Environment*, 38(21): 3431-3442.
- Webb, E.K., Pearman, G.I. and Leuning, R., 1980. Correction of flux measurements for density effects due to heat and water-vapor transfer. *Quarterly Journal of the Royal Meteorological Society*, 106(447): 85-100.
- Wilczak, J.M., Oncley, S.P. and Stage, S.A., 2001. Sonic anemometer tilt correction algorithms. *Boundary-Layer Meteorology*, 99(1): 127-150.
- Wild, O., 2007. Modelling the global tropospheric ozone budget: exploring the variability in current models. *Atmospheric Chemistry and Physics*, 7(10): 2643-2660.
- Wilson, K.L. and Birks, J.W., 2006. Mechanism and elimination of a water vapor interference in the measurement of ozone by UV absorbance. *Environmental Science & Technology*, 40(20): 6361-6367.
- Zahn, A. et al., 2012. A fast and precise chemiluminescence ozone detector for eddy flux and airborne application. *Atmospheric Measurement Techniques*, 5(2): 363-375.

APPENDIX D

Influence of meteorology and anthropogenic pollution on chemical divergence of the NO-NO₂-O₃ triad above and within a natural grassland canopy

D. Plake¹, M. Sörgel¹, P. Stella^{1*}, A. Held² and I. Trebs^{1**}

[1] Max Planck Institute for Chemistry, Biogeochemistry Department, P. O. Box 3060, 55020 Mainz, Germany.

[2] University of Bayreuth, Junior Professorship in Atmospheric Chemistry, Bayreuth, Germany.

* now at: AgroParisTech, UMR INRA/ AgroParisTech SAD-APT, Paris, France

** now at: Centre de Recherche Public - Gabriel Lippmann, Department Environment and Agrobiotechnologies, 41 rue du Brill, L-4422 Belvaux, Luxembourg

Submitted to Biogeosciences: 09 May 2014

Abstract

The detailed understanding on surface-atmosphere exchange of reactive trace gas species is a crucial precondition for reliable modeling of processes in atmospheric chemistry. Plant canopies significantly impact the surface-atmosphere exchange. In the past, many studies focused on taller forest canopies or crops, where the bulk plant material is concentrated in the uppermost canopy layer. However, within grasslands, a land-cover class that globally covers vast terrestrial areas, the canopy structure is fundamentally different, as the main biomass is concentrated in the lowest canopy part. This has obvious implications for aerodynamic in-canopy transport, and consequently also impacts on global budgets of key species in atmospheric chemistry such as nitric oxide (NO), nitrogen dioxide (NO₂) and ozone (O₃).

This study presents for the first time a comprehensive data set of directly measured in-canopy transport times and aerodynamic resistances, chemical timescales, Damköhler numbers, trace gas and micrometeorological measurements for a natural grassland canopy. Special attention is paid to the impact of contrasting meteorological and air chemical conditions on in-canopy transport and chemical divergence. Our results show that the grassland canopy is decoupled throughout the day. In the lower canopy, the measured transport times are fastest during nighttime, which is due to convection during

nighttime and stable stratification during daytime in this layer. This was found inverse in the layer above. During periods of low wind speeds and high NO_x ($\text{NO}+\text{NO}_2$) levels, the canopy decoupling its effect on transport was found especially distinct. The aerodynamic resistance in the lower canopy was with around 1000 s m^{-1} as high as values from literature representing the lowest meter of an Amazonian rain forest canopy. The aerodynamic resistance representing the bulk canopy was found more than 3–4 times higher as in forests. Calculated Damköhler numbers (ratio of transport and chemical timescale) indicated a strong flux divergence for the $\text{NO}-\text{NO}_2-\text{O}_3$ triad within the canopy during daytime. At that time, the timescale of NO_2 plant uptake ranged from 90 to 160 s and was the fastest relevant timescale. Thus, our results clearly reveal that grassland canopies of similar structure have a strong potential to recapture NO , which before might have been emitted by the soil below. Furthermore, a photo-chemical O_3 production above the canopy was observed, which resulted from a surplus of NO_2 from the $\text{NO}-\text{NO}_2-\text{O}_3$ photostationary state. The O_3 production was one order of magnitude during high NO_x than during low NO_x periods and resulted in an O_3 flux underestimation, which was observed for the first time.

1 Introduction

Nitric oxide (NO) and nitrogen dioxide (NO_2) play a crucial role in air chemistry since they act as key catalysts for ozone (O_3) production and are therefore involved in the generation of hydroxyl radicals (OH) (Crutzen, 1973). The most significant atmospheric source for O_3 is initiated by photochemical dissociation of NO_2 and subsequent reaction of the resulting oxygen (O) atom with NO :



When O_3 is present, it may oxidize NO and re-form NO_2 :



In the absence of additional reactions, R1–R3 represent a null cycle. Beside R1–R3, NO is oxidized by OH radicals constituting an additional important net O_3 production pathway in the troposphere (Warneck, 2000).

Dry-deposition to terrestrial surfaces, especially to plant canopies, is an important sink for tropospheric O_3 and NO_2 . The uncertainties of dry deposition estimates are substantially higher for NO_2 , because its net ecosystem exchange can be bi-directional depending on the ambient NO_2 levels (Lerdau et al., 2000). O_3 instead is exclusively deposited to surfaces. In contrast, NO is known to be mainly net emitted from nearly all soil types. Biogenic NO soil emissions contribute significantly with $\sim 20\%$ to the global NO_x ($\text{NO}+\text{NO}_2$) emissions (IPPC, 2007), highlighting the need of careful investigations on NO soil-atmosphere exchange.

A major challenge for studies investigating surface-atmosphere exchange fluxes of these reactive trace gases is the presence of plant canopies. These significantly modify the turbulent properties of the surface that drive trace gas exchange. Most previous studies focused on taller canopies such as forests. However, grassland canopies represent a highly important land cover class covering globally 41 % and Europe-wide 19 % of the terrestrial land surface (Kasanko et al., 2011; Suttie et al., 2005). In contrast to forests, grasslands feature the main bulk plant area density near the soil (e.g., Jäggi et al., 2006;

Ripley and Redman, 1976), accompanied with mean distances between plant elements of only some millimeters (Aylor et al., 1993). Organized coherent structures govern turbulence dynamics within and above plant canopies (Finnigan, 2000). The mean in-canopy transport is slower than above the canopy. This modification of in-canopy transport has important implications for global atmospheric chemistry. Plant canopies and the soil below are biologically actively emitting and taking up reactive trace gases, and they may provide sufficient time for fast chemical reactions to occur within the canopy (Nemitz et al., 2009). Subsequently they modify surface exchange fluxes. For instance, ammonia can be released by a part of the canopy and taken up by another (Denmead et al., 2007; Nemitz et al., 2000). In addition, recapturing of NO_2 originating from biogenic soil NO emissions after reaction with O_3 within plant canopies (Rummel et al., 2002) is accounted for in global models by a so-called canopy reduction factor for NO_x (Yienger and Levy, 1995). However, these estimates are based on only one single experiment in the Amazon Basin (Bakwin et al., 1990), and the subsequent model analysis (Jacob and Wofsy, 1990). Canopy reduction for grasslands and other ecosystems were not studied in detail up to now. Consequently, the contrasting canopy structure of grassland and forest ecosystems highlight the need for a detailed analysis.

Net ecosystem exchange fluxes are typically measured at a certain height above the canopy. They rely on the constant flux assumption (e.g., Swinbank, 1968), which however, may be violated for reactive trace gases within or just above the vegetation. To assess the potential chemical divergence of exchange fluxes, the Damköhler number (DA) has commonly been applied (e.g., Rinne et al., 2012). DA is calculated as the ratio of the transport time (τ_{tr}) and the characteristic chemical timescale (τ_{ch}):

$$DA = \frac{\tau_{tr}}{\tau_{ch}} \quad (1)$$

Hence, DA above unity indicate chemical reactions to occur significantly faster than the transport (flux divergence), whereas DA smaller than 0.1 indicate the reverse case. The range in-between is commonly addressed as a critical range, where an impact of chemistry cannot be excluded (Stella et al., 2013). In this paper, we present directly measured transport times, chemical timescales and corresponding Damköhler numbers for three layers above and within a natural grassland canopy under contrasting meteorological and air chemical conditions. For the first time, such a comprehensive analysis involving trace gas and micrometeorological measurements is made for a grassland canopy. Furthermore, the consequences of in-canopy processes for NO_x canopy reduction and simultaneously measured O_3 deposition fluxes will be discussed.

2 Material and Methods

2.1 Site description

We performed an intensive field experiment from July to September 2011 at the estate of the Mainz-Finthen Airport in Rhineland-Palatinate, Germany. The vegetation at the site was nutrient-poor grassland with a mean canopy height (h_c) of 0.6 m and a leaf area index (LAI) of 4.8. A list of species and an LAI profile are given in Plake et al. (2014), with the latter indicating a high biomass density below 0.2 m corresponding to 85 % of the total LAI . Topographically located on a plateau 150 m above the

Rhine valley, the site was situated about 9 km south-west of the city center of Mainz. The site was surrounded by villages and motorways in a distance of 2 to 6 km and 4 to 15 km, respectively. The surrounding area was mainly characterized by agricultural use for vineyards, orchards and crops. The fetch was largest in south-western direction without significant anthropogenic pollution sources.

2.2 Experimental setup

A vertical Thoron (Tn) profile system was operated at $z_1 = 0.04$ m, $z_2 = 0.2$ m and $z_3 = 0.8$ m for the direct determination of transport times (for details see Plake and Trebs, 2013). Vertical profiles of NO, NO₂, O₃ and CO₂ were measured at z_1 , z_2 , z_3 and additionally at $z_4 = 4.0$ m by a system described in Plake et al. (2014). This study is based on simultaneous operation of both vertical profile systems at identical heights and, thus, evaluates the period from 19 August to 26 September 2011. Vertical profiles of temperature (HMT337, Vaisala, Helsinki, Finland), wind speed and direction (WS425, Vaisala, Helsinki, Finland) were installed at 0.2 m, 0.8 m, 1.5 m, 2.5 m, 4.0 m. Soil temperature (107L, Campbell Scientific Inc., Logan, USA) was measured at -0.02 m. Global radiation (G) and the NO₂ photolysis frequency (j_{NO_2}) were measured at a height of 2.5 m with a net radiometer (CNR1, Kipp&Zonen, Delft, Netherlands), and a filter radiometer (Meteorology Consult GmbH, Glashütten, Germany), respectively. The data of temperature, wind and radiation were recorded by a data logger (CR3000, Campbell Scientific) every 10 seconds. A three dimensional sonic anemometer (CSAT-3, Campbell Scientific) placed at $z_{ref} = 3.0$ m measured 3D wind and temperature at 20 Hz and the data were recorded by a CR3000 data logger. The friction velocity (u_*) and stability functions (z/L) were computed using the TK3 software (see Mauder and Foken, 2011). eddy covariance fluxes of O₃ were simultaneously measured, which are described in detail by Plake et al. (2014).

2.3 Theory

The data analysis was carried out for three individual layers (L_{1-3}), which were named in ascending order starting at the soil surface. Hence, L_1 was the lower canopy layer between the corresponding measurement heights z_{1-2} ($\Delta z(L_1) = 0.16$ m), L_2 the upper canopy layer between z_{2-3} ($\Delta z(L_2) = 0.6$ m), and L_3 the layer above the canopy between z_3 and z_{ref} ($\Delta z(L_3) = 2.2$ m). As shown in Plake et al. (2014) the vertical trace gas gradients between z_{ref} and z_4 were negligible, allowing the use of mixing ratios measured at z_4 for L_3 .

2.3.1 Chemical timescales

The overall chemical timescale τ_{ch} (in s) of the NO-NO₂-O₃ triad (Lenschow, 1982) was calculated for each layer (L_i , $i = 1, 2, 3$) as:

$$\tau_{ch}(L_i) = \frac{2}{\sqrt{j_{NO_2}(L_i) \cdot k_1(L_i) \cdot (N_{O_3}(L_i) + N_{NO}(L_i))^2 + 2j_{NO_2}(L_i) \cdot k_1(L_i) \cdot (N_{O_3}(L_i) + N_{NO}(L_i) + 2N_{NO_2}(L_i))^2}} \quad (2)$$

where N_{O_3} , N_{NO} and N_{NO_2} were number densities (in molecules cm⁻³) of O₃, NO and NO₂ for L_{1-3} , and k_3 the reaction rate constant of R3 (in cm³ molecule⁻¹ s⁻¹) according to Atkinson et al. (2004). Geometric means of mixing ratios for L_{1-3} were used to account for non-linear profiles.

2.3.2 NO₂ photolysis within the canopy

The data gaps in the measured time series of j_{NO_2} (in s⁻¹) above the canopy were filled using the parameterization of j_{NO_2} as a function of G (in W m⁻²) by Trebs et al. (2009). This approach was also used to parameterize in-canopy j_{NO_2} from a vertical in-canopy profile of G . The latter was calculated as function of the LAI profile using the method of Monsi and Saeki (1953):

$$G(LAI) = G_0 \cdot \exp(-k_{ex} \cdot LAI) \quad (3)$$

where G_0 (in W m⁻²) is the above-canopy G and k_{ex} is the dimensionless extinction coefficient of the canopy. In this study, the extinction coefficient of barley ($k_{ex} = 0.69$ by Monteith and Unsworth (1990)) was used. First $G(LAI)$ was deduced and then converted into j_{NO_2} . Finally, geometric means of j_{NO_2} were calculated for $j_{NO_2}(L_{1-3})$.

2.3.3 Transport times

For L_3 , height integrated transport times $\tau_{tr}(L_3)$ (in s) were derived by multiplying the aerodynamic resistance ($R_a(L_3)$) (e.g., Erisman et al., 1994; Hicks et al., 1987) with the layer thickness ($\Delta z(L_3)$) (cf. Stella et al., 2013):

$$\tau_{tr}(L_3) = R_a(L_3) \cdot \Delta z(L_3) \quad (4)$$

$$R_a(L_3) = \frac{1}{\kappa \cdot u_*} \left[\ln \left(\frac{z_{ref} - d}{z_3 - d} \right) - \Psi_H \left(\frac{z_{ref} - d}{L} \right) + \Psi_H \left(\frac{z_3 - d}{L} \right) \right] \quad (5)$$

where κ was the von-Kàrmàn constant of 0.4, d the displacement height ($d = 0.75 \cdot h_c$), Ψ_H the stability correction function for heat and L the Obukhov length.

In the canopy, $\tau_{tr}(L_i, i = 1, 2)$ were derived from the vertical Tn profiles (Lehmann et al., 1999; Plake and Trebs, 2013):

$$\tau_{tr}(L_i) = \ln \left[\frac{C_{Tn_{z_l}}(L_i)}{C_{Tn_{z_u}}(L_i)} \right] / \lambda \quad (6)$$

where $C_{Tn_{z_l}}$ and $C_{Tn_{z_u}}$ were the measured Tn concentrations (in Bq m⁻³) at the lower (z_l) and upper (z_u) heights of L_i , and λ the radioactive decay rate $\lambda = \ln 2 / T_{0.5} = 0.0125$ s⁻¹ (Hänsel and Neumann, 1995).

3 Results

3.1 Meteorological conditions and mixing ratios

Fig. 1a displays the dominance of south westerly winds at the site during 45 % of the field experiment and their relation to relatively low NO_x levels (< 3 ppb). Contrastingly, winds from the north eastern sector were characterized by high NO_x levels often above 13 ppb (Fig. 1a). The wind speed (ws) at the site was also related to the NO_x levels. Fig. 1b reveals that in cases when $ws > 3$ m s⁻¹ NO_x levels were mostly < 5 ppb, whereas during $ws < 3$ m s⁻¹ the NO_x levels sometimes reached 40 ppb. The measured CO₂ levels generally showed a similar pattern, while O₃ levels exhibited the opposite dependency on ws .

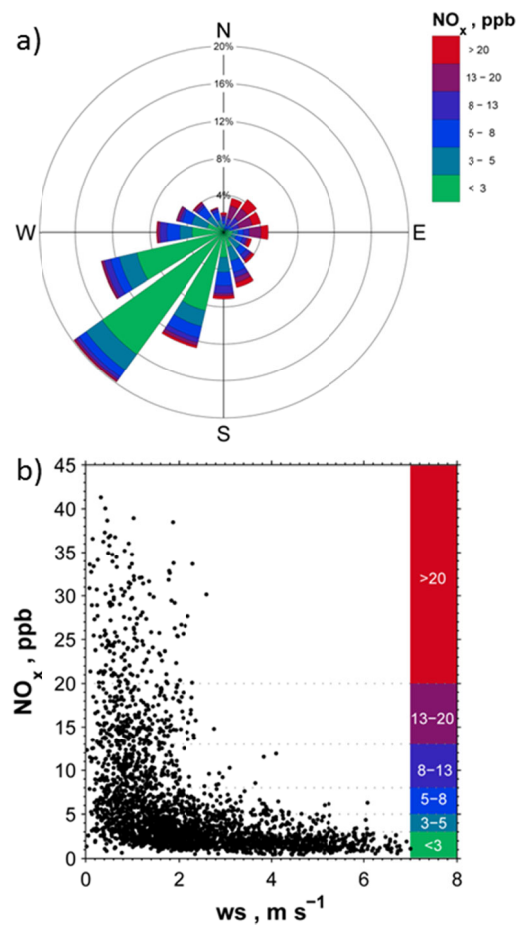


Fig. 1. (a) Frequency distribution of wind direction related to NO_x mixing ratios; (b) NO_x mixing ratios as function of ws at the Mainz-Finthen grassland site.

For further data analysis, defined criteria allowed to account for these specific relationships. In order to clearly separate entire days (24 h) of contrasting conditions from each other, the criteria were defined as low NO_x or high NO_x periods when (i) the mean daytime ws was $> 3 \text{ m s}^{-1}$ and the wind direction mainly ranged between 180 and 270° , or (ii) the mean daytime ws was $< 3 \text{ m s}^{-1}$ and the wind direction was mainly outside $180 - 270^\circ$, respectively. The wind direction definition was fulfilled during 96 % of the low NO_x periods and during 84 % of the high NO_x periods. Following these criteria, we identified eleven and nine days as low and high NO_x periods, respectively, which were separately analyzed.

3.2 Vertical profile of trace gases

Since the wind field is the driver of vertical exchange of scalars such as trace gases between vegetation and the atmosphere (Finnigan, 2000), it affects their vertical distribution. Passive tracers such as Rn and CO_2 are used especially at nighttime as indicators for vertical exchange processes within plant canopies (e.g., Nemitz et al., 2009; Trumbore et al., 1990). Generally, the nighttime ws values of the low and high NO_x periods were accordingly higher and lower, respectively. This was reflected by the

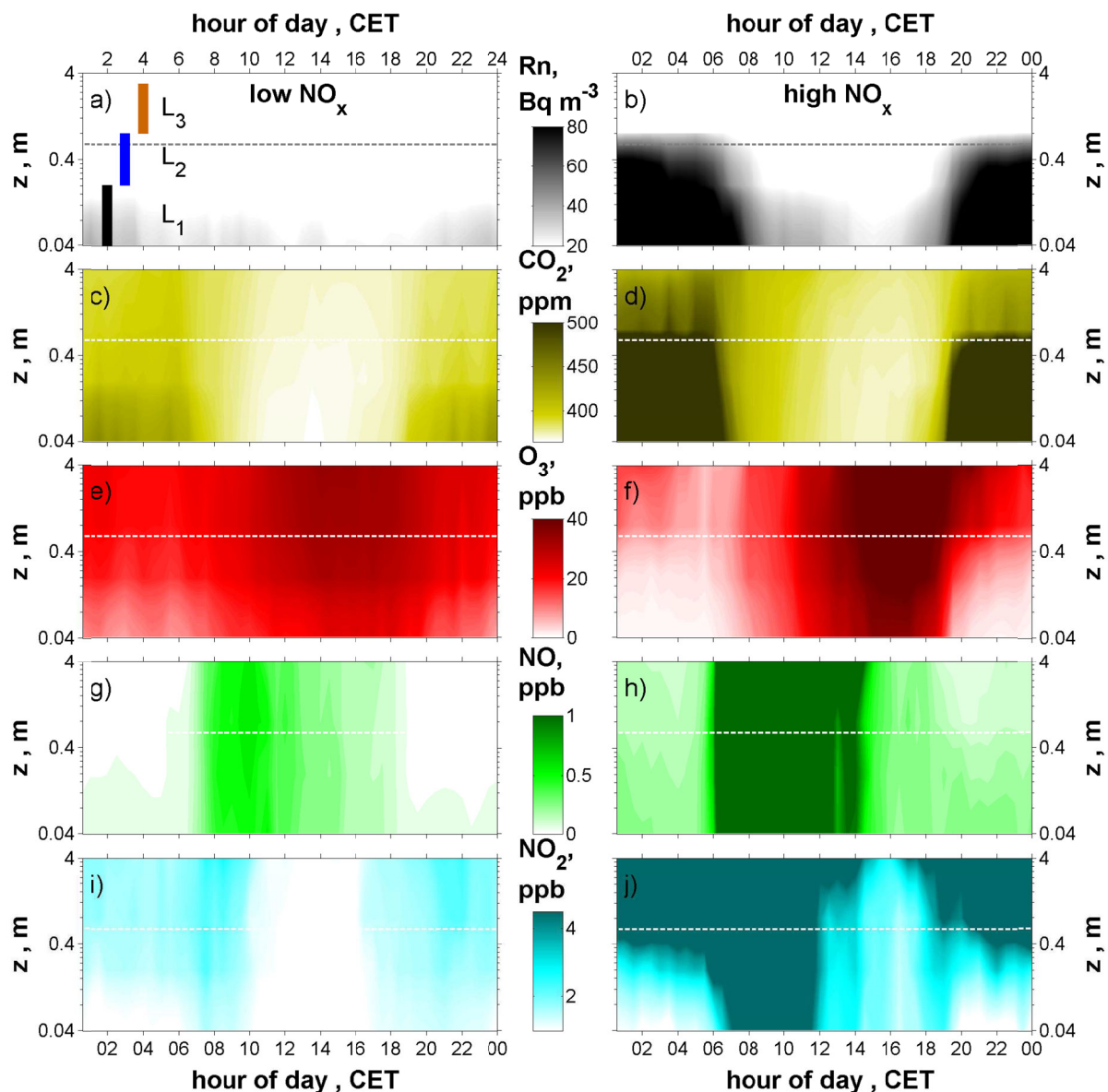


Fig. 2. Time height cross sections indicating the median vertical distribution of (a,b) Rn, (c,d) CO₂, (e,f) O₃, (g,h) NO and (i,j) NO₂ during low NO_x (left panels) and high NO_x (right panels) conditions at the Mainz-Finthen grassland site. The canopy height (dotted line) and L₁₋₃ are also shown. The plots were made using the *contourf* function of MATLAB.

in-canopy concentrations of both Rn and CO₂ (Fig. 2a–d). Consequently, during nighttime when both gases are exclusively emitted by soil, a weak enrichment within the canopy (Fig. 2a,c) reflected higher *ws* and exchange during the low NO_x periods. In comparison, during the high NO_x periods a strong in-canopy CO₂ and Rn accumulation was observed (Fig. 2b,d). During daytime photosynthesis prohibits the use of CO₂ as passive tracer, whereas Rn profiles are still useful. The vertical exchange is generally enhanced during daytime causing dilution of the in-canopy Rn concentrations, which was especially pronounced in the low NO_x periods (Fig. 2a) and less evident during the high NO_x periods (Fig. 2b).

The vertical distribution of O_3 (Fig. 2e,f) reflected a typical pattern with lower mixing ratios closer to the ground and higher mixing ratios above. The diurnal O_3 maximum occurred during the afternoon around 16:00 CET (= UTC+1). Nevertheless, in the low NO_x periods the diurnal O_3 maximum was much less pronounced compared to the high NO_x periods with 35 ppb and 50 ppb, respectively. Furthermore, characteristic vertical O_3 distributions were observed during the low and high NO_x periods. Nighttime O_3 gradients were less pronounced during the low NO_x than during the high NO_x periods. Median in-canopy values of O_3 were 10-20 ppb and 20-25 ppb above during the low NO_x periods (Fig. 2e). During the high NO_x periods 1-6 ppb were measured in the canopy and 10-25 ppb above (Fig. 2f).

During both the low and the high NO_x periods, significantly enhanced NO mixing ratios prevailed during the morning hours from 06:00 to 14:00 CET (Fig. 2g,h) with median diurnal maxima of 0.6 ppb and 7.2 ppb, respectively, both occurring at 10:00 CET (not visible in Fig. 2h due to scaling). The NO mixing ratios decreased afterwards to reach nighttime minima. These were characterized by small vertical NO gradients during both periods. During low NO_x nights, NO appeared to be mainly present in the in-canopy air layer, with median mixing ratios at z_1 and z_2 of ≤ 0.1 ppb. The median values at z_1 and z_2 during the high NO_x periods were ≤ 0.3 ppb, respectively.

NO_2 mixing ratios were generally found to increase with height (Fig. 2i,j), featuring significantly stronger vertical differences during the high NO_x periods. Similar to NO, also NO_2 mixing ratios were enhanced throughout the profile during the morning hours of both, low and high NO_x periods, with corresponding values of 1–2.5 ppb and 6–14 ppb, respectively. At nighttime, comparable NO_2 mixing ratios of around 1 ppb prevailed during both periods at z_1 . They showed clearly stronger gradients above the canopy during the high NO_x periods. The diurnal NO_2 minima during low and high NO_x periods were observed between 12-16 CET and 14-16 CET, respectively.

3.3 Vertical profile of chemical timescales

The obtained values for τ_{ch} were generally higher during nighttime than during daytime (Fig. 3a,d,g) and decrease from L_3 to L_1 . The validity of our applied criteria for separation between low and high NO_x periods, is shown by the median values (brown and green lines) nearly adjoining the interquartile range of the overall data set. Significantly higher τ_{ch} values prevailed during nighttime of the high NO_x periods, ranging from 300 to 2500 s in L_{1-3} . In contrast, low NO_x periods were characterized by τ_{ch} of 250–800 s in L_{1-3} . However, during daytime τ_{ch} was within 100–200 s in L_{1-3} for both periods. During the low NO_x periods τ_{ch} values were slightly higher compared to the high NO_x periods.

3.4 Vertical profile of transport times

The median $\tau_{tr}(L_3)$ of all data Fig. 3b was one order of magnitude smaller during noon than at midnight with 30 and 200 s, respectively. As for τ_{ch} (Sect. 3.3), also in the case of τ_{tr} the medians of the low and high NO_x periods adjoining the interquartile range of the overall data set. For example, $\tau_{tr}(L_3)$ in the low NO_x periods never exceeded $\tau_{tr}(L_3)$ in the high NO_x periods (cf. Fig. 3b). The difference of $\tau_{tr}(L_3)$ between noon and midnight was largest in the high NO_x and smallest during the low NO_x periods with 470 and 40 s, respectively. Compared to L_{1-2} (Fig. 3e,h), the extreme values of the entire

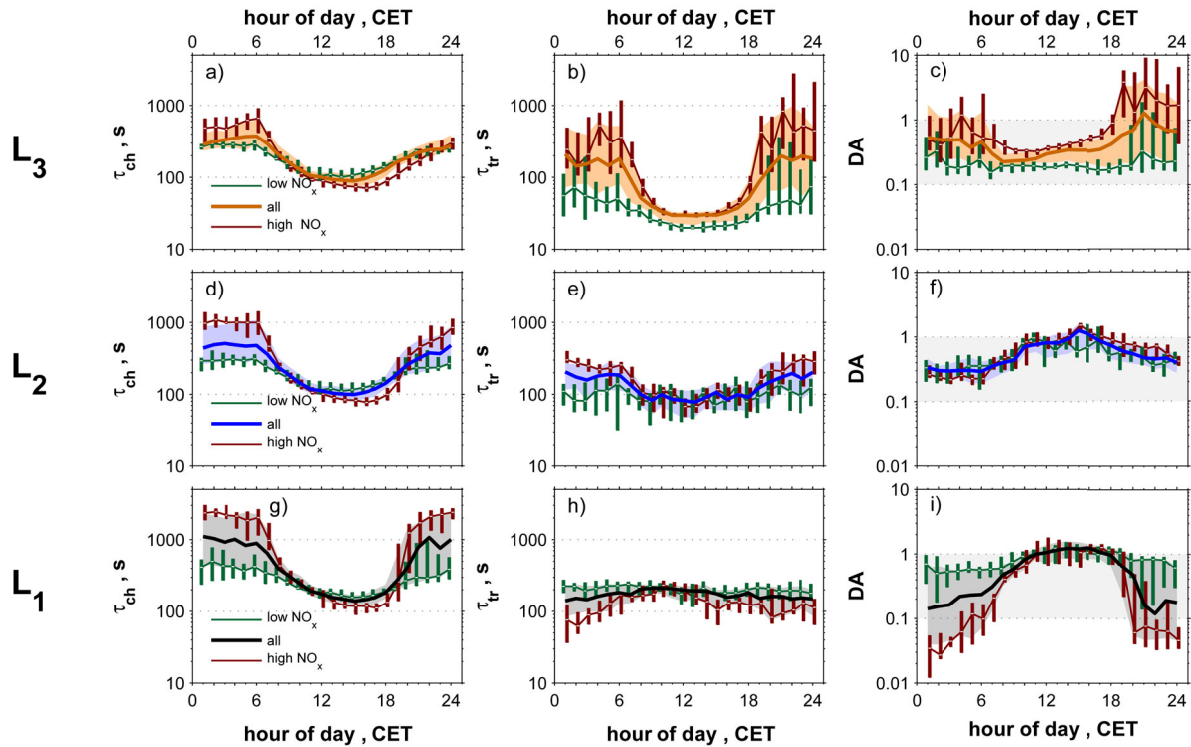


Fig. 3. Diurnal courses of (a, d, g) $\tau_{ch}(L_{1-3})$, (b, e, h) $\tau_{tr}(L_{1-3})$ and (c, f, i) $DA(L_{1-3})$ considering all data from 19 August to 26 September 2011 (medians and shaded interquartile ranges) and the low NO_x and high NO_x periods (green and brown medians and interquartile boxes) at the Mainz-Finthen grassland site.

τ_{tr} data set were be found above the canopy in L_3 . The τ_{tr} minimum was during daytime of the low NO_x periods, and the maximum during nighttime of the high NO_x periods.

The diurnal course of the entire $\tau_{tr}(L_2)$ data set in Fig. 3e exhibited a similar pattern as in L_3 , with higher $\tau_{tr}(L_2)$ during nighttime than during daytime. Representative nighttime and daytime values were 200 and 100 s, respectively, and a similar nighttime separation between the low and high NO_x periods as in Fig. 3b was observed.

In contrast, both diurnal $\tau_{tr}(L_1)$ median values that represented all data and the high NO_x periods (Fig. 3h) were slightly higher during daytime between 08:00 and 13:00 CET than at nighttime with around 200 and 75 – 175 s, respectively. In the low NO_x periods, the median $\tau_{tr}(L_1)$ was relatively stable throughout the day with about 200 s. The pattern of $\tau_{tr}(L_1)$ was generally opposite to L_{2-3} , with faster $\tau_{tr}(L_1)$ in the high NO_x periods than in the low NO_x periods.

3.5 Vertical profile of Damköhler numbers

The values for $DA(L_3)$ presented in Fig. 3c were generally smaller during daytime than during nighttime. They exhibited a diurnal minimum of 0.2 and a maximum of 1.3 at 08:00 and 21:00 CET, respectively. In the low NO_x periods, the difference of the $DA(L_3)$ median to unity was highest

($0.2 < DA(L_3) < 0.3$), whereas in the high NO_x periods $DA(L_3)$ remained at higher median values ($0.3 < DA(L_3) < 3.9$).

In contrast, the diurnal course of $DA(L_2)$ in Fig. 3f exhibited its maximum of 1.25 at 15:00 CET and nighttime minima of about 0.3. The difference in $DA(L_2)$ between the low and high NO_x periods was not as pronounced as for $DA(L_3)$. It became most obvious from 15:00 to 24:00 CET with lower $DA(L_2)$ in the low NO_x periods. Hence, both $DA(L_{2,3})$ values throughout the day were found within the critical range or above under all conditions.

Interestingly, the diurnal course of $DA(L_1)$ (Fig. 3i) appeared to mirror that of $DA(L_3)$, with highest and lowest DA during daytime and nighttime, respectively. The diurnal median of $DA(L_1)$ partly exhibited values below 0.1 (transport dominates) during nighttime of the high NO_x periods, values above unity (chemistry dominates) from 12:00 to 17:00 CET under all conditions, and between 0.1 and unity during nighttime in the overall data set and in the low NO_x periods.

4 Discussion

4.1 Transport times and resistances

4.1.1 Thermal stratification

The diurnal courses of the temperature differences $\Delta T(L_{1-3})$ in Fig. 4a–c describe the stability in each layer. They clearly indicated contrasting stability conditions in L_1 and L_{2-3} . During daytime, negative values of $\Delta T(L_{2-3})$ reflected turbulent conditions, while positive $\Delta T(L_1)$ reflected stable conditions. In contrast, at nighttime these conditions were reversed. Similar stratifications are observed for other canopies (cf. Jacobs et al., 1994; Kruijt et al., 2000; Nemitz et al., 2000), and are known to decouple the lower canopy from above (cf. Fig. 4d). Canopy coupling regimes are typically classified according to the detection of coherent structures in high-frequency time series of scalars such as temperature (e.g. Dupont and Patton, 2012; Foken et al., 2012). In our data, set $\Delta T(L_1)$ explained that $\tau_{tr}(L_1)$ was generally smaller, i.e. transport was faster, during night than daytime (Fig. 3h). Correspondingly, $\Delta T(L_{2-3})$ elucidated that $\tau_{tr}(L_{2-3})$ were smaller during day than nighttime (Fig. 3b,e). The soil released stored heat as thermal plumes during nighttime, that drove an in-canopy nighttime convection and reached up to the height of the temperature inversion as explained by Dupont and Patton (2012) or Jacobs et al. (1994). This resulted in lower $\tau_{tr}(L_1)$ during nighttime. The $\tau_{tr}(L_1)$ maximum from 08:00 to 13:00 CET could accordingly been attributed to positive $\Delta T(L_1)$ values at that time indicating a stable stratification. In all layers the thermal stratification was stronger during the high NO_x periods and weaker during the low NO_x periods (Fig. 4a–c). As higher wind speed yielded better mixing during the low NO_x periods, the vertical temperature differences were smaller.

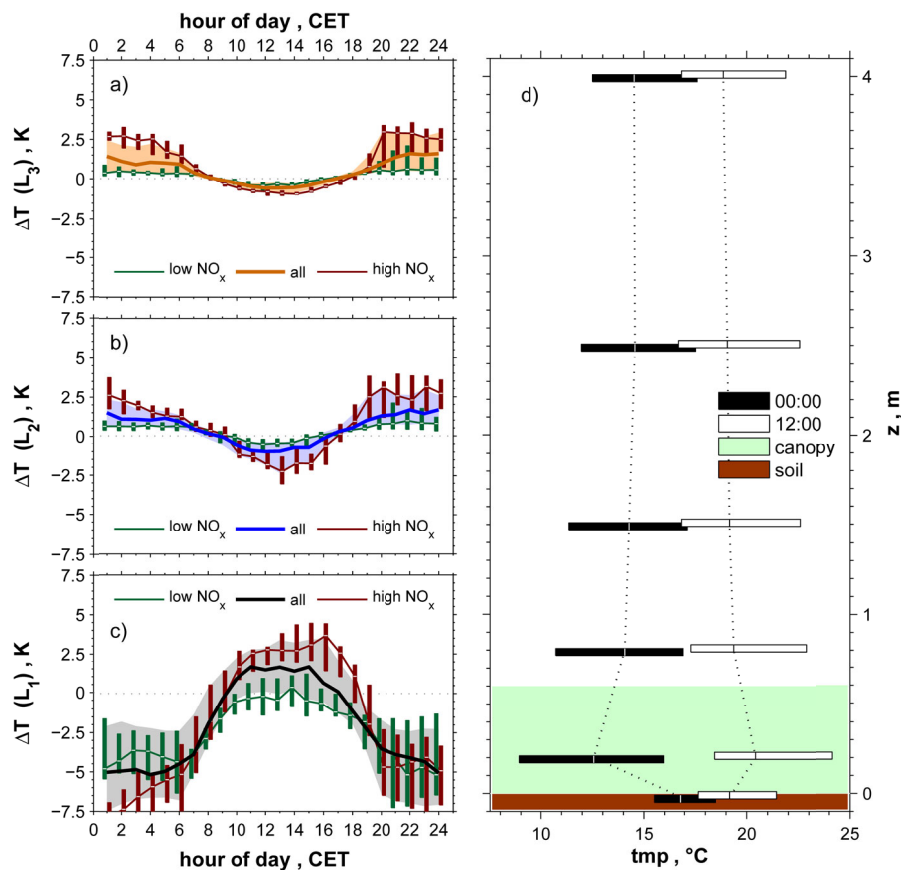


Fig. 4. (a)–(c) Diurnal courses of measured $\Delta T(L_{1-3})$ considering all data from 19 August to 26 September 2011 (medians and shaded interquartile ranges) and the low and high NO_x periods (green and brown medians and interquartile ranges); note: $\Delta T(L_1, L_3)$ do not fully cover L_1 and L_3 (Sect. 2.3) due to availability of measurements (Sect. 2.2); (a) $\Delta T(L_3)$: 2.5 – 0.8 m; (b) $\Delta T(L_2)$: 0.8 – 0.2 m; (c) $\Delta T(L_1)$: 0.2 – 0.02 m (soil temperature). (d) Median vertical temperature profiles and interquartile boxes representing the thermal stratification at 00:00 and 12:00 CET considering all data from 19 August to 26 September 2011 at the Mainz-Finthen grassland site.

4.1.2 Aerodynamic resistances and transport times

Aerodynamic resistances (R_a) are important input parameters for modeling studies on surface-atmosphere exchange fluxes. They represent transport times through a layer, normalized by the layer thickness ($R_a = \tau_{tr}/\Delta z$). In cases when the thicknesses of two layers under consideration differ, the effectiveness of transport can be represented by the corresponding aerodynamic resistances. On the other hand, transport times are required to evaluate the influence of chemical reactions on fluxes (e.g., DA).

Aerodynamic in-canopy resistances (R_{ac}) are typically parameterized as function of u_* and LAI (e.g., Personne et al., 2009; van Pul and Jacobs, 1994). These parameterizations are based on experiments above e.g., crops such as maize (van Pul and Jacobs, 1994) and consider a homogeneous vertically leaf distribution (Personne et al., 2009). However, this approximation may differ substantially within

grassland canopies, as their structure is characterized by high biomass density in the lowest layer (cf. Sect. 2.1).

The usefulness of our results is underlined by the direct assessment of measured R_{ac} values. By utilizing Eq. 6 we can assess R_{ac} for different canopy layers (L_1 , L_2 and for the whole canopy ($\tau_{tr}(z_1, z_3)$; $\Delta z = z_3 - z_1$)) within the grassland canopy (cf. Fig. 5). In the lower canopy, $R_{ac}(L_1)$ was generally highest with medians of 900 to 1000 s m^{-1} during nighttime and 1000 to 1300 s m^{-1} during daytime (Fig. 5). In comparison, Gut et al. (2002) found the aerodynamic resistance in the lowest meter of an Amazonian rain forest canopy in a similar range and showing the same diurnal pattern with 600 s m^{-1} during nighttime and 1700 s m^{-1} during daytime.

As found for the transport times, the diurnal course was inversed in the layers above (Fig. 5). In the upper canopy, the median of $R_{ac}(L_2)$ typically ranged around 300 s m^{-1} during nighttime and around 150 s m^{-1} during daytime. In comparison, above the canopy the median of $R_a(L_3)$ (Eq. 5) was substantially lower with around 80 and 15 s m^{-1} during night and daytime, respectively. Consequently, the aerodynamic resistances in and above the canopy ($R_{ac}(L_{1,2})$ and $R_a(L_3)$) differed by almost two orders of magnitude during daytime, and by one order of magnitude during nighttime. Accordingly, the efficiency of aerodynamic transport decreased with height, even if the transport times were partly shorter in L_1 compared to L_3 . The R_{ac} for the whole canopy (Fig. 5) ranged in-between $R_{ac}(L_1)$ and $R_{ac}(L_2)$ with 440 s m^{-1} during nighttime and 360 s m^{-1} during daytime. The opposite diurnal courses of both, $R_{ac}(L_1)$ and $R_{ac}(L_2)$ have an impact on R_{ac} , which in turn showed a smaller diurnal variation. As L_2 contained around 80 % of the layer thickness between z_1 and z_3 (cf. Fig. 5), R_{ac} was closer to $R_{ac}(L_2)$.

The median transport time through the 0.6 m high natural grassland canopy (also referred to as “canopy flushing time”) was presented in the related study of Plake and Trebs (2013) for the same experiment. It was measured using the vertical thoron profile between z_1 and z_3 (Eq. 6). The canopy flushing time is consistent with the sum of $\tau_{tr}(L_1)$ and $\tau_{tr}(L_2)$ in this manuscript (cf. Fig. 7 below) and represented the in-canopy layer down to $0.07 \cdot h_c$ (z_1/h_c). It was determined to be ≤ 6 min exhibiting only small day/ nighttime variation. Simon et al. (2005) reported canopy flushing times based on radon measurements within a 40 m high rain forest canopy. For the layer between h_c and $0.13 \cdot h_c$ (canopy top to trunk space), they determined flushing times of around 60 min during any time of the day. As in the grassland canopy in Mainz-Finthen, nighttime in-canopy convection accounted for the small day/ nighttime variation in their study. Normalization of their canopy flushing time by the layer thickness yielded R_{ac} in the order of 100 s m^{-1} , which is around 3–4 times lower than the corresponding R_{ac} of the grassland site. Other studies (Holzinger et al., 2005; Rummel, 2005) based on surface renewal models reported somewhat lower flushing times. Rummel (2005) found flushing times in a 32 m high rain forest canopy of ≤ 200 s during daytime, which correspond to R_{ac} values ≤ 10 s m^{-1} . In the same way Holzinger et al. (2005) determined flushing times of 90 s during daytime and around 300 s during nighttime within a 6 m high scrubby pine forest. Corresponding R_{ac} values were in the order of 20 and 60 s m^{-1} , respectively.

Thus, it is important to note that even if the canopy height of natural grassland canopies is small compared to forests (around 1–10 %); the corresponding canopy flushing times can be shorter or even

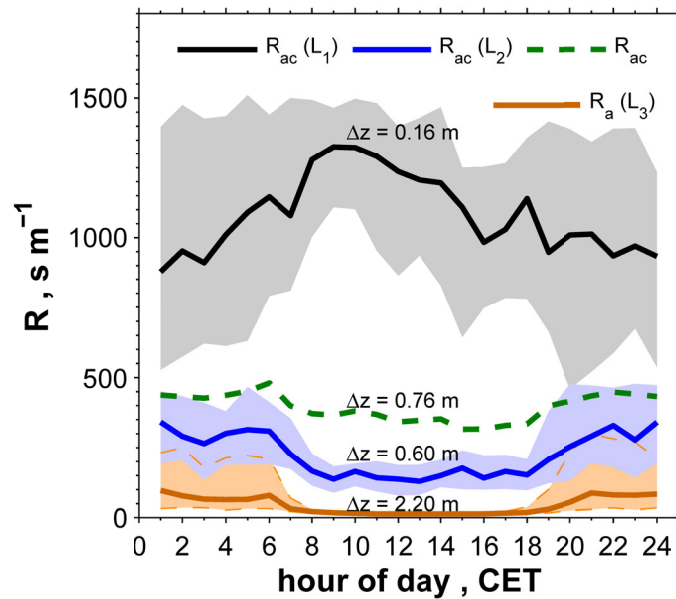


Fig. 5. Diurnal courses of in-canopy aerodynamic resistances for each individual canopy layer ($R_{ac}(L_1)$, $R_{ac}(L_2)$) and for the entire grassland canopy (R_{ac}) at the Mainz-Finthen site (median and shaded interquartile ranges). For comparison, the aerodynamic resistance above the canopy is also displayed ($R_a(L_3)$). The layer thickness (Δz) is indicated. The plots includes all data from 19 August until 26 September 2011.

longer within grassland than in forest canopies (10–400 %). The typically high biomass density in the lower canopy of grasslands (e.g., Jäggi et al., 2006; Nemitz et al., 2009) is the most obvious explanation. It provides a large aerodynamic resistance ($> 900 \text{ s m}^{-1}$) in a small layer adjacent to the ground (here: $R_{ac}(L_1)$). The aerodynamic resistance is large enough to increase the overall aerodynamic resistance of the whole canopy (R_{ac}) by 50 % and 140 % during night and daytime, respectively. Consequently, R_{ac} of the grassland canopy was found at least 3–4 times higher than R_{ac} values representing corresponding in-canopy layers of forests taken from literature.

Plake and Trebs (2013) compared their directly measured transport times with the parameterizations of van Pul and Jacobs (1994) and Personne et al. (2009). They found that none of the parameterizations was able to reproduce the entire diurnal course of the in-canopy transport. An agreement with the measured transport times was either found during daytime (Personne et al., 2009) or nighttime (van Pul and Jacobs, 1994), underlining the need for more direct measurements on in-canopy transport.

4.2 Chemical timescales

The non-linear profiles of NO, NO₂ and O₃ might have introduced uncertainties in $\tau_{ch}(L_{1-3})$. The potential uncertainties due to averaging were investigated by determining the individual $\tau_{ch}(z_{1-4})$ and their subsequent comparison with $\tau_{ch}(L_{1-3})$. In L_1 , L_2 and L_3 they were found to be $\leq 13 \%$, $\leq 4 \%$ and $\leq 2 \%$, respectively, during daytime under any condition. During nighttime, the uncertainties in L_2 and L_3 were found to be 6 and 2 % during the low NO_x periods and 57 % and 13 % during the high NO_x

periods, respectively. In L_1 the uncertainty during nighttime was 30 % under all conditions. Furthermore, the in-canopy parameterization of j_{NO_2} might have introduced additional uncertainties since (i) in reality the attenuation of in-canopy radiation might be more complex than described by Eq. 3, and (ii) the parameterization of j_{NO_2} from G is prone to uncertainties of >40 % for $G < 100 \text{ W m}^{-2}$, 10 – 40 % for $G = 100\text{--}500 \text{ W m}^{-2}$ and $\leq 10\%$ for $G > 500 \text{ W m}^{-2}$ (Trebs et al., 2009).

The diurnal maxima and minima of $\tau_{ch}(L_{1-3})$ (Fig. 3a,d,g) were found to coincide with the O_3 minima and maxima (Fig. 2e,f), respectively. The impact of the terms in Eq. 2 on $\tau_{ch}(L_3)$ was examined by a correlation coefficient analysis. It was found to be highest for O_3 followed by NO_2 and NO with $r = -0.57$, $r = 0.46$ and $r = -0.07$, respectively. As the average air-chemical situation in Mainz-Finthen, was characterized by a surplus of O_3 compared to NO_2 or NO (cf. Sect. 3.2), the magnitude of $\tau_{ch}(L_3)$ was most affected by the mixing ratios of O_3 . NO in contrast, was generally less abundant, which explained the low overall impact on $\tau_{ch}(L_3)$. Only in high NO_x situations, when NO levels were above 5 ppb (cf. Sect. 3.1), an increased impact on $\tau_{ch}(L_3)$ was found.

Fig. 6a summarizes the chemical timescales. The temporal variation in τ_{ch} , expressed by higher nighttime and lower daytime values, can be considered as a rather typical pattern based on the diurnal courses of NO , NO_2 and O_3 (Fig. 2e–j) and their strong photochemical link. The vertical variation in $\tau_{ch}(L_{1-3})$ was on one hand caused by the attenuation of j_{NO_2} in the canopy, and on the other hand by generally increasing mixing ratios of NO , NO_2 and O_3 with height (Fig. 2e–j). It should be noted, that the latter was a site characteristic issue. Insignificant NO soil emissions were measured by Plake et al. (2014), and were underlined by weak in-canopy NO gradients (Fig. 2g,h). As already seen in the last paragraph, generally low NO , NO_2 and O_3 mixing ratios tend to cause high τ_{ch} values and vice versa. Consequently, at a site with higher NO emissions as e.g., an intensively managed agricultural field, the vertical τ_{ch} profile would most likely feature smaller vertical differences.

The extremely high $\tau_{ch}(L_1)$ during nighttime of the high NO_x periods (Fig. 6a) were a direct consequence of canopy decoupling (cf. Sect. 4.1.1). Transport of O_3 or NO_2 into the lower canopy was suppressed by the temperature inversion (cf. Fig. 2f,j). The residual O_3 and NO_2 molecules were convectively circulated within the lower canopy and, subsequently deposited efficiently to surfaces until both almost disappeared in the early morning (Fig. 2f,j). Thus, the negligible NO emissions together with the suppressed supply of O_3 and NO_2 from above, yielded simultaneously very low mixing ratios of all three species, that in turn led to the extremely high $\tau_{ch}(L_1)$ values.

Our results are in line with those of Stella et al. (2013) who reported median diurnal τ_{ch} of 80-300 s and 150-600 s above and within the canopy, respectively, of an intensively managed meadow. Their in-canopy τ_{ch} maximum was somewhat lower than in Mainz-Finthen, which might be attributed to NO soil emissions or averaging of different layers.

Since Eq. 2 exclusively considers R1 and R3, additional reactions may have biased the obtained τ_{ch} values to a certain extent. For instance, the oxidation of NO and NO₂ by peroxy radicals (Sect. 1), or reactions between volatile organic compounds (VOCs) and O₃ (e.g., Atkinson and Arey, 2003) might have influenced ambient NO, NO₂ and O₃ levels. Simultaneously measured VOC mixing ratios featured very small values at our site (e.g., isoprene < 0.7 ppb, monoterpene < 0.3 ppb, J. Kesselmeier, personal communication). Thus, the latter reaction could be considered of minor importance, whereas information on peroxy radicals was unfortunately not available.

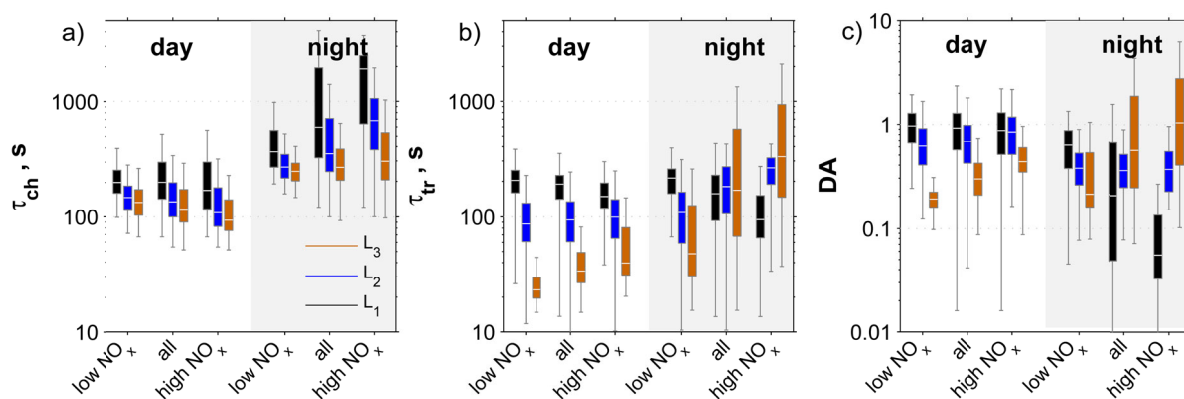


Fig. 6. Comparison of box plot statistics for $\tau_{ch}(L_{1-3})$, $\tau_{tr}(L_{1-3})$ and $DA(L_{1-3})$ during daytime and nighttime including all data from 19 August until 26 September 2011 separated for the low and high NO_x periods at the Mainz-Finthen grassland site.

4.3 Influence of meteorology and air pollution on vertical Damköhler number profiles

The summarized daytime $DA(L_{1-3})$ in Fig. 6c exhibited a pattern of decreasing DA values with layer height. Thus, the likelihood of chemical divergence was indicated to decrease from L_1 to L_3 . Throughout L_1 to L_3 , the τ_{ch} values (Fig. 6a) showed a lower variation compared to the corresponding τ_{tr} (Fig. 6b). Therefore, the daytime DA profile was mainly caused by the vertical τ_{tr} profile.

Interestingly, the nighttime DA of all and the high NO_x periods data showed opposite vertical profiles, indicating an increasing likelihood of chemical divergence with increasing layer height (L_1 to L_3). This was especially pronounced during nighttime of the high NO_x periods, where the only instance without indication for a flux divergence within the entire data set was found for L_1 . The reasons for this were (i) the extraordinary high $\tau_{ch}(L_1)$ (Fig. 6a and Sect. 4.2), and (ii) the reversed vertical transport time profiles during nighttime (fastest in L_1) of the high NO_x periods (Fig. 6b). This finding agrees very well with Rummel (2005) who found at nighttime the transport timescale in the lowest layer of an Amazonian rainforest to be faster than the chemical timescale.

Above the canopy, the order of magnitude (Fig. 6c) and the median diurnal course (Fig. 3c) of DA compared well with Stella et al. (2013). But the in-canopy DA in Stella et al. (2013) was smaller than

the DA above the canopy throughout the entire day, which is in contrast to our study. Considering the canopy flushing time given in Plake and Trebs (2013) (cf. Sect. 4.1.2) and the $\tau_{ch}(L_2)$ (cf. Fig. 6a), a comparable in-canopy DA in Mainz-Finthen was be in the order of 2 and 1 for day and nighttime, respectively. Thus, in-canopy DA in our study are significantly higher than above the canopy throughout the day. As the canopy height in Stella et al. (2013) was only around 0.2 m, the corresponding transport time was faster with 80 s at noon, which explains the lower in-canopy DA compared to our study. Finally it should be noted that, DA values within plant canopies are not fully representative for all processes, since besides transport and chemistry, additional sources and sinks for trace gases exist within plant canopies. These are specific for each trace gas and will be further discussed below.

4.4 Implications for measured fluxes

4.4.1 Potential NO_x canopy reduction

Within the canopy, $DA(L_{1-2})$ (Fig. 3f,i; Fig. 6c) indicated that chemical reactions exhibited a larger influence on the $\text{NO-NO}_2\text{-O}_3$ triad during daytime than during night. However, reactive traces gases in canopies are deposited to soil and vegetation elements. Trace gases can be efficiently taken up by plants due adsorption/ absorption on cuticles and diffusion through stomata. On the other hand, particularly NO is simultaneously produced by microbial processes and is subsequently released from soil. Although, the latter process could be neglected in this study due to insignificant NO soil emissions (Sect. 4.2), the uptake of NO_2 by plants, however, was investigated in order to draw general conclusions on NO_x canopy reduction within natural grasslands canopies. Hence, additional information on the characteristic time scale of plant uptake of NO_2 was required. Such timescales $\tau_u(\text{NO}_2)$ integrated over the whole canopy (L_{1+2}) were estimated based on a resistance model (Baldochi, 1988), following an approach of Rummel (2005) as:

$$\tau_u(x) = \left(\frac{1}{R_{L_x}} \cdot \frac{\Delta LAI}{\Delta z} \right)^{-1} \quad (7)$$

where x denoted the trace gas of interest (here $x = \text{NO}_2$) and R_{L_x} was the leaf resistance of x :

$$R_{L_x} = \left(\frac{1}{R_{bl_x} + R_{s_x} + R_{mes_x}} + \frac{2}{R_{bl_x} + R_{cut_x}} \right)^{-1} \quad (8)$$

with R_{bl_x} being the leaf boundary layer resistance of x calculated according to Personne et al. (2009), R_{s_x} the stomatal resistance of x taken from Plake et al. (2014), R_{mes_x} the mesophyll resistance set to 200 s m^{-1} for NO_2 and R_{cut_x} the cuticular resistance set to 9999 s m^{-1} due to its unimportance for NO_2 (both values were taken from Stella et al. (2013)).

During daytime, $\tau_u(\text{NO}_2)$ was typically found to be the shortest amongst all timescales relevant for NO_2 typically ranging between 90 and 160 s between 09:00 and 17:00 CET (Fig. 7). This timescale was closely followed by $\tau_{ch}(L_{1+2})$ exhibiting values between 100 and 200 s in the same time window, but with a shorter lasting minimum. In contrast, the values of $\tau_{tr}(L_{1+2})$, the canopy flushing time, ranged from 250 to 290 s (Fig. 7) during this time. For a similar canopy with significant NO soil emissions, this would imply an efficient in-canopy conversion of NO to NO_2 during daytime, followed by an effective NO_2 plant uptake as the transport was found to be 2-3 times slower. Furthermore, the bi-

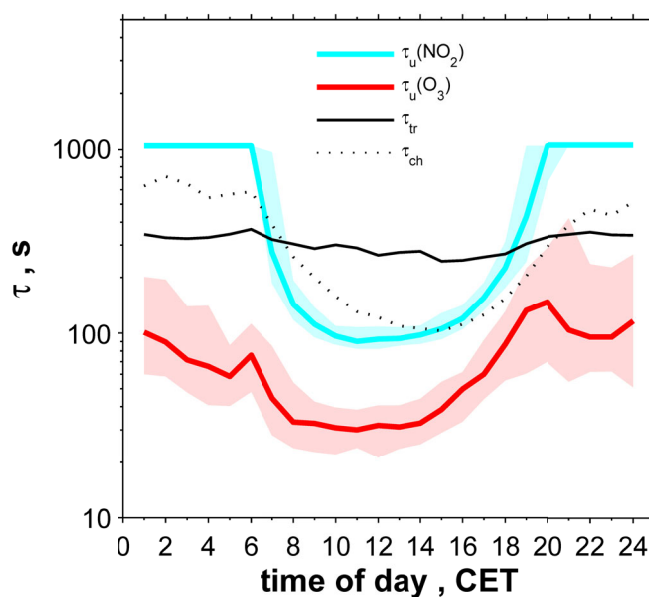


Fig. 7. Comparison of median diurnal $\tau_u(NO_2)$, $\tau_u(O_3)$, τ_{tr} and τ_{ch} with interquartile ranges for the whole canopy layer (L_{1+2}) considering all data from 19 August to 26 September 2011 at the Mainz-Finthen grassland site.

omass density within the lowest 0.2 m of the canopy (i) strongly inhibits the transport, especially in L_1 during daytime (Fig. 5; Fig. 6b), and (ii) dampens the photolysis of NO_2 at the soil-canopy interface, the location where NO is usually emitted. This indicates strong NO_x canopy reduction occurring in such grassland ecosystems during daytime, if the precondition of significant NO soil emissions is fulfilled.

However, during nighttime, $\tau_u(NO_2)$ was found to be very large (Fig. 7), hence, the role of turbulence-chemistry interactions ($DA(L_{1-2})$) was dominating over biological uptake processes. In L_1 the transport of soil-emitted NO would be slowest under relatively windy nighttime situations (low NO_x periods in Fig. 3h). Thus, a considerably high mixing ratio of O_3 within the canopy (Fig. 2e) would lead to an efficient formation of NO_2 indicated by $DA(L_{1-2})$ close to unity. The uptake of NO_2 by plants would be insignificant (see above), and only soil deposition would lead to a small NO_2 depletion. Most likely, such nighttime conditions would lead to simultaneous NO_2 and NO canopy emission fluxes.

However, during nights with low w_s (high NO_x periods), the temperature inversion constitutes a “canopy lid”. Within the canopy (L_{1+2}) the reaction of residual O_3 (cf. Sect. 4.2) and soil-emitted NO would compete with the O_3 surface deposition. Subsequently, a mixture of NO and NO_2 would be trapped inside the canopy. Besides some minor in-canopy NO_2 losses (see above), a distinct NO and NO_2 release may occur in the morning hours, which has been observed for forests (cf. Dorsey et al., 2004; Foken et al., 2012; Jacob and Wofsy, 1990).

4.4.2 Influence on O₃ deposition flux

Similar to NO₂, the application of in-canopy *DA* values for O₃ remains difficult, since plant uptake and deposition to plant surfaces and the soil are additional O₃ pathways besides chemistry. The characteristic timescale of O₃ plant uptake and soil deposition $\tau_u(O_3)$, shown in Fig. 7, was estimated using Eqs. 7 and 8, with $x = O_3$, R_{mes_x} set to 0 s m⁻¹ (Erisman et al., 1994) and $R_{cut_x} = R_{ns_x} - R_{soil_x}$ (e.g., Lamaud et al., 2009). R_{ns_x} was taken from Plake et al. (2014) and $R_{soil_x} = 240$ s m⁻¹ according to Lamaud et al. (2009). $\tau_u(O_3)$ ranged between 30 and 150 s, which clearly illustrates the dominance of in-canopy O₃ plant uptake and soil deposition. $\tau_u(O_3)$ was significantly faster than both $\tau_{tr}(L_{1-2})$ and $\tau_{ch}(L_{1-2})$ during the entire day (values are given in Sect. 4.4.1).

Consequently, only *DA* above the canopy, i.e. $DA(L_3)$ in this study, are valid as an indicator for potential O₃ flux divergence. Because the $DA(L_3)$ always exceeded 0.1 (Fig. 3c, Fig. 6c), a chemical flux divergence could not be excluded at the Mainz-Finthen site. Furthermore, $DA > 1$ (Fig. 3c) during the early evening hours clearly indicated potential flux divergence. In the low NO_x periods, the probability of flux divergence was lowest. The influence of chemistry on O₃ deposition fluxes determined by Plake et al. (2014) at the Mainz-Finthen grassland site will be discussed below. The median O₃ fluxes ranged from about -1.5 to -6 nmol m² s⁻¹ during night and daytime, respectively.

Due to negligible NO soil emissions, a chemical flux divergence in L_3 resulting from counter-directed fluxes of NO and O₃ was very unlikely. Nevertheless, we used a simplified method proposed by Duyzer et al. (1995) based on R1 and R3 and the law of mass conservation. The flux divergence is approximated by the correction factor α_{O_3} as:

$$\alpha_{O_3} = \frac{\phi_x}{\kappa \cdot u_*} \cdot [k_1 \cdot (N_{NO} \cdot F_{O_3}^* + N_{O_3} \cdot F_{NO}^*) - j_{NO_2} \cdot F_{NO_2}^*] \quad (9)$$

where $\phi_x = \phi_{O_3} = \phi_H$ was the stability correction function for heat (Högström, 1988), $F_{O_3}^*$ the measured O₃ flux at z_{ref} determined by the eddy covariance method (cf. Plake et al., 2014) and F_{NO}^* and $F_{NO_2}^*$ the corresponding NO and NO₂ fluxes determined by the dynamic chamber technique (cf. Plake et al., 2014). The estimated O₃ deposition flux at z_3 (F_{z_3}) was then calculated as:

$$F_{z_3} = F_{z_{ref}} + \int_{z_3}^{z_{ref}} \left(\frac{\partial F}{\partial z} \right)_z dz = F_{O_3}^* + \alpha_{O_3} \cdot z_3 \cdot \left(1 + \ln \frac{z_{ref}}{z_3} \right) \quad (10)$$

where the term $\int_{z_3}^{z_{ref}} \left(\frac{\partial F}{\partial z} \right)_z dz$ was the integrated flux divergence within L_3 . The resulting median O₃ flux divergence was quantified to be less than 1 %, confirming the a priori assumption of irrelevant O₃ flux divergence.

Nevertheless, we examined the influence of the enhanced NO mixing ratios in the morning hours (Sect. 3.2, Fig. 2g,h), accompanied by very low O₃/NO ratios (Fig. 8) on the measured O₃ fluxes. A chemically induced O₃ flux $F_c(O_3)$ due to production $P(O_3)$ or loss $L(O_3)$ of O₃ by R1 and R3 integrated over the air column of L_3 was quantified according to Rummel et al. (2007) as:

$$F_c(O_3) = P(O_3) - L(O_3) = \int_{z_3}^{z_{ref}} \frac{\mu_{NO_2}(z) \cdot \rho_d(z)}{\tau_{NO_2}(z)} \cdot dz - \int_{z_3}^{z_{ref}} \frac{\mu_{O_3}(z) \cdot \rho_d(z)}{\tau_{O_3}(z)} \cdot dz \quad (11)$$

where ρ_d (in mol m⁻³) was the molar density of dry air. τ_{NO_2} and τ_{O_3} (in s) were the chemical depletion times of NO₂ and O₃, respectively:

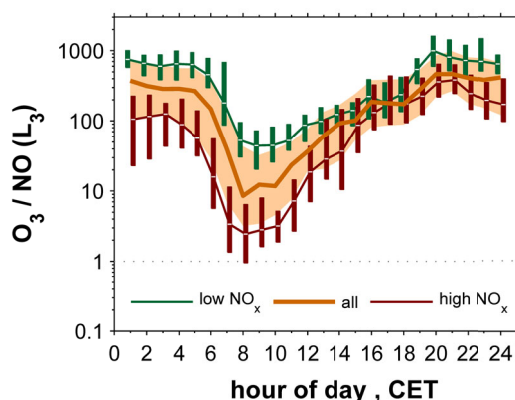


Fig. 8. Diurnal course of the O_3 to NO ratio in L_3 considering all data from 19 August to 26 September 2011 (median and shaded interquartile range) and separated for the low NO_x and high NO_x periods (medians and interquartile boxes) at the Mainz-Finthen grassland site.

$$\tau_{NO_2} = \frac{1}{j_{NO_2}} \quad (12)$$

$$\tau_{O_3} = \frac{1}{k_1 \cdot N_{NO}} \quad (13)$$

Fig. 9a displays the diurnal courses of $P(O_3)$ and $L(O_3)$ exhibiting median values of 0 to $1.9 \text{ nmol m}^{-2} \text{ s}^{-1}$ and 0 to $-1.4 \text{ nmol m}^{-2} \text{ s}^{-1}$, respectively. The maximum median values were related to the enhanced NO_x levels in the morning. The resulting median net $F_c(O_3)$ in Fig. 9b ranged between 0.6 and $-0.05 \text{ nmol m}^{-2} \text{ s}^{-1}$, representing a net O_3 production during daytime and a net loss during nighttime. Repeatedly, the medians of low and high NO_x periods adjoined the interquartile range of the overall data set, showing a variability of one order of magnitude of net $F_c(O_3)$ during daytime. Considering the median values of all data, the measured O_3 deposition flux would change by around +10 % during daytime and -3 % during nighttime. This finding is interesting, as to our knowledge previous studies only reported O_3 losses when dealing with the chemical flux divergence of O_3 . The outbalancing of the reactions of O_3 with NO (e.g., Dorsey et al., 2004) or VOCs (e.g., Kurpius and Goldstein, 2003) emitted by soil or plants, respectively, resulted in net O_3 loss. The O_3 production in our study was attributed to a deviation from the NO - NO_2 - O_3 photostationary state by a surplus of NO_2 , based on NO oxidation by e.g. peroxy radicals or other oxidants. Unfortunately, we were not able to assess the impact of these reactions on the calculated chemical timescales as measurements of peroxy radicals were not available. The NO_2 surplus might have originated from simultaneous emissions of non-methane hydrocarbons, carbon monoxide (CO) and NO from motorways surrounding the site in a distance of some kilometers. Under daytime conditions and high NO_x levels peroxy radicals are formed that react with NO resulting in net O_3 production (Seinfeld and Pandis, 2006). Although, this O_3 production might also prevail at other experimental sites, this effect is most likely balanced or even exceeded by the destruction of O_3 due to biogenic soil NO emissions.

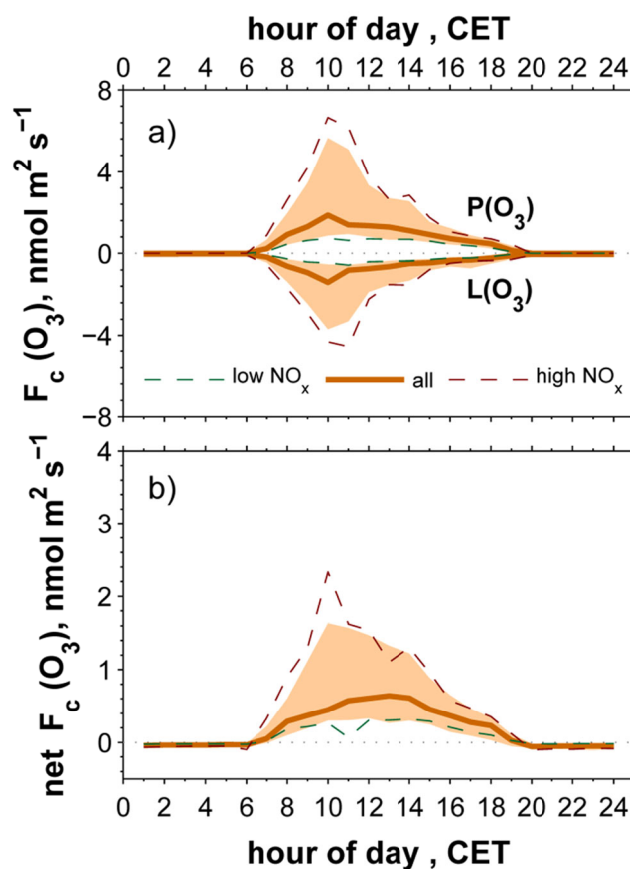


Fig. 9. Diurnal courses showing (a) $P(O_3)$ and $L(O_3)$ and (b) $F_c(O_3)$ (Eq. 11) for L_3 considering all days from 19 August to 26 September 2011 (medians and shaded interquartile ranges) and separated for the low and high NO_x periods (medians) at the Mainz-Finthen grassland site.

5 Conclusions

For the first time, we simultaneously measured transport times (aerodynamic resistances), vertical profiles of $\text{NO-NO}_2\text{-O}_3$ mixing ratios and micrometeorological quantities within and above a natural grassland canopy. The obtained data were analyzed to gain insights about the potential NO_x canopy reduction in the grassland canopy, and to analyze the effect of chemistry on fluxes of purely depositing compounds, such as O_3 . We observed two extreme regimes characterized by a) high wind speed and low NO_x mixing ratios (low NO_x periods) and b) low wind speed and high NO_x mixing ratios (high NO_x periods). Our study highlights that (i) as a result of in-canopy convection, nighttime transport in the lowest canopy layer is fastest during highly stable conditions above the canopy related to low wind speed (high NO_x periods), and (ii) the opposite pattern prevails during daytime of the low NO_x periods.

Interestingly, our results on transport-chemistry interactions within the grassland canopy are partly comparable to those found in the Amazonian rainforest, although the vertical canopy structure differs

substantially. Natural grasslands exhibit very high biomass densities in the lowest canopy part. Thus, the aerodynamic resistance in the lowest canopy layer (0.04–0.2 m) was found to be of the same magnitude ($> 900 \text{ s m}^{-1}$) and to feature the same diurnal pattern (higher during daytime, lower at night) as the aerodynamic resistance in the lowest meter of an Amazonian rain forest. The in-canopy aerodynamic resistance representing the whole grassland canopy was at least 3–4 times higher than in-canopy aerodynamic resistances of forest canopies taken from literature. Our results reveal that even if the canopy height of natural grassland canopies is small compared to forests (around 1–10 %), the corresponding canopy flushing times can be shorter or even longer within grassland than in forest canopies (10–400 %). The canopy flushing times exhibited only small day/night variability, which is well in accordance with a detailed study on flushing times within an Amazonian rain forest (Simon et al., 2005). The small day/night variability is caused by the compensating transport efficiencies in lower and upper canopy layers during day and nighttime for both canopy types.

The canopy flushing time of the grassland was found to be ≤ 6 min and the chemical timescale of the NO-NO₂-O₃ triad during daytime ranged between 1–3 min. This has obvious implications e.g., for soil-emitted reactive compounds such as NO, implying fast chemical conversion of NO to NO₂ within the grass canopy. During daytime the plant uptake of NO₂ was shown to be 2–3 times faster than the canopy flushing time. Inevitably, this leads to a strong potential NO_x canopy reduction in the presence of biogenic NO soil emissions. Due to the extensive global terrestrial coverage with grassland canopies, this finding is highly relevant for the application of global chemistry and transport models. We determined a median net chemical O₃ production of 10 % during daytime within the air column between the flux measurement and the canopy, which was due to the absence of biogenic NO soil emission in our study. Hence, in contrast to previous studies our measured O₃ deposition flux by eddy covariance is slightly underestimated. The flux divergence for O₃ was one order of magnitude larger during the high NO_x than during the low NO_x periods. In-canopy Damköhler numbers were shown to be relevant for NO₂ only under nighttime conditions, due to the minor role of NO₂ uptake by plants at this time. Above the canopy Damköhler numbers indicated a potential flux divergence, but did not provide a hint for the observed chemical production of O₃. The only instance without indication for a flux divergence within the entire data set was found during nighttime of the high NO_x periods in the lowest canopy layer.

Acknowledgements

This project was funded by the Max Planck Society. We are grateful to J.-C. Mayer for the installation and the maintenance of meteorological sensors and for supporting the data evaluation. We are indebted to A. Moravek for his support with the eddy covariance measurements and the corresponding data evaluation and the fruitful discussions on many details of this study.

References

- Atkinson, R. and Arey, J., 2003. Gas-phase tropospheric chemistry of biogenic volatile organic compounds: a review. *Atmospheric Environment*, 37: S197-S219.
- Atkinson, R. et al., 2004. Evaluated kinetic and photochemical data for atmospheric chemistry: Volume I - gas phase reactions of O_(x), HO_(x), NO_(x) and SO_(x) species. *Atmospheric Chemistry and Physics*, 4: 1461-1738.
- Aylor, D.E., Wang, Y.S. and Miller, D.R., 1993. Intermittent wind close to the ground within a grass canopy. *Boundary-Layer Meteorology*, 66(4): 427-448.
- Bakwin, P.S. et al., 1990. Emission of nitric-oxide (NO) from tropical forest soils and exchange of NO between the forest canopy and atmospheric boundary-layers. *Journal of Geophysical Research-Atmospheres*, 95(D10): 16755-16764.
- Baldocchi, D., 1988. A multi-layer model for estimating sulfur-dioxide deposition to a deciduous oak forest canopy. *Atmospheric Environment*, 22(5): 869-884.
- Crutzen, P., 1973. Discussion of chemistry of some minor constituents in stratosphere and troposphere. *Pure and Applied Geophysics*, 106(5-7): 1385-1399.
- Denmead, O.T., Freney, J.R. and Dunin, F.X., 2007. Gas exchange between plant canopies and the atmosphere: Case-studies for ammonia. *Atmospheric Environment*, 42(14): 3394-3406.
- Dorsey, J.R. et al., 2004. Oxidized nitrogen and ozone interaction with forests. I: Experimental observations and analysis of exchange with Douglas fir. *Quarterly Journal of the Royal Meteorological Society*, 130(600): 1941-1955.
- Dupont, S. and Patton, E.G., 2012. Momentum and scalar transport within a vegetation canopy following atmospheric stability and seasonal canopy changes: the CHATS experiment. *Atmospheric Chemistry and Physics*, 12(13): 5913-5935.
- Duyzer, J.H., Deinum, G. and Baak, J., 1995. The interpretation of measurements of surface exchange of nitrogen-oxides - correction for chemical-reactions. *Philosophical Transactions of the Royal Society a-Mathematical Physical and Engineering Sciences*, 351(1696): 231-248.
- Erisman, J.W., Vanpul, A. and Wyers, P., 1994. Parametrization of surface-resistance for the quantification of atmospheric deposition of acidifying pollutants and ozone. *Atmospheric Environment*, 28(16): 2595-2607.
- Finnigan, J., 2000. Turbulence in plant canopies. *Annual Review of Fluid Mechanics*, 32: 519-571.
- Foken, T. et al., 2012. Coupling processes and exchange of energy and reactive and non-reactive trace gases at a forest site - results of the EGER experiment. *Atmospheric Chemistry and Physics*, 12(4): 1923-1950.
- Gut, A. et al., 2002. Exchange fluxes of NO₂ and O₃ at soil and leaf surfaces in an Amazonian rain forest. *Journal of Geophysical Research-Atmospheres*, 107(D20): LBA 27-1-LBA 27-15.
- Hänsel, H. and Neumann, W., 1995. *Physik*. Spektrum, Akad. Verl., Heidelberg, Berlin, Oxford.
- Hicks, B.B., Baldocchi, D.D., Meyers, T.P., Hosker, R.P. and Matt, D.R., 1987. A preliminary multiple resistance routine for deriving dry deposition velocities from measured quantities. *Water Air and Soil Pollution*, 36(3-4): 311-330.
- Högström, U., 1988. Non-dimensional wind and temperature profiles in the atmospheric surface-layer - a re-evaluation. *Boundary-Layer Meteorology*, 42(1-2): 55-78.
- Holzinger, R., Lee, A., Paw, K.T. and Goldstein, A.H., 2005. Observations of oxidation products above a forest imply biogenic emissions of very reactive compounds. *Atmospheric Chemistry and Physics*, 5: 67-75.
- IPPC, 2007. *Climate Change 2007: the physical science basis*. Contribution of working group I to the fourth assessment report of the Intergovernmental Panel on Climate Change. University Press, Cambridge, UK.

- Jacob, D.J. and Wofsy, S.C., 1990. Budgets of reactive nitrogen, hydrocarbons, and ozone over the amazon-forest during the wet season. *Journal of Geophysical Research-Atmospheres*, 95(D10): 16737-16754.
- Jacobs, A.F.G., Vanboxel, J.H. and Elkilani, R.M.M., 1994. Nighttime free-convection characteristics within a plant canopy. *Boundary-Layer Meteorology*, 71(4): 375-391.
- Jäggi, M., Ammann, C., Neftel, A. and Fuhrer, J., 2006. Environmental control of profiles of ozone concentration in a grassland canopy. *Atmospheric Environment*, 40(28): 5496-5507.
- Kasanko, M., Palmieri, A. and Coyette, C., 2011. Land cover/ land use statistics. In: C. Coyette and H. Schenk (Editors), *Agriculture and Fishery Statistics*. Eurostat, Luxembourg, pp. 158.
- Kruijt, B. et al., 2000. Turbulence statistics above and within two Amazon rain forest canopies. *Boundary-Layer Meteorology*, 94(2): 297-331.
- Kurpius, M.R. and Goldstein, A.H., 2003. Gas-phase chemistry dominates O₃ loss to a forest, implying a source of aerosols and hydroxyl radicals to the atmosphere. *Geophysical Research Letters*, 30(7).
- Lamaud, E. et al., 2009. Partitioning of ozone deposition over a developed maize crop between stomatal and non-stomatal uptakes, using eddy-covariance flux measurements and modelling. *Agricultural and Forest Meteorology*, 149(9): 1385-1396.
- Lehmann, B.E., Lehmann, M., Neftel, A., Gut, A. and Tarakanov, S.V., 1999. Radon-220 calibration of near-surface turbulent gas transport. *Geophysical Research Letters*, 26(5): 607-610.
- Lenschow, D.H., 1982. Reactive trace species in the boundary-layer from a micrometeorological perspective. *Journal of the Meteorological Society of Japan*, 60(1): 472-480.
- Lerdau, M.T., Munger, L.J. and Jacob, D.J., 2000. Atmospheric chemistry - the NO₂ flux conundrum. *Science*, 289(5488): 2291.
- Mauder, M. and Foken, T., 2011. Documentation and instruction manual of the eddy-covariance software package TK3. *Arbeitsergebnisse Nr. 46(46)*.
- Monsi, M. and Saeki, T., 1953. Über den Lichtfaktor in den Pflanzengesellschaften und seine Bedeutung für die Stoffproduktion. *Japanese Journal of Botany*, 14: 22-52.
- Monteith, J.L. and Unsworth, M.H., 1990. *Principles of environmental physics*. E. Arnold, London, New York, 291 pp.
- Nemitz, E. et al., 2009. Turbulence characteristics in grassland canopies and implications for tracer transport. *Biogeosciences*, 6(8): 1519-1537.
- Nemitz, E. et al., 2000. Sources and sinks of ammonia within an oilseed rape canopy. *Agricultural and Forest Meteorology*, 105(4): 385-404.
- Personne, E. et al., 2009. SURFATM-NH₃: a model combining the surface energy balance and bi-directional exchanges of ammonia applied at the field scale. *Biogeosciences*, 6(8): 1371-1388.
- Plake, D. et al., 2014. Comparison of ozone deposition measured with the dynamic chamber and the eddy covariance method. *Agricultural and Forest Meteorology*, submitted.
- Plake, D. and Trebs, I., 2013. An automated system for selective and continuous measurements of vertical thoron profiles for the determination of transport times near the ground. *Atmospheric Measurement Techniques*, 6(4): 1017-1030.
- Rinne, J. et al., 2012. Effect of chemical degradation on fluxes of reactive compounds - a study with a stochastic Lagrangian transport model. *Atmospheric Chemistry and Physics*, 12(11): 4843-4854.
- Ripley, E.A. and Redman, R.E., 1976. Grassland. In: J.L. Monteith (Editor), *Vegetation and the atmosphere*. Acad. Press, London.
- Rummel, U., 2005. Turbulent exchange of ozone and nitrogen oxides between an Amazonian rain forest and the atmosphere, University of Bayreuth, Bayreuth, 246 pp.
- Rummel, U., Ammann, C., Gut, A., Meixner, F.X. and Andreae, M.O., 2002. Eddy covariance measurements of nitric oxide flux within an Amazonian rain forest. *Journal of Geophysical Research-Atmospheres*, 107(D20).

- Rummel, U. et al., 2007. Seasonal variation of ozone deposition to a tropical rain forest in southwest Amazonia. *Atmospheric Chemistry and Physics*, 7(20): 5415-5435.
- Seinfeld, J.H. and Pandis, S.N., 2006. *Atmospheric chemistry and physics : from air pollution to climate change*. Wiley, Hoboken, NJ, 1203 pp.
- Simon, E. et al., 2005. Lagrangian dispersion of Rn-222, H₂O and CO₂ within Amazonian rain forest. *Agricultural and Forest Meteorology*, 132(3-4): 286-304.
- Stella, P. et al., 2013. Measurements of nitrogen oxides and ozone fluxes by eddy covariance at a meadow: evidence for an internal leaf resistance to NO₂. *Biogeosciences*, 10(9): 5997-6017.
- Suttie, J.M., Reynolds, S.G. and Batello, C., 2005. Introduction. In: J.M. Suttie, S.G. Reynolds and C. Batello (Editors), *Grasslands of the world*. FAO, Rome.
- Swinbank, W.C., 1968. A comparison between predictions of dimensional analysis for constant-flux layer and observations in unstable conditions. *Quarterly Journal of the Royal Meteorological Society*, 94(402): 460-&.
- Trebs, I. et al., 2009. Relationship between the NO₂ photolysis frequency and the solar global irradiance. *Atmospheric Measurement Techniques*, 2(2): 725-739.
- Trumbore, S.E., Keller, M., Wofsy, S.C. and Dacosta, J.M., 1990. Measurements of soil and canopy exchange-rates in the Amazon rain-forest using Rn-222. *Journal of Geophysical Research-Atmospheres*, 95(D10): 16865-16873.
- van Pul, W.A.J. and Jacobs, A.F.G., 1994. The conductance of a maize crop and the underlying soil to ozone under various environmental-conditions. *Boundary-Layer Meteorology*, 69(1-2): 83-99.
- Warneck, P., 2000. *Chemistry of the natural atmosphere*. Academic Press, San Diego, California, 927 pp.
- Yienger, J.J. and Levy, H., 1995. Empirical-model of global soil-biogenic NO_x emissions. *Journal of Geophysical Research-Atmospheres*, 100(D6): 11447-11464.

Erklärungen

(§ 5 Nr. 4 PromO)

Hiermit erkläre ich, dass keine Tatsachen vorliegen, die mich nach den gesetzlichen Bestimmungen über die Führung akademischer Grade zur Führung eines Doktorgrades unwürdig erscheinen lassen.

(§ 8 S. 2 Nr. 5 PromO)

Hiermit erkläre ich mich damit einverstanden, dass die elektronische Fassung meiner Dissertation unter Wahrung meiner Urheberrechte und des Datenschutzes einer gesonderten Überprüfung hinsichtlich der eigenständigen Anfertigung der Dissertation unterzogen werden kann.

(§ 8 S. 2 Nr. 7 PromO)

Hiermit erkläre ich eidesstattlich, dass ich die Dissertation selbständig verfasst und keine anderen als die von mir angegebenen Quellen und Hilfsmittel benutzt habe. Ich habe die Dissertation nicht bereits zur Erlangung eines akademischen Grades anderweitig eingereicht und habe auch nicht bereits diese oder eine gleichartige Doktorprüfung endgültig nicht bestanden.

(§ 8 S. 2 Nr. 9 PromO)

Hiermit erkläre ich, dass ich keine Hilfe von gewerblichen Promotionsberatern bzw. -vermittlern in Anspruch genommen habe und auch künftig nicht nehmen werde.

Mainz, den

Daniel Plake